INSTITUTE OF PHYSICS PUBLISHING REPORTS ON PROGRESS IN PHYSICS

Rep. Prog. Phys. **69** (2006) 233–299 doi:10.1088/0034-4885/69/1/R05

Neutron and x-ray diffraction studies of liquids and glasses

Henry E Fischer[1,4], **Adrian C Barnes**[2] **and Philip S Salmon**[3]

[1] Institut Laue-Langevin, 6 rue Jules Horowitz, B.P. 156, 38042 Grenoble cedex 9, France
[2] H.H. Wills Physics Laboratory, University of Bristol, Tyndall Avenue, Bristol BS8 1TL, UK
[3] Department of Physics, University of Bath, Bath BA2 7AY, UK

E-mail: fischer@ill.fr, a.c.barnes@bristol.ac.uk, p.s.salmon@bath.ac.uk

Received 11 August 2005
Published 30 November 2005
Online at stacks.iop.org/RoPP/69/233

Abstract

The techniques of neutron diffraction and x-ray diffraction, as applied to structural studies of liquids and glasses, are reviewed. Emphasis is placed on the explanation and discussion of the experimental techniques and data analysis methods, as illustrated by the results of representative experiments. The disordered, isotropic nature of the structure of liquids and glasses leads to special considerations and certain difficulties when neutron and x-ray diffraction techniques are applied, especially when used in combination on the same system. Recent progress in experimental technique, as well as in data analysis and computer simulation, has motivated the writing of this review.

(Some figures in this article are in colour only in the electronic version)

[4] Author to whom correspondence should be sent.

Contents

1. Introduction

Given the wide range and long history of neutron and x-ray diffraction techniques used to study liquids and glasses, the scope of this review needs to be defined. We do not attempt to give a complete summary of the systems studied to date, or to cite all the major participants in the history of this field. We are mainly concerned with providing a rather pedagogic summary of the diffraction techniques as illustrated by the results of representative experiments, along the lines of previous publications by, for example, Barnes *et al* (2003) and Suck *et al* (1993).

Two early reviews of diffraction studies of liquids were written by Kruh (1962) for x-ray diffraction and by Furukawa (1962) for neutron, x-ray and electron diffraction, where both reviews included some discussion of the experimental techniques and data analysis methods. A thorough review of neutron diffraction studies on molecular liquids, molten salts and both aqueous and non-aqueous solutions has been given by Neilson and Adya (1996), and Neuefeind (2002) presents a brief review of high-energy x-ray diffraction studies of liquids. The application of x-ray and neutron diffraction techniques to glasses and the data analysis methods have been discussed by Wright (1996, 1994, 1993, 1974) and others. A recent book deals with applications of x-ray and neutron scattering methods to polymer science (Roe 2000). The dynamical aspects of disordered materials, including liquids and glasses, have recently been reviewed by Price *et al* (2003). We choose to cite such reviews rather than repeat too much of what has already been published.

The special physical properties of liquids (Egelstaff 1992, Hansen and McDonald 1990, Cusack 1987, Temperley *et al* 1968) and of glasses (Boolchand 2000, Feltz 1993, Elliott 1990, Cusack 1987, Zallen 1983) are largely due to these systems being disordered, isotropic and generally homogeneous. The microscopic structure of liquids and glasses is generally described in terms of probabilistic atomic distribution functions—see, for example, Ziman (1979) for a general discussion of the structure and dynamics of disordered systems. In this review, we consider a liquid to be a fluid of solid-like density, where by definition the atoms are free to diffuse throughout the medium and do not remain at their initial positions. Occasionally we will treat the dilute limit of such a system, i.e. a fluid of gas-like density. We also assume the ergodic principle for liquids (and other fluids). In our case this means that an average of 'snapshots' of local structures across a large sample of the liquid (obtained experimentally) is equivalent to the time average of any local structure. Here 'local structure' refers to that within the coherence volume of an incident quantum that diffracts in the sample (discussed in section 2.1). We will consider a glass to be an amorphous material made from a liquid via sufficiently rapid cooling so as to prevent any crystallization (Zallen 1983, Zachariasen 1932), where techniques of production include conventional bulk quenching, melt-spinning and splat-cooling.

By 'diffraction' we mean scattering of incident quanta by the sample and detection of all scattered quanta regardless of any energy exchange with particles undergoing atomic motion in the sample. Standard general references are the books by Bacon (1975) for neutron diffraction and Warren (1990) for x-ray diffraction, as well as Als-Nielsen and McMorrow (2001) for the case of x-ray synchrotron radiation. See also the HERCULES series on large-scale facilities, which contains chapters on the application of neutron and synchrotron radiation to condensed matter studies (Baruchel *et al* 1993, 1994). The diffusive and vibrational motions of the atoms in a liquid or a glass can be measured by both inelastic neutron scattering (INS) and inelastic x-ray scattering (IXS), but a discussion of these methods is beyond the scope of this review. The reader is referred to Hempelmann (2000), Zabel (1993), Richter *et al* (1989) and Beé (1988) for INS and to Chen and Kotlarchyk (1997), Burkel (1991) and Schulke (1991) for IXS.

Useful compilations of information and data for neutron and x-ray scattering techniques are given in the *Neutron Data Booklet* (Dianoux and Lander 2002) and the *X-ray Data Booklet*

(Thompson and Vaughan 2001). A thorough compilation of information on neutron, x-ray and electron diffraction techniques, including data correction factors as well as methods for the production and detection of the quanta, can be found in the *International Crystallography Tables* (volume C) edited by Prince (2004 3rd edn) and by Wilson and Prince (1999 2nd edn).

For a monatomic system, a single probabilistic function called the pair-distribution function is used to describe the spatial correlations between pairs of atoms. In a polyatomic liquid or glass, this concept is extended such that the probability of finding one type of atom (e.g. H) at a given distance from another (e.g. O) is related to the *partial* pair-distribution function for those chemical species in that system. In all materials the existence of chemical bonding will give rise to short-range and intermediate-range structural order but not to long-range periodic order as in the case of crystals (see, e.g. Salmon *et al* (2005)). The determination of this order in terms of partial pair-distribution functions is therefore fundamental to an understanding of many physical properties of liquids and glasses.

The Fourier transform of a (partial) pair-distribution function leads to a reciprocal space function known as the (partial) structure factor. Neutron and x-ray diffraction techniques measure the differential scattering cross-section that is essentially proportional to the structure factor of a monatomic system, or to a weighted sum of partial structure factors for a polyatomic system. From a series of diffraction experiments on a given polyatomic system for which the scattering power of the atoms is varied (e.g. by isotopic substitution in neutron diffraction), it is often possible to determine, with accuracy, its partial structure factors and thereby its partial pair-distribution functions.

The need for high accuracy and absolute normalization of the measured intensities makes diffraction measurements on liquids and glasses particularly challenging, and the data analysis generally involves a variety of delicate corrections and careful interpretation. Specialized instruments include the D4c (Fischer *et al* 2002), 7C2 (Ambroise *et al* 1984) and SLAD (Wannberg *et al* 1997) reactor–source neutron diffractometers, the SANDALS (Soper 1989), GEM (Hannon 2005), LAD (Howells and Hannon 1999), HIT-II (Fukunaga *et al* 1993) and GLAD (Ellison *et al* 1993) pulsed-source neutron diffractometers, the BW5 (Bouchard *et al* 1998), BL04B2 (Kohara *et al* 2001) and 11-ID-C (Rütt *et al* 2001) high-energy x-ray beamlines and the anomalous scattering x-ray beamline ID1 (Lequien *et al* 1995). As neutrons and x-rays have fundamentally different interactions with matter, diffraction experiments made using these methods can provide complementary information and, in certain cases, considerable advantage can be had in the determination of partial structure factors by combining the two techniques. However, the absolute accuracy needed for the correct combination of the two types of diffraction data makes the data analysis even more complicated.

An alternative and complementary approach to such partial structure factor (and partial pair-distribution function) determination is that of reverse Monte Carlo (RMC) modelling (Keen *et al* 2005a, McGreevy 2001, 1995, McGreevy and Pusztai 1988), whose range of application continues to increase. The RMC method refines iteratively a three-dimensional structural model of the system that is consistent with one or more data sets from structure measurements, be they neutron diffraction, x-ray diffraction, EXAFS (extended x-ray absorption fine structure) spectroscopy, NMR (nuclear magnetic resonance), etc. There is no interatomic or intermolecular potential involved in RMC modelling, which can be an advantage in many cases.

The method of empirical potential structural refinement (EPSR) is similar in concept to RMC but refines self-consistently a potential as well as a three-dimensional model for the system (Soper 2001, 1998, 1996a). The EPSR method has had a productive application to molecular liquids and ionic solutions.

The development of techniques for extreme thermodynamic conditions has opened up new areas of research in x-ray and neutron diffraction studies of liquids and glasses. As high-temperature studies are oftentimes limited by chemical reaction between the sample and container, requiring special container materials (e.g. Simonet *et al* (1998)), the advent of containerless techniques such as aerodynamic levitation has led to sample temperatures exceeding 2000 °C for liquids in x-ray (Hennet *et al* 2002, Krishnan and Price 2000, Krishnan *et al* 1997, Landron *et al* 1997) and neutron (Landron *et al* 2003, 2001, 2000) diffraction experiments. For electrically conducting liquid samples at high-temperature, the technique of electromagnetic levitation has been used in x-ray (e.g. Kimura *et al* (2001)) and neutron (e.g. Schenk *et al* (2002)) diffraction studies, as well as in EXAFS work (e.g. Egry *et al* (1996)). Both levitation techniques have the added advantage of permitting significant undercooling of the liquid sample.

Due to relatively low attenuation effects, conventional (i.e. bulky) high-pressure cells can be used in neutron diffraction (e.g. Pfleiderer *et al* (2000)) and high-energy x-ray diffraction (e.g. Heusel *et al* (2002)) experiments, although the cell wall material is generally chosen to have small coherent scattering. New advances in very high-pressure instrumentation, including large volume presses such as the Paris–Edinburgh cell adapted to neutron diffraction (e.g. Klotz *et al* (2005, 2002)) and synchrotron x-ray diffraction (e.g. Mezouar *et al* (1999)), have extended the pressure range to tens of giga-pascals (GPa). Such 'anvil'-type cells have been used for the study of liquid samples under high-pressure and high-temperature, e.g. in the high-energy synchrotron x-ray diffraction work of Katayama and Tsuji (2003), Crichton *et al* (2001) and Katayama *et al* (2000). A different type of cell has been developed by Tamura *et al* (1998) for energy-dispersive synchrotron x-ray diffraction and is suitable for liquids at high-temperature and high-pressure (see also Hosokawa and Tamura (2004)). Diamond anvil cells have also been used to study liquids at high pressures and temperatures (Falconi *et al* 2005, Gregoryanz *et al* 2005).

We begin this review by briefly considering the pertinent theoretical background for diffraction by liquids and glasses, distinguishing the cases for monatomic and polyatomic systems. For clarity we will limit the early discussion to scattering lengths that are independent of wavevector transfer and incident energy, sufficient for most cases of neutron diffraction, and later generalize the discussion to include these dependences for the more complex case of x-ray diffraction. This mode of presentation allows a concise and clear notation for the mathematics of the theoretical background while maintaining a good measure of generality.

Separate sections then discuss the diffraction techniques and their data treatment, with emphasis placed on the methods used for determining the partial structure factors of polyatomic liquids and glasses: isotopic substitution in neutron diffraction, anomalous dispersion in x-ray diffraction and the combination of neutron and x-ray diffraction techniques. The discussion of neutron diffraction techniques is most pertinent to the case of a monochromatic incident beam (i.e. reactor source), but elements particular to pulsed-source diffraction are also discussed and/or cited.

Finally, we feel that the growing importance and utility of data modelling and simulation methods, also noted by Price *et al* (2003) for dynamical studies, merit their discussion in a separate section, which is followed by the conclusions section.

2. Basic theoretical background for diffraction by liquids and glasses

The formalism reviewed in this section holds for both neutron and x-ray diffraction and starts with a system that comprises point-like scattering centres. The results thus obtained can then be readily generalized to the case of extended scattering centres, or atoms, by superimposing these

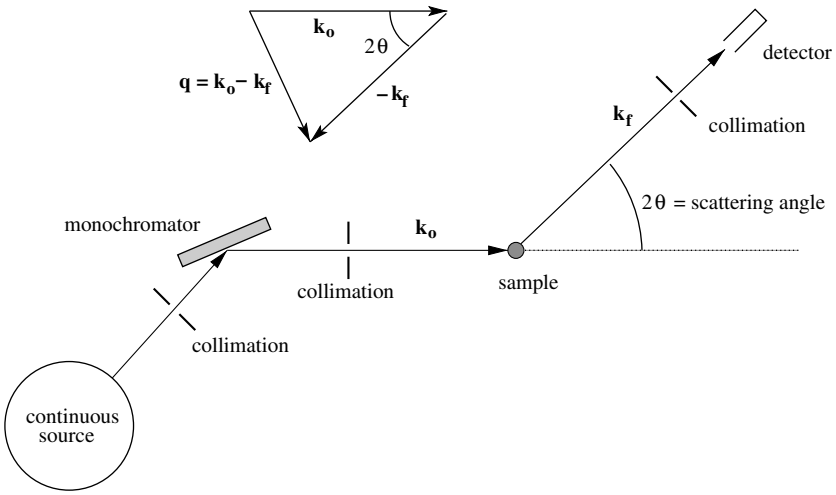

Figure 1. Schematic of a typical diffraction experiment from a continuous source of neutrons or x-rays. The scattering triangle of wavevectors is shown at the top.

centres on each and every point. Similar unified formalisms have been presented elsewhere (e.g. Champeney (1973), Leadbetter and Wright (1972d)). For more fundamental descriptions of the scattering processes involved for liquids and glasses the reader is referred to Lovesey (1984 vol 1 chapter 5), Squires (1978 chapter 5), Bacon (1975 chapter 16) or Sjölander (1965) for neutrons and to Guinier (1994 chapter 3), Warren (1990 chapter 10) or James (1962 chapter 10) for x-rays. A general quantum mechanical treatment of scattering theory can be found in Schiff (1968 chapters 5 and 9).

2.1. *Differential scattering cross-section for diffraction*

Consider a collimated beam of quanta (neutrons or x-rays) incident on a sample composed of one or more point-like scattering centres, as depicted in figure 1. Let us first treat the case of a monochromatic incident beam where all quanta have the same incident wavelength, λ_o, and let us represent the wavepacket of each incident quantum by a simple plane wave:

$$\Psi_{\rm inc} = \psi_{\rm inc}\, {\rm e}^{{\rm i}[\boldsymbol{k}_o\cdot\boldsymbol{r}-\omega_o t]} \equiv \psi_o\, {\rm e}^{{\rm i}\boldsymbol{k}_o\cdot\boldsymbol{r}}, \tag{2.1}$$

where $\psi_{\rm inc}$ is the amplitude, $\boldsymbol{k}_o$ is the incident wavevector of magnitude $k_o = 2\pi/\lambda_o$ and $\boldsymbol{r}$ is the position of the quantum. For neutrons, the incident energy $\hbar\omega_o = \hbar^2 k_o^2/2m_n$, where m_n is the mass of the neutron, and for x-rays $\hbar\omega_o = \hbar c k_o$, where c is the speed of light in vacuum. For simplicity, we will assume that the incident energy, $\hbar\omega_o$, of a quantum is much larger than any energy exchange, $\hbar\omega$, that occurs on scattering from the sample. Also, if λ_o is very much larger than the diameter of the scattering centre, the scattering will be isotropic (i.e. S-wave scattering). Then, for a single scattering centre i at the origin of coordinates, the wavepacket of the scattered quantum is represented by a spherical wave:

$$\Psi_{\rm scatt,1} = \frac{-\psi_o b_i}{R} {\rm e}^{{\rm i}k_f R}, \tag{2.2}$$

where R is the distance from the scattering centre and k_f is the magnitude of the final wavevector $\boldsymbol{k}_f$. Since we are assuming $\hbar\omega_o \gg \hbar\omega = \hbar\omega_o - \hbar\omega_f$, where $\hbar\omega_f$ is the final energy of the quantum, we have $\hbar\omega_f \approx \hbar\omega_o$ which means that we have been able to factor out

a common time dependence, $\exp(-\mathrm{i}\omega_o t)$, from the incident and scattered waves and incorporate it into the ψ_o term. In addition, we have $k_f \approx k_o$ for both x-rays and neutrons. The constant b_i is the *scattering length* for scattering centre i, has dimensions of length, is in general complex-valued and its magnitude and sign depend on the properties of the interaction between the quantum and scattering centre. The leading minus sign in equation (2.2) results from the convention in neutron scattering that a positive scattering length corresponds to a repulsive scattering potential (e.g. Squires (1978) p 8), and in the case of x-ray scattering it indicates that the radiated electric field is phase-shifted on scattering by π with respect to the incident field (e.g. Als-Nielsen and McMorrow (2001) p 7). Note that we are ignoring for the moment any polarization of the quantum or scattering centre.

If the scattering centre i is not at the origin but at a position $\boldsymbol{r}_i$ then, provided $R \gg r_i$, an additional phase shift of $\boldsymbol{q}\cdot\boldsymbol{r}_i$ can be deduced where $\boldsymbol{q} = \boldsymbol{k}_o - \boldsymbol{k}_f$ is called the scattering vector. Hence, for a sample comprising N point-like scattering centres i, each having a scattering length b_i,

$$\Psi_{\mathrm{scatt,N}} = \frac{-\psi_o}{R}\mathrm{e}^{\mathrm{i}k_f R}\sum_{i=1}^{N} b_i \mathrm{e}^{\mathrm{i}\boldsymbol{q}\cdot\boldsymbol{r}_i} \tag{2.3}$$

at a distant point defined by $\boldsymbol{R}$, taken to be parallel to $\boldsymbol{k}_f$, where we place a detector of area $\mathrm{d}S \ll R^2$ subtending a small solid angle $\mathrm{d}\Omega = \mathrm{d}S/R^2$ with respect to the sample. The upper part of figure 1 shows the so-called scattering triangle, which relates the vectors $\boldsymbol{k}_o$, $\boldsymbol{k}_f$ and $\boldsymbol{q}$ to the scattering angle 2θ of $\boldsymbol{k}_f$ with respect to $\boldsymbol{k}_o$.

We define the differential scattering cross-section for diffraction by

$$\frac{\mathrm{d}\sigma}{\mathrm{d}\Omega} \stackrel{\mathrm{def}}{=} \frac{\text{number of quanta scattered per second towards the detector into } \mathrm{d}\Omega}{\Phi\,\mathrm{d}\Omega}, \tag{2.4}$$

where the flux Φ is the number of incident quanta per second per unit cross-sectional area of the incident beam. For typical units of $\mathrm{cm}^{-2}\,\mathrm{s}^{-1}$ for flux and steradian (str) for $\mathrm{d}\Omega$ the units of $\mathrm{d}\sigma/\mathrm{d}\Omega$ become cm^2/str or, more conveniently, barn/str where 1 barn = $10^{-24}\,\mathrm{cm}^2$. By choosing a suitable normalization of the wavefunctions (e.g. Mott (1962)), the incident flux is given by $\Phi = v_o|\Psi_{\mathrm{inc}}|^2 = v_o\psi_o^2$, where v_o is the group velocity of the incident quanta, and the flux of scattered particles across area $\mathrm{d}S$, which defines the numerator of equation (2.4), is given by $v_f|\Psi_{\mathrm{scatt}}|^2\,\mathrm{d}S$ where v_f is the final velocity. For x-ray diffraction $v_o = v_f = c$ and for neutron diffraction $v_f = \hbar k_f/m_n \approx v_o$ since we have assumed $\hbar\omega_f \approx \hbar\omega_o$ such that $k_f \approx k_o$. Hence the velocity factors will cancel, and we can write for a single scattering centre at the origin:

$$\left.\frac{\mathrm{d}\sigma}{\mathrm{d}\Omega}\right|_1 = \frac{|\Psi_{\mathrm{scatt},1}|^2\,\mathrm{d}S}{|\Psi_{\mathrm{inc}}|^2\,\mathrm{d}\Omega} = \frac{(\psi_o^2|b_i|^2/R^2)(R^2\,\mathrm{d}\Omega)}{\psi_o^2\,\mathrm{d}\Omega} = |b_i|^2 \quad \text{or} \quad b_i^2, \tag{2.5}$$

giving isotropic scattering as expected. Note that here, as elsewhere in this review, b^2 represents the norm-squared of a scattering length. For the sample of N scattering centres, the expression for the differential scattering cross-section becomes

$$\frac{\mathrm{d}\sigma}{\mathrm{d}\Omega}(\boldsymbol{q}) = \overline{\left\langle\left|\sum_{i=1}^{N} b_i \mathrm{e}^{\mathrm{i}\boldsymbol{q}\cdot\boldsymbol{r}_i}\right|^2\right\rangle} = \left\langle\sum_{i,j}^{N} \overline{b_i b_j^*}\,\mathrm{e}^{\mathrm{i}\boldsymbol{q}\cdot\boldsymbol{r}_{ij}}\right\rangle, \tag{2.6}$$

where the vector $\boldsymbol{r}_{ij} = \boldsymbol{r}_i - \boldsymbol{r}_j$ gives the relative position of scattering centres i and j.

The averages in equation (2.6) require some explanation. Firstly, the atoms in a real sample continually undergo thermal displacement over the course of a diffraction experiment. The positions of the scattering centres are therefore, not, fixed, and the brackets $\langle\ \rangle$ denote a thermal average of these positions corresponding to the different states of the scattering system (i.e. the sample) that are accessible at a given temperature, as weighted by a Boltzmann factor

and appropriate degeneracy factors (e.g. Lovesey (1984) vol 1 p 9). Secondly, we have to consider the nature of the incident quantum and its interaction with the scattering centres, taking into account the distribution of b_i values over the scattering centre positions.

For definiteness, consider the case of a large sample (e.g. $N \approx N_A$ where N_A is the Avogadro constant) comprising a single element, or chemical species, having Z electrons. In x-ray diffraction, the photons scatter from the atomic electron density, and each scattering centre is identified with an 'atomic position' or 'atomic site' insofar as the atomic electron density is roughly centred on the nucleus. Since the atomic scattering length at a given incident energy depends only on Z, the horizontal bars in equation (2.6) can be omitted; there is a unique scattering length for each possible site. In neutron diffraction, the neutrons will scatter from the nuclei and also, for magnetic atoms, from unpaired electrons. For simplicity, we will consider only the former and identify the scattering centres with the nuclei. Then the scattering length (for a given incident energy) at a site depends on the isotopic mass of the nucleus that occupies that site and also on the relative orientation of the isotope's nuclear spin state with respect to the incident neutron's spin state. The horizontal bars in equation (2.6) then represent an average over an ensemble of samples of identical structure and isotopic composition where, for each member of the ensemble, the neutron scattering lengths are distributed differently over the sites (cf Squires (1978) p 21). In making this average, it is usual to assume that there is no correlation (a) between nuclear spin state and site, (b) between the nuclear spins themselves and (c) between isotopic mass and site. In the case of a sample comprising several chemical species, the neutron scattering lengths for each chemical species must be distributed appropriately amongst the available sites for that chemical species.

In neutron diffraction, the b_i in equations (2.2)–(2.6) represent so-called 'bound' scattering lengths. However, this nomenclature does not mean that the nuclei are perfectly fixed (see the appendix of Sears (1978) for a discussion). Rather, the use of bound values for neutron scattering lengths within the Fermi pseudo-potential formalism ensures that if a single nucleus is sufficiently well localized with respect to its chemical environment, the required result of isotropic scattering (see equation (2.2)) is obtained (e.g. Lovesey (1984) vol 1 p 11). From equation (2.5) it follows, for a system comprising a single bound nucleus at the origin, that the total scattering cross-section is $\sigma_{\text{scatt}} = 4\pi b_i^2$ (again ignoring polarization effects). By comparison, for an isolated 'free' nucleus as in the case of a perfect gas, this cross-section becomes $\sigma_{\text{scatt}}^{\text{free}} = 4\pi a_i^2$ where $a_i = b_i M_i/(m_n + M_i)$ is called the free scattering length and M_i is the nuclear mass (e.g. Bacon (1975) p 32). At thermal neutron energies, the imaginary part of b_i (which is related to the absorption cross-section) is generally very small because absorption resonances are rare at diffraction wavelengths—notable exceptions occur for ^{103}Rh, ^{113}Cd, ^{149}Sm, ^{151}Eu, ^{155}Gd, ^{157}Gd, ^{164}Dy, ^{167}Er, ^{176}Lu, ^{180}Ta, ^{191}Ir and others (Sinclair 1993, Mughabghab *et al* 1981). It should be noted that the real part of b_i also varies strongly near these resonances as a function of the incident neutron energy—Cossy *et al* (1989) outline a procedure for calculating the real and imaginary parts of energy-dependent neutron scattering lengths and apply it to the case of ^{164}Dy.

In x-ray diffraction, the b_i refer to Rayleigh–Thomson scattering lengths for photons that scatter from electrons in bound atomic orbitals (see e.g. Maslen *et al* (1995) p 476). As the x-rays scatter not from the point-like atomic nuclei but from spatially extended electron density distributions (i.e. orbitals and bonds), each scattering centre is associated with a scattering length *density* distribution that is described by an r-dependent function. The finite extent of this distribution in real-space results in a q-dependent modulation of the x-ray scattering length in reciprocal space, in other words, an atomic form factor (see section 4.1). For x-ray diffraction, absorption effects are in general considerably stronger than for off-resonance neutron diffraction, i.e. the imaginary part of b_i cannot be ignored, and

the energy dependence of the real part should always be taken into account. A q-dependent form factor also occurs in the case of neutron scattering from magnetic atoms. It is therefore necessary to take this scattering into account when analysing the diffraction patterns measured for magnetic materials, e.g. when there is paramagnetic scattering from rare-earth ions (Wasse and Salmon 1999).

In deriving equation (2.6) it was not necessary to assume elastic scattering events, i.e. that there was no energy exchange between the incident quantum and sample. Instead, we made the so-called *static approximation* in which the energy exchange, $\hbar\omega$, is considered to be very small compared with the incident energy $\hbar\omega_o$. In order to appreciate the validity of this approximation it is important to note that the scattered quanta in a diffraction experiment are counted by the detector regardless of their energy exchanges with the sample. The measurement thus amounts to an integration of the double differential scattering cross-section, $\mathrm{d}^2\sigma/\mathrm{d}\Omega\,\mathrm{d}E$, at constant detector angle 2θ and over all possible energy exchanges:

$$\left.\frac{\mathrm{d}\sigma}{\mathrm{d}\Omega}\right|_{\mathrm{meas}} = \int_{-\infty}^{+\hbar\omega_o} \mathrm{d}(\hbar\omega)\frac{\mathrm{d}^2\sigma}{\mathrm{d}\Omega\,\mathrm{d}E}\epsilon(E_f), \tag{2.7}$$

where $E = \hbar\omega = E_o - E_f$ represents the energy loss of the quanta, all having incident energy $E_o = \hbar\omega_o$. The efficiency $\epsilon(E_f)$ of the detector is in general a function of the final energy E_f. For x-rays we can write $\hbar\omega = \hbar ck_o - \hbar ck_f$ and for neutrons $\hbar\omega = (\hbar^2/2m_n)(k_o^2 - k_f^2)$. Within the static approximation, $E_o = \hbar\omega_o \gg \hbar\omega$ so that the upper limit of the integral in equation (2.7) can be extended to infinity. It can also be shown that the integration over $\hbar\omega$ then occurs at constant $\boldsymbol{q}$ (see e.g. Squires (1978) p 78, Lomer and Low (1965) p 12). Then equation (2.7) reduces to the expression

$$\left.\frac{\mathrm{d}\sigma}{\mathrm{d}\Omega}\right|_{\mathrm{meas}}^{\mathrm{sa}} = \epsilon(E_o)\int_{-\infty}^{+\infty}\mathrm{d}(\hbar\omega)\left.\frac{\mathrm{d}^2\sigma}{\mathrm{d}\Omega\,\mathrm{d}E}\right|_{\boldsymbol{q}} = \epsilon(E_o)\frac{\mathrm{d}\sigma}{\mathrm{d}\Omega}(\boldsymbol{q}), \tag{2.8}$$

where we have assumed that the detector efficiency is insensitive to any (small) energy transfer. The static approximation therefore leads to a differential scattering cross-section given by equation (2.6), and correction terms, due to the inelastic nature of scattering events, may apply.

In practice, a sample at a given temperature will have a spectrum of possible thermal excitations and therefore, in general, an energy exchange of maximum possible magnitude $\hbar\omega_{\mathrm{max}}$ with the incident quantum. The static approximation will therefore be valid if $E_o \gg \hbar\omega_{\mathrm{max}}$. We can also examine this condition in terms of timescales. The energy $\hbar\omega_{\mathrm{max}}$ leads to a minimum characteristic time of atomic motion $\tau_{\mathrm{min}} \sim \omega_{\mathrm{max}}^{-1}$, corresponding to a period of atomic vibration in a solid or a relaxation time in a liquid (Squires (1978) pp 81–2). The quantum's incident energy $E_o = \hbar\omega_o$ leads to a characteristic time for diffraction, often called the 'snapshot' time $\tau_{\mathrm{snapshot}} \sim \omega_o^{-1}(a/\lambda_o)$, that corresponds to the timescale for an incident quantum (x-ray or neutron) to travel one interatomic distance a, which in diffraction experiments is generally of the order of the incident quantum wavelength λ_o. The static approximation is valid when $\hbar\omega_o \gg \hbar\omega_{\mathrm{max}}$ and therefore when $\tau_{\mathrm{snapshot}} \ll \tau_{\mathrm{min}}$. In other words, the structure of the sample is relatively static during the time the quantum wavepacket takes to pass from one atom to the next, and so the scattering event results in a relatively instantaneous 'snapshot' of the local structure, validating the use of time-independent positions $\boldsymbol{r}_i$ for the scattering centres in equation (2.6) (see also Turchin (1965) p 105).

The minimum characteristic time of atomic motion depends on the composition and temperature of the sample but typically $\tau_{\mathrm{min}} \sim 10^{-13}$–$10^{-12}$ s, corresponding to energies of the order of several millielectronvolts. The incident energies of x-rays at atomic diffraction wavelengths are sufficiently high (several kiloelectronvolts) such that the static approximation is comfortably valid. For neutron diffraction, however, the lower incident energies commonly

used (tens or a few hundred millielectronvolts) correspond to snapshot times in the range 10^{-15} s $\lesssim \tau_{\text{snapshot}} \lesssim 10^{-13}$ s, generally only about 1 or 2 orders of magnitude smaller than τ_{min} (e.g. Squires (1978) pp 78–83). This incomplete validity of the static approximation in the case of neutron scattering results in the need for inelasticity corrections (discussed in section 3.1) to the differential scattering cross-section given by equation (2.8).

In an actual neutron or x-ray diffraction experiment, a complete diffraction pattern (or *diffractogram*) is made by averaging the snapshots taken of the system by each of the incident quanta, i.e. it is made from summing up the contributions to $\mathrm{d}\sigma/\mathrm{d}\Omega$ that arise from the scattered intensity from all the coherence volumes in the sample (see, e.g. Sinha *et al* (1998) for the case of x-ray diffraction). A coherence volume can be thought of as the 'size' of the wavepacket of each quantum that diffracts somewhere in the sample and increases in size with the collimation and monochromaticity of the beam (e.g. Rauch and Werner (2000) section 4.2.5, Als-Nielsen and McMorrow (2001) section 1.5), i.e. it is dependent on the resolution function of the diffractometer. Scattering centres that lie within a coherence volume will give rise to interference effects, and the converse applies if the scattering centres do not satisfy this condition. Hence, there is a cutoff function in real-space associated with the coherence volumes and it follows, from the properties of Fourier transforms, that the measured intensity in reciprocal-space will be represented by the differential scattering cross-section of equation (2.6) or (2.8) *after* it has been convoluted with the resolution function of the diffractometer (Sinha *et al* 1998). In the extreme case of a single coherence volume in the illuminated part of the sample, we have diffraction-limited 'speckle' scattering (Sutton *et al* 1991)—such experiments are now possible at synchrotron x-ray sources and can give information on, for example, the dynamics of equilibrium critical fluctuations at the order–disorder transition in a binary alloy (Brauer *et al* 1995). It is worthwhile noting that since an incident quantum interacts with many scattering centres within its coherence volume, the centre-of-mass coordinates for the scattering event are accurately represented by coordinates in the sample's (i.e. laboratory's) frame of reference.

As already mentioned, the static approximation does not correspond to purely elastic scattering where all the energy exchanges, $\hbar\omega = 0$. Elastic scattering relates to diffraction from only the time-averaged atomic positions in the sample as can be appreciated from consideration of the Heisenberg Uncertainty principle $\Delta E \Delta t \sim \hbar$ in quantum mechanics: to equate exactly the incident and final energies of a scattered quantum an infinite timescale is required for the scattering event (e.g. Turchin (1965) p 106). For a liquid, atoms do not have well-defined equilibrium positions because of their diffusive motion, and the time-averaged atomic density is therefore uniform. In consequence, there is no elastic scattering from a liquid (Squires (1978) chapter 5). However, a given atom moving in a liquid will generally have a well-defined local coordination environment produced by successive neighbours, and this structure corresponds to the average of the *instantaneous* snapshots taken in a diffraction measurement. Within the formalism of van Hove (1954) correlation functions, the time-dependent pair-correlation function of the scattering system, $G(r, t)$, is evaluated at $t = \infty$ in the case of elastic scattering and is evaluated at $t = 0$ in the static approximation (see, e.g. Squires (1978) chapter 4). For a glass, the structure can be viewed in terms of the thermal motion of atoms about time-independent mean positions. The instantaneous position of an atom will therefore average in time to form a 'thermal cloud' about its mean position, leading to Debye–Waller factors in the diffracted intensity. In the case of a glass, it is possible to measure purely elastic scattering, and the coherent differential scattering cross-sections for the static approximation and elastic scattering differ by terms that involve the Debye–Waller factors of the chemical species (Wright and Sinclair 1985, Leadbetter and Wright 1972d).

Finally, it may be deduced from equation (2.4) that the intensity $I(\boldsymbol{q})$ in counts-per-second as measured by a detector of solid angle $\mathrm{d}\Omega$ is given by

$$I(\boldsymbol{q}) = \Phi \frac{\mathrm{d}\sigma}{\mathrm{d}\Omega}(\boldsymbol{q})\,\mathrm{d}\Omega, \tag{2.9}$$

where Φ is the incident flux on the sample, the differential scattering cross-section is given by equation (2.6), and here we assume perfect efficiency of detection ($\epsilon(E_f) = 1$). Note that the measured intensity is explicitly a function of only the scattering vector $\boldsymbol{q}$ which for a quantum of incident wavelength λ_o is related to the scattering angle 2θ via

$$q = |\boldsymbol{q}| = 2k_o \sin\theta = \frac{4\pi}{\lambda_o}\sin\theta. \tag{2.10}$$

This equation follows from the scattering triangle in figure 1 and is valid when $k_f = k_o$ (elastic scattering) or when $k_f \approx k_o$ (the static approximation). For a sample of overall isotropic structure, such as a polycrystalline powder, glass or liquid, it is not necessary to specify the azimuthal angle ϕ of the scattered quanta, as the diffraction pattern has conical symmetry (Debye–Scherrer diffraction).

A diffractogram of a liquid or a glass can therefore be obtained by varying either 2θ or λ_o or both. In the case of x-rays, energy-dispersive diffraction, wherein $\lambda_o = hc/E_o$ is varied at constant 2θ, is seldom used because of the complication of E_o-dependent cross-sections, although it may be advantageous when the detector's angular range is constrained by the sample environment (e.g. a high-pressure cell). For neutrons, there is significant complementarity between monochromatic angle-dispersive diffraction at reactor sources (fixed λ_o) and time-of-flight techniques at pulsed sources (variable λ_o and 2θ), especially concerning resolution effects and inelasticity corrections. Some schematic comparisons between diffraction techniques at reactor and pulsed sources are given by Windsor (1986), while Carpenter and Yelon (1986) discuss the characteristics of the neutron sources themselves. Soper *et al* ((2000) appendix B) define a 'C-number' for counting-rate comparisons of different neutron diffractometers, which is a function of q and proportional to the intensity scattered from a standard vanadium sample. For completeness, we mention that neutron diffractograms can also be obtained by measuring the sample's total cross-section as a function of incident energy (Sinclair and Wright 1983).

2.2. *The case of a monatomic system*

As discussed above, a monatomic sample (single atomic number Z) can have a distribution of scattering lengths for neutron diffraction (e.g. Squires (1978) pp 21–4). Assuming that there is no correlation between the scattering lengths and positions of different scattering centres in the sample, we can consider two cases for each term in the summation of equation (2.6):

$$\begin{aligned} \overline{b_i b_j^*} &= \overline{b_i b_i^*} = \overline{b^2} \qquad i = j \text{ (same site)}, \\ \overline{b_i b_j^*} &= \overline{b_i}\;\overline{b_j^*} = \overline{b}^2 \qquad i \neq j \text{ (different sites)}, \end{aligned} \tag{2.11}$$

so that the differential scattering cross-section becomes

$$\begin{aligned} \frac{\mathrm{d}\sigma}{\mathrm{d}\Omega}(\boldsymbol{q}) &= \overline{b}^2 \left\langle \sum_{i,j\neq i}^{N} \mathrm{e}^{\mathrm{i}\boldsymbol{q}\cdot\boldsymbol{r}_{ij}} \right\rangle + N\overline{b^2} \\ &= \overline{b}^2 \left\langle \sum_{i,j}^{N} \mathrm{e}^{\mathrm{i}\boldsymbol{q}\cdot\boldsymbol{r}_{ij}} \right\rangle + N(\overline{b^2} - \overline{b}^2), \end{aligned} \tag{2.12}$$

where again the brackets $\langle\,\rangle$ denote a thermal average. The first line of equation (2.12) separates the contributions to $\mathrm{d}\sigma/\mathrm{d}\Omega$ into a 'distinct' term (the diffraction interference from different

atomic sites) and a 'self' term (the isotropic diffraction from individual atomic sites). By defining the *interference function* $H(\boldsymbol{q})$ as

$$H(\boldsymbol{q}) \stackrel{\text{def}}{=} \frac{1}{N}\left\langle \sum_{i,j\neq i}^{N} \mathrm{e}^{\mathrm{i}\boldsymbol{q}\cdot\boldsymbol{r}_{ij}} \right\rangle, \tag{2.13}$$

which is dimensionless and for a disordered structure converges to 0 as $q \to \infty$, we can write the differential scattering cross-section per atom as

$$\begin{aligned} \frac{1}{N}\left[\frac{\mathrm{d}\sigma}{\mathrm{d}\Omega}(\boldsymbol{q})\right] &= \frac{1}{N}\left[\frac{\mathrm{d}\sigma}{\mathrm{d}\Omega}(\boldsymbol{q})\right]^{\text{distinct}} + \frac{1}{N}\left[\frac{\mathrm{d}\sigma}{\mathrm{d}\Omega}(\boldsymbol{q})\right]^{\text{self}} \\ &= \overline{b}^2 H(\boldsymbol{q}) + \overline{b^2}, \end{aligned} \tag{2.14}$$

showing explicitly the dependence on $\boldsymbol{q}$ only. Note that we are assuming the atoms of mass M to be distinguishable so that the system can be treated classically, i.e. that their thermal de Broglie wavelength

$$\Lambda = \sqrt{\frac{2\pi\hbar^2}{k_B T M}}, \tag{2.15}$$

is much smaller than their mean atomic separation, where k_B is the Boltzmann constant and T the absolute temperature (e.g. Mandl (1988)).

Alternatively, and more commonly for monatomic systems, $\mathrm{d}\sigma/\mathrm{d}\Omega$ is decomposed into a 'coherent' part and an 'incoherent' part, as shown by the second line in equation (2.12). The coherent part concerns diffraction from all atomic sites, including the 'self-scattering' from a single atom, but is independent of the distribution in scattering lengths; it is a function of the average scattering length alone. The incoherent part, by contrast, is independent of the spatial correlation of the atomic sites and depends only on the distribution of scattering lengths present in the sample, leading to isotropic diffraction. We thereby define the coherent and incoherent scattering lengths,

$$b_{\text{coh}} \stackrel{\text{def}}{=} \overline{b} \qquad \text{and} \qquad b^2_{\text{incoh}} \stackrel{\text{def}}{=} (\overline{b^2} - \overline{b}^2) = \overline{|b - \overline{b}|^2}, \tag{2.16}$$

as simply the average and standard deviation of the sample's scattering length distribution, respectively. Obviously, $b_{\text{incoh}} = 0$ in the case of x-ray diffraction from a monatomic sample. Tables of neutron b_{coh} and b_{incoh} values for natural isotopic compositions and for individual isotopes are given by, for example, Sears (1992). Note that it is possible in neutron diffraction to have a contribution to the measured intensity from spin incoherence (e.g. for a sample comprising a single isotope with non-zero spin), from isotope incoherence (e.g. for a sample comprising several spinless isotopes) or from both spin and isotope incoherence (Squires (1978) pp 21–4).

By defining the *(static) structure factor* $S(\boldsymbol{q})$ as

$$S(\boldsymbol{q}) \stackrel{\text{def}}{=} \frac{1}{N}\left\langle \sum_{i,j}^{N} \mathrm{e}^{\mathrm{i}\boldsymbol{q}\cdot\boldsymbol{r}_{ij}} \right\rangle = H(\boldsymbol{q}) + 1, \tag{2.17}$$

which is dimensionless and converges to 1 for $q \to \infty$, we can write the differential scattering cross-section per atom for a monatomic sample in the more familiar form:

$$\begin{aligned} \frac{1}{N}\left[\frac{\mathrm{d}\sigma}{\mathrm{d}\Omega}(\boldsymbol{q})\right] &= \frac{1}{N}\left[\frac{\mathrm{d}\sigma}{\mathrm{d}\Omega}(\boldsymbol{q})\right]^{\text{coh}} + \frac{1}{N}\left[\frac{\mathrm{d}\sigma}{\mathrm{d}\Omega}(\boldsymbol{q})\right]^{\text{incoh}} \\ &= \overline{b}^2 S(\boldsymbol{q}) + (\overline{b^2} - \overline{b}^2) \\ &= b^2_{\text{coh}} S(\boldsymbol{q}) + b^2_{\text{incoh}}, \end{aligned} \tag{2.18}$$

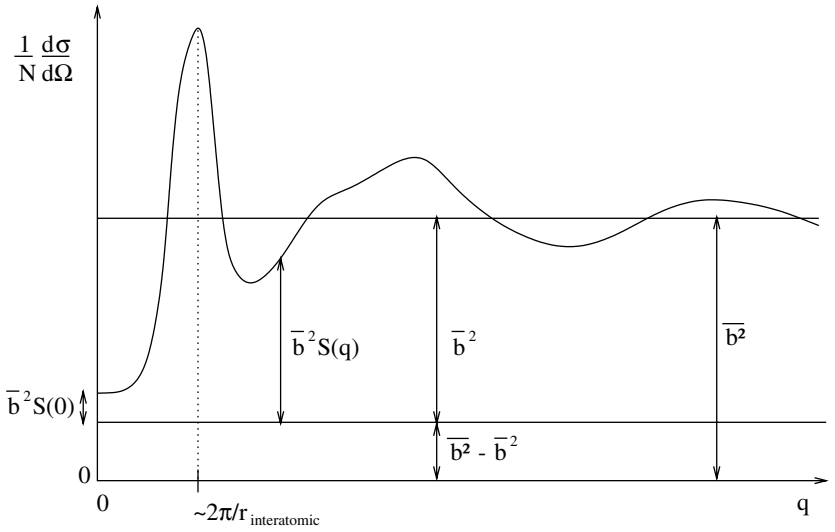

Figure 2. Differential scattering cross-section per atom $(1/N)\mathrm{d}\sigma/\mathrm{d}\Omega = \overline{b}^2 S(q) + (\overline{b^2} - \overline{b}^2)$ for a monatomic liquid or glass. The position of the first peak is inversely proportional to the interatomic distance, $r_{\text{interatomic}}$.

where the $\boldsymbol{q}$-dependence is again emphasized. Note that the above expression can be derived from equation (2.14) by the simple operation of subtracting the coherent self-scattering $\overline{b}^2$ from the second term and adding it to the first. Figure 2 shows the differential scattering cross-section per atom for a typical monatomic liquid or glass. We emphasize that $S(\boldsymbol{q})$ depends only on the relative coordinates of the scattering centres in the system and is independent of the nature of the probe–system interaction.

It follows from equation (2.8) that the (static) structure factor $S(\boldsymbol{q})$ can be expressed in terms of a more general quantity $S(\boldsymbol{q}, \omega)$ which is known as the (coherent) *dynamic* structure factor (van Hove 1954):

$$S(\boldsymbol{q}) = \int_{-\infty}^{+\infty} \mathrm{d}(\hbar\omega) S(\boldsymbol{q}, \omega), \tag{2.19}$$

where $\hbar\omega$ is the energy transfer between the incident quantum and the sample and $S(\boldsymbol{q}, \omega)$ is in turn directly proportional to the double differential scattering cross-section for coherent scattering $\mathrm{d}^2\sigma/(\mathrm{d}\Omega\,\mathrm{d}E)|_{\text{coh}}$. As mentioned earlier, in reality the integration is limited by the (maximum) incident energy of the beam, thus leading to the 'snapshot' time, τ_{snapshot}, and possible inelasticity corrections (discussed in section 3.1).

The structure of a monatomic sample can be described in real space (figure 3) in terms of its *pair-distribution function* $g(\boldsymbol{r})$ which is proportional to the probability of finding an atom at a position $\boldsymbol{r}$ relative to a reference atom taken to be at the origin. The functions $S(\boldsymbol{q})$ and $g(\boldsymbol{r})$ are related by the Fourier transforms:

$$S(\boldsymbol{q}) - 1 = \rho_o \int [g(\boldsymbol{r}) - 1]\, \mathrm{e}^{\mathrm{i}\boldsymbol{q}\cdot\boldsymbol{r}}\, \mathrm{d}\boldsymbol{r} \tag{2.20}$$

and

$$g(\boldsymbol{r}) - 1 = \frac{1}{\rho_o (2\pi)^3} \int [S(\boldsymbol{q}) - 1]\, \mathrm{e}^{-\mathrm{i}\boldsymbol{q}\cdot\boldsymbol{r}}\, \mathrm{d}\boldsymbol{q}, \tag{2.21}$$

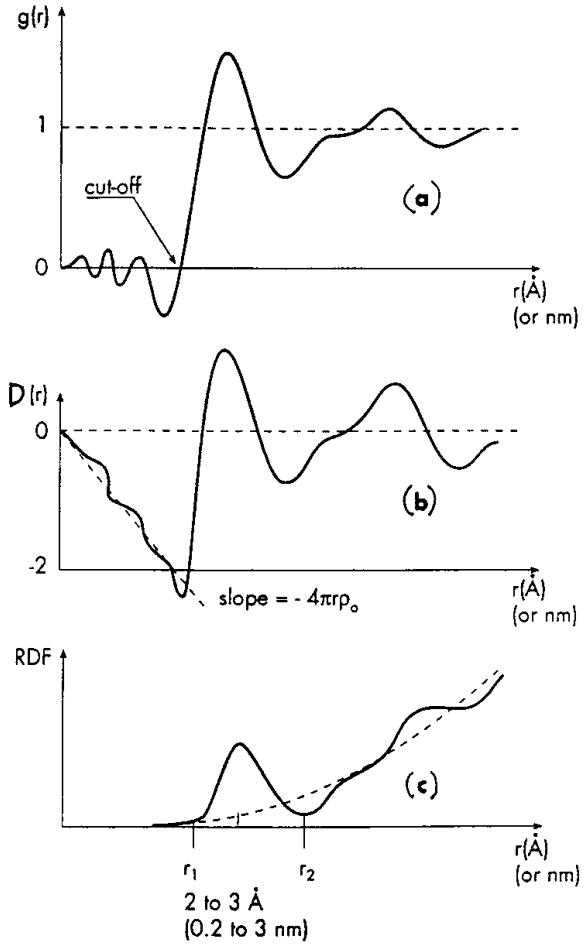

Figure 3. Real-space functions for a monatomic liquid or glass: (*a*) pair-distribution function $g(r)$, (*b*) density function $D(r)$ and (*c*) radial distribution function RDF(r). The 'cut-off' in (*a*) refers to a possible truncation point for performing a back-Fourier transformation to test the self-consistency of a measured data set. Figure after Chieux (1993).

where ρ_o is the atomic number density. By construction, $g(\boldsymbol{r})$ is dimensionless. The '-1' term in the integrand of equation (2.20) represents the subtraction of the forward scattering at $\boldsymbol{q} = 0$ since

$$\rho_o \int \mathrm{e}^{\mathrm{i}\boldsymbol{q}\cdot\boldsymbol{r}}\,\mathrm{d}\boldsymbol{r} = \rho_o V \delta_{\boldsymbol{q},0} = N\delta_{\boldsymbol{q},0}, \tag{2.22}$$

where V is the volume of the sample and $\delta_{\boldsymbol{q},0}$ is the Kronecker delta which has the property $\delta_{\boldsymbol{q},0} = 1$ when $\boldsymbol{q} = 0$ and $\delta_{\boldsymbol{q},0} = 0$ when $\boldsymbol{q} \neq 0$. As discussed for equation (2.18), the '-1' term in the integrand of equation (2.21) represents, in turn, the subtraction of the coherent self-scattering so that the Fourier transform is taken of only the distinct part $H(\boldsymbol{q}) = S(\boldsymbol{q}) - 1$ of the diffractogram. We will see later that this remains the case for a polyatomic sample.

In the case of a liquid or glass sample for which the average structure is isotropic, only the vector norms $r = |\boldsymbol{r}|$ and $q = |\boldsymbol{q}|$ are relevant. By averaging over the relative orientations of $\boldsymbol{r}$ and $\boldsymbol{q}$, the exponential terms in equations (2.13), (2.20) and (2.21) can be written as

zeroth-order spherical-Bessel functions (Debye 1915) thereby simplifying the expression for the static structure factor:

$$S(q) = 1 + \frac{1}{N}\left\langle \sum_{i,j\neq i}^{N} \frac{\sin(qr_{ij})}{(qr_{ij})} \right\rangle, \tag{2.23}$$

as well as the expressions for the Fourier transforms:

$$S(q) - 1 = \frac{4\pi\rho_o}{q}\int_0^\infty r[g(r) - 1]\sin(qr)\,\mathrm{d}r \tag{2.24}$$

and

$$g(r) - 1 = \frac{1}{2\pi^2 r\rho_o}\int_0^\infty q[S(q) - 1]\sin(qr)\,\mathrm{d}q, \tag{2.25}$$

whence $S(q \to \infty) = 1$ and $g(r \to \infty) = 1$. In a real diffraction experiment for a liquid or glass sample, this orientational average is obtained from the sum of diffraction contributions of different coherence volumes within the sample. For a monatomic system one also defines the *density function* $D(r)$ as

$$D(r) \stackrel{\text{def}}{=} 4\pi r\rho_o[g(r) - 1] = \frac{2}{\pi}\int_0^\infty q[S(q) - 1]\sin(qr)\,\mathrm{d}q, \tag{2.26}$$

whose slope at small r is proportional to ρ_o since $g(r)$ is exactly zero for r-values below a certain minimum interatomic distance. The *radial distribution function* RDF(r), given by

$$\mathrm{RDF}(r) \stackrel{\text{def}}{=} 4\pi r^2\rho_o\, g(r), \tag{2.27}$$

can be integrated to obtain the average number of neighbouring atoms in a coordination shell:

$$\overline{n} = \int_{r_1}^{r_2} \mathrm{RDF}(r)\,\mathrm{d}r = 4\pi\rho_o\int_{r_1}^{r_2} g(r)r^2\,\mathrm{d}r, \tag{2.28}$$

where r_1 and r_2 are the distances corresponding, for example, to consecutive minima in $g(r)$—the deeper the minima, the more robust the delimitation of atomic shells. The average number of atoms in the first (i.e. innermost) shell is often called the *coordination number*. It should be noted that there is often some confusion about the meaning of the coordination number. Firstly, it does not mean that every atom in the structure has this number of atoms around it; the coordination number is an *average*—hence it is quite reasonable to have a non-integral number. Secondly, the definition of the limits of the first shell in equation (2.28) is somewhat arbitrary and various methods for quoting coordination numbers are often used, e.g. integrating to the first minimum in $g(r)$, fitting and integrating peaks in $g(r)$ (see, e.g. Pings (1968)).

In practice, the finite maximum q-value that is accessible in diffraction experiments, $q_{\max}$, leads to peak broadening in real space after Fourier transformation as well as to non-physical oscillations in $g(r)$ and in other r-space functions. Such 'truncation ripples' can be reduced via prudent modulation of the experimental $S(q)$ by a damping function before Fourier transformation (e.g. Lorch (1969)), being equivalent to a coarsening of the r-space resolution. Alternatively, the step-function describing the experimental q-range, $M(q \leqslant q_{\max}) = 1$, $M(q > q_{\max}) = 0$, can be Fourier-transformed to produce the r-space modification function

$$M(r) = \frac{1}{\pi}\int_0^{q_{\max}} \cos(qr)\,\mathrm{d}q \tag{2.29}$$

with which theoretical r-space functions should be convolved before comparison or fitting to Fourier-transformed diffraction data (e.g. Petri *et al* (2000), Waser and Schomaker (1953)). For example, the modified pair-distribution function becomes

$$rg'(r) = rg(r) \otimes M(r), \tag{2.30}$$

where $\otimes$ denotes the one-dimensional convolution operator. A minimum noise procedure has also been developed to estimate uncertainties in $g(r)$ resulting from the Fourier transformation of measured $S(q)$ (Soper *et al* 1993). Limitations associated with the Fourier transformation (or inversion) of diffraction data have also been discussed by Leadbetter and Wright (1972b) and by Waser and Schomaker (1953).

It should also be mentioned that coherent diffraction techniques, such as variable coherence electron diffraction (Gibson and Treacy 1997, Treacy and Gibson 1996) and other fluctuation microscopy techniques (see review by Treacy *et al* (2005)), can give information about higher-order (3- and 4-body) distribution/correlation functions that are relevant to medium range order in glasses. See also Soper (2001), Evans (1990) and Schofield (1968) for a discussion of higher-order correlation functions relevant to diffraction.

Finally, there is a useful thermodynamic limit for the static structure factor of a monatomic system:

$$S(0) = \rho_o \chi_T k_B T, \tag{2.31}$$

where χ_T is the isothermal compressibility, k_B the Boltzmann constant and T the absolute temperature. In the case of an ideal (monatomic) gas, the pressure $P = \rho_o k_B T$ and $\chi_T = 1/P$, so that $S(0) = 1$. For a (monatomic) liquid having larger ρ_o but much smaller χ_T, we have $S(0) < 1$ except for state points close to the liquid/gas critical point.

2.3. *The case of a polyatomic system*

In a monatomic system all the atoms are chemically identical, and we can normally assume that there is no correlation between scattering length and atomic position in the sample. This assumption allowed the derivation of equation (2.18) which we used to define a dimensionless structure factor $S(q)$ having a simple thermodynamic limit. For a polyatomic system, we can still assume a random assignment of (neutron) scattering lengths over the sites occupied by a given chemical species α (having atomic number Z_α), but different α have different isotopes and therefore different scattering length distributions for neutron diffraction and, of course, different x-ray scattering lengths that depend on Z_α. Different chemical species also have different interatomic interactions (chemical bonding) and so do not in general occupy each other's sites. Therefore, a polyatomic system will usually have an overall correlation between scattering length and atomic position in the sample. This correlation prevents, except for special cases, the definition of a single dimensionless structure factor for a polyatomic system; instead we are obliged to consider several *partial* structure factors.

We can however generalize equation (2.14) to a system of n chemical species, again separating 'distinct' and 'self' terms:

$$\frac{1}{N}\left[\frac{\mathrm{d}\sigma}{\mathrm{d}\Omega}(q)\right] = F(q) + \sum_{\alpha}^{n} c_\alpha \overline{b_\alpha^2}, \tag{2.32}$$

where $F(q)$ is the *total interference function* and c_α is the concentration of chemical species α (such that $\sum_\alpha^n c_\alpha = 1$). The second term of equation (2.32) is therefore the mean of the scattering length squared of each chemical species as averaged over the entire sample:

$$\sum_{\alpha}^{n} c_\alpha \overline{b_\alpha^2} = \overline{b^2} \qquad \text{where } \overline{b_\alpha^2} = b_{\mathrm{coh},\alpha}^2 + b_{\mathrm{incoh},\alpha}^2. \tag{2.33}$$

Since for a polyatomic system we are generally interested in describing the distribution of one chemical species around another, it is convenient to choose the convention of

Faber and Ziman (1965) for defining *partial structure factors* $S_{\alpha\beta}(q)$ by decomposing $F(q)$ in the following manner:

$$F(q) \overset{\text{def}}{=} \sum_{\alpha,\beta}^{n} c_\alpha c_\beta \overline{b}_\alpha \overline{b}^*_\beta [S_{\alpha\beta}(q) - 1], \tag{2.34}$$

where each $S_{\alpha\beta}(q)$ is a function that is dependent only on the distribution of α atoms around β atoms (or vice-versa). It should be noted that a different definition for partial structure factors due to Ashcroft and Langreth (1967) is also commonly used, especially in papers on theory and computer simulation. The relationship between the Ashcroft–Langreth, $S^{\text{AL}}_{\alpha\beta}(q)$, and Faber–Ziman, $S_{\alpha\beta}(q)$, partial structure factors is given by (e.g. Cusack (1987) section 3.12)

$$S^{\text{AL}}_{\alpha\beta}(q) = \delta_{\alpha\beta} + (c_\alpha c_\beta)^{1/2}[S_{\alpha\beta}(q) - 1], \tag{2.35}$$

where $\delta_{\alpha\beta}$ is the Kronecker delta. In this review we shall mostly confine ourselves to the Faber–Ziman (FZ) description, which had in fact been proposed earlier by Fournet (1957).

As mentioned earlier, the complex conjugate ($\overline{b}^*_\beta$) is rarely necessary for neutron diffraction, and the averaging bars ($\overline{b}_\alpha$) are superfluous for x-ray diffraction. However, the scattering lengths for the latter have significant dependences on both q and incident energy E_o that will be considered later.

By analogy with equation (2.23), the FZ partial structure factors for an isotropic system can be written as

$$S_{\alpha\beta}(q) = S_{\beta\alpha}(q) = 1 + \frac{1}{c_\alpha c_\beta N}\left\langle \sum_{i,j\neq i}^{N_\alpha, N_\beta} \frac{\sin(qr_{ij})}{(qr_{ij})} \right\rangle, \tag{2.36}$$

where $N_\alpha = c_\alpha N$ is the number of α atoms and i and j refer to sites among the α and β atoms, respectively. Evidently the equivalence of sites $i = j$ is only possible within a single chemical species (i.e. for $\alpha = \beta$). Fourier transformation of the $S_{\alpha\beta}(q)$ leads to the *partial pair-distribution functions* $g_{\alpha\beta}(r)$:

$$S_{\alpha\beta}(q) - 1 = \frac{4\pi\rho_o}{q}\int_0^\infty r[g_{\alpha\beta}(r) - 1]\sin(qr)\,\mathrm{d}r, \tag{2.37}$$

$$g_{\alpha\beta}(r) - 1 = \frac{1}{2\pi^2 r\rho_o}\int_0^\infty q[S_{\alpha\beta}(q) - 1]\sin(qr)\,\mathrm{d}q, \tag{2.38}$$

where ρ_o is still the total number density of atoms. Note that $S_{\alpha\beta}(q \to \infty) = 1$ for all α, β in analogy to the $S(q)$ of a monatomic system. The $g_{\alpha\beta}(r)$ are a measure of the probability of finding a β atom at a distance r from an α atom (e.g. Fournet (1957) p 317). More precisely, the *partial coordination number* $\overline{n}^\beta_\alpha$ (i.e. the average number of β atoms in a spherical shell around an α atom) is found through integration of a partial radial distribution function:

$$\overline{n}^\beta_\alpha = 4\pi\rho_o c_\beta \int_{r_1}^{r_2} g_{\alpha\beta}(r) r^2\,\mathrm{d}r. \tag{2.39}$$

A Fourier transform of $F(q)$ defines the *total pair-correlation function* $G(r)$ as

$$\begin{aligned} G(r) &\overset{\text{def}}{=} \frac{1}{2\pi^2 r\rho_o}\int_0^\infty qF(q)\sin(qr)\,\mathrm{d}q \\ &\overset{\text{N}}{=} \sum_{\alpha,\beta}^{n} c_\alpha c_\beta \overline{b}_\alpha \overline{b}^*_\beta [g_{\alpha\beta}(r) - 1], \end{aligned} \tag{2.40}$$

which is a simple weighted sum of the $g_{\alpha\beta}(r)$ only in the case of neutron 'N' diffraction for which the scattering lengths are q-independent.

For neutron and x-ray diffraction studies of glasses, one often defines the *total correlation function* $T(r)$ as

$$T(r) \stackrel{\text{def}}{=} 4\pi r\rho_o \left[G(r) + \sum_{\alpha,\beta}^{n} c_\alpha c_\beta \bar{b}_\alpha \bar{b}_\beta^* \right], \tag{2.41}$$

where

$$\sum_{\alpha,\beta}^{n} c_\alpha c_\beta \bar{b}_\alpha \bar{b}_\beta^* = \left| \sum_{\alpha}^{n} c_\alpha \bar{b}_\alpha \right|^2 = \bar{b}^2 \tag{2.42}$$

and $\bar{b} = \sum_\alpha^n c_\alpha \bar{b}_\alpha$ is the mean scattering length as averaged over the entire sample. The $T(r)$ function is theoretically zero below a certain minimum distance between atoms and has the advantage of peaks that are *symmetrically* broadened by a finite $q_{\max}$ (Wright 1980). It also leads directly to a *total radial distribution function* $R(r)$ via

$$R(r) \stackrel{\text{def}}{=} rT(r). \tag{2.43}$$

In practice, experimental results for diffraction by (especially polyatomic) liquids and glasses should be compared with theory/simulation in *both* r-space and q-space, as well as with results from other experimental techniques, so as to fully appreciate the significance of single features such as a 'first sharp diffraction peak' (FSDP) (see, e.g. Salmon (1994)).

Note that we are following the convention of Enderby (1993) and others who reserve the symbols S [i.e. $S(q)$, $S_{\alpha\beta}(q)$] and g [i.e. $g(r)$, $g_{\alpha\beta}(r)$] as well as $H(q)$ and $D(r)$ for monatomic systems or partial functions and employ the symbols F [i.e. $F(q)$, $\Delta_x F(q)$] and G [i.e. $G(r)$, $\Delta_x G(r)$] as well as $T(r)$ for polyatomic systems. Some researchers define $H_{\alpha\beta}(q) \stackrel{\text{def}}{=} S_{\alpha\beta}(q) - 1$ for convenience (e.g. Soper and Luzar (1992)) while others use $A_{\alpha\beta}(q)$ instead of $S_{\alpha\beta}(q)$ to denote the Faber–Ziman (FZ) partial structure factors. A review of different types of notation for these and other functions is given by Keen (2001).

By taking the limit as $r \to 0$ in equation (2.38) we obtain a sum-rule that can be useful for checking the normalization of partial structure factors (Norman 1957, Krogh-Moe 1956):

$$\int_0^\infty q^2[S_{\alpha\beta}(q) - 1]\,\mathrm{d}q = -2\pi^2\rho_o, \tag{2.44}$$

where ρ_o is again the total atomic number density. As seen from equation (2.25), this sum-rule also holds for a monatomic system, where $S(q)$ replaces $S_{\alpha\beta}(q)$.

Bhatia and Thornton (1970) define for a binary system an alternative set of partial structure factors, $S_{NN}(q)$, $S_{CC}(q)$ and $S_{NC}(q)$, describing, respectively, the distributions of atomic number density, of concentration and the correlation between the two. The measured total interference function $F(q)$ can be expressed in terms of Bhatia–Thornton (BT) partial structure factors as

$$F(q) = |\langle b\rangle|^2 S_{NN}(q) + |\bar{b}_1 - \bar{b}_2|^2 S_{CC}(q) + [\langle b\rangle(\bar{b}_1^* - \bar{b}_2^*) + \langle b\rangle^*(\bar{b}_1 - \bar{b}_2)]S_{NC}(q) - (c_1\bar{b}_1^2 + c_2\bar{b}_2^2), \tag{2.45}$$

where c_1 and c_2 are the atomic concentrations and $\langle b\rangle = c_1\bar{b}_1 + c_2\bar{b}_2$ is the overall average scattering length. Fourier transformation leads to the BT partial pair-distribution functions $g_{NN}(r)$, $g_{CC}(r)$ and $g_{NC}(r)$.

The Bhatia–Thornton and Faber–Ziman formalisms are connected by simple linear combinations involving only the concentrations c_1 and c_2 of the two species

(e.g. Cusack (1987)):

$$\begin{aligned} S_{NN}(q) &= c_1^2 S_{11}(q) + c_2^2 S_{22}(q) + 2c_1c_2S_{12}(q), \\ S_{CC}(q) &= c_1c_2[1 + c_1c_2(S_{11}(q) + S_{22}(q) - 2S_{12}(q))], \\ S_{NC}(q) &= c_1c_2[c_1(S_{11}(q) - S_{12}(q)) - c_2(S_{22}(q) - S_{12}(q))], \end{aligned} \tag{2.46}$$

where the coefficients differ slightly from those for the r-space functions:

$$\begin{aligned} g_{NN}(r) &= c_1^2 g_{11}(r) + c_2^2 g_{22}(r) + 2c_1c_2g_{12}(r), \\ g_{CC}(r) &= c_1c_2[g_{11}(r) + g_{22}(r) - 2g_{12}(r)], \\ g_{NC}(r) &= c_1[g_{11}(r) - g_{12}(r)] - c_2\,[g_{22}(r) - g_{12}(r)]. \end{aligned} \tag{2.47}$$

The number–number partial structure factor, $S_{NN}(q)$, concerns the sites of all the scattering nuclei without regard to the chemical species decorating those sites and therefore represents the 'colour-blind' scattering cross-section, i.e. $S_{NN}(q)$ would be measured directly if both chemical species had the same average (i.e. coherent) scattering length. The concentration–concentration partial structure factor, $S_{CC}(q)$, describes the ordering of the two chemical species with respect to the sites specified by $S_{NN}(q)$. When there is a preference for like or unlike neighbours at a given distance, corresponding positive or negative peaks will appear in $g_{CC}(r)$, respectively. For an ideal (solid or liquid) solution, in which the two chemical species mix randomly without volume change or heat of mixing, all three FZ partial structure factors are equal and hence $S_{CC}(q) = c_1c_2$, i.e. constant. Conversely, any q-dependence in $S_{CC}(q)$ indicates non-ideal substitution between the two species. Note that if the sample is a 'zero alloy', having $\langle b \rangle = 0$, then $S_{CC}(q)$ is measured directly in a diffraction experiment. The real-space counterpart of $S_{NC}(q)$, namely $g_{NC}(r)$, describes the correlation between sites and their occupancy by a given chemical species. If the sample is an ideal solution then there is no correlation between site and chemical species, so that $S_{NC}(q) = 0$ and therefore all q-dependence in $F(q)$ (and hence all structural information) is contained in $S_{NN}(q)$. Salmon (1992) gives a thorough discussion of Bhatia–Thornton partial structure factors for 2 : 1 binary systems MX_2. The Bhatia–Thornton (1970) structure factors in the $q \to 0$ limit are more directly expressed in terms of thermodynamic quantities than are those of Faber–Ziman (1965), and their general behaviour at low-q can be usefully related to the moments of the corresponding partial pair-distribution functions (Salmon 2005). In addition, the fact that the measured intensity in a diffraction experiment is positive or zero provides numerical limits on the BT partial structure factors, namely $S_{NN}(q) \geqslant 0$, $S_{CC}(q) \geqslant 0$ and $S_{NN}(q)S_{CC}(q) \geqslant S_{NC}^2(q)$ (Bhatia and Thorton 1970). Equivalent expressions for the Faber–Ziman partial structure factors are given by Enderby *et al* (1966).

2.4. *The case of a molecular liquid or gas*

For a molecular liquid of N_{mol} molecules containing m atoms per molecule, either of the same or different chemical species, the total differential scattering cross-section in the static approximation can again be separated into incoherent and coherent terms:

$$\left[\frac{\mathrm{d}\sigma}{\mathrm{d}\Omega}(q)\right] = \left[\frac{\mathrm{d}\sigma}{\mathrm{d}\Omega}(q)\right]^{\mathrm{incoh}} + \left[\frac{\mathrm{d}\sigma}{\mathrm{d}\Omega}(q)\right]^{\mathrm{coh}} \tag{2.48}$$

where $[\mathrm{d}\sigma/\mathrm{d}\Omega(q)]^{\mathrm{incoh}} = N_{\mathrm{mol}} \sum_i^m b_{\mathrm{incoh},i}^2$, the index i refers to sites on the same molecule and $b_{\mathrm{incoh},i}$ is the incoherent scattering length of the chemical species at site i (recall that $b_{\mathrm{incoh},i} = 0$ in the case of x-ray diffraction). It is then convenient to further separate the coherent term

into its contributions from self, intramolecular and intermolecular terms (e.g. Bertagnolli *et al* (1976)):

$$\left[\frac{\mathrm{d}\sigma}{\mathrm{d}\Omega}(q)\right]^{\mathrm{coh}} = \left[\frac{\mathrm{d}\sigma}{\mathrm{d}\Omega}(q)\right]^{\mathrm{coh}}_{\mathrm{self}} + \left[\frac{\mathrm{d}\sigma}{\mathrm{d}\Omega}(q)\right]^{\mathrm{coh}}_{\mathrm{intra}} + \left[\frac{\mathrm{d}\sigma}{\mathrm{d}\Omega}(q)\right]^{\mathrm{coh}}_{\mathrm{inter}} \tag{2.49}$$

where $[\mathrm{d}\sigma/\mathrm{d}\Omega(q)]^{\mathrm{coh}}_{\mathrm{self}} = N_{\mathrm{mol}} \sum_i^m \overline{b_i^2}$ and $\overline{b}_i$ is the coherent scattering length of the chemical species at site i. If the mean relative positions of the atoms in a molecule remain the same (e.g. there are no internal rotations) and the vibrational motion can be approximated as being harmonic then provided the liquid is isotropic,

$$\left[\frac{\mathrm{d}\sigma}{\mathrm{d}\Omega}(q)\right]^{\mathrm{coh}}_{\mathrm{intra}} = N_{\mathrm{mol}} \sum_{i,j\neq i}^{m} \overline{b}_i \overline{b}_j^* \frac{\sin(qr_{ij})}{(qr_{ij})} \mathrm{e}^{-\langle \delta r_{ij}^2 \rangle q^2/2}, \tag{2.50}$$

where i and j refer to sites on the same molecule, for which r_{ij} is the modulus of their mean separation, and in the Debye–Waller term $\langle \delta r_{ij}^2 \rangle = \langle u_i^2 \rangle + \langle u_j^2 \rangle$ where $\langle u_i^2 \rangle$ is one component of the mean squared vibrational amplitude for the atom at site i. The intermolecular term, for an isotropic liquid, is then

$$\left[\frac{\mathrm{d}\sigma}{\mathrm{d}\Omega}(q)\right]^{\mathrm{coh}}_{\mathrm{inter}} = \left\langle \sum_{y,z\neq y}^{N_{\mathrm{mol}}} \sum_{k,l}^{m} \overline{b}_k \overline{b}_l^* \frac{\sin(qr_{kylz})}{(qr_{kylz})} \right\rangle, \tag{2.51}$$

where k and l refer to sites on different molecules y and z, respectively, for which $r_{kylz} = |\boldsymbol{r}_{ky} - \boldsymbol{r}_{lz}|$ is their separation. Note that the intramolecular and intermolecular differential scattering cross-sections contain no self-scattering terms.

Since the molecular structure is usually known and not sought in the experiment, in general the incoherent, coherent, self and intramolecular terms can be calculated or fitted and then subtracted from the total differential scattering cross-section, leaving the intermolecular term which can be written as a linear combination of partial intermolecular structure factors $S^{\mathrm{inter}}_{\alpha\beta}(q)$:

$$\frac{1}{N}\left[\frac{\mathrm{d}\sigma}{\mathrm{d}\Omega}(q)\right]^{\mathrm{coh}}_{\mathrm{inter}} = \sum_{\alpha,\beta}^{n} c_\alpha c_\beta \overline{b}_\alpha \overline{b}_\beta^* [S^{\mathrm{inter}}_{\alpha\beta}(q) - 1], \tag{2.52}$$

where $N = mN_{\mathrm{mol}}$ is the total number of atoms and n the number of chemical species. Each $S^{\mathrm{inter}}_{\alpha\beta}(q)$ thus involves correlations only between α and β atoms on different molecules—useful for e.g. isolating solvent-solute structures.

It is often useful to consider the correlations between the centres of different molecules which we define by vectors $\boldsymbol{R}_{cy}$ and $\boldsymbol{R}_{cz}$. Following Page (1972), Egelstaff *et al* (1971) and Zachariasen (1935), we can then write the coherent differential scattering cross-section as

$$\left[\frac{\mathrm{d}\sigma}{\mathrm{d}\Omega}(q)\right]^{\mathrm{coh}} = N_{\mathrm{mol}} \left| \sum_i^m \overline{b}_i \right|^2 S_{\mathrm{mol}}(q), \tag{2.53}$$

where the structure factor for the molecular assembly is defined by

$$S_{\mathrm{mol}}(q) \overset{\mathrm{def}}{=} f_1(q) + \frac{1}{N_{\mathrm{mol}}} \left\langle \sum_{y,z\neq y}^{N_{\mathrm{mol}}} \mathrm{e}^{-\mathrm{i}\boldsymbol{q}\cdot(\boldsymbol{R}_{cy}-\boldsymbol{R}_{cz})} \right\rangle f_2(q), \tag{2.54}$$

and it is assumed, in deducing the second term, that the orientation of molecule y relative to molecule z is statistically independent of their relative separation (Gray and Gubbins (1984) give useful expressions for the case of relative orientations being correlated with molecular

separation). The *intra*molecular form factor $f_1(q)$ characterises the scattering from a single molecule and is given by

$$f_1(q) = \frac{1}{N_{\rm mol}\left|\sum_i^m \overline{b}_i\right|^2}\left(\left[\frac{{\rm d}\sigma}{{\rm d}\Omega}(q)\right]_{\rm self}^{\rm coh} + \left[\frac{{\rm d}\sigma}{{\rm d}\Omega}(q)\right]_{\rm intra}^{\rm coh}\right), \tag{2.55}$$

where the r_{ij} in equation (2.50) still refer to the relative separation of sites within the same molecule. For an isotropic liquid, the *inter*molecular form factor $f_2(q)$, which includes orientational correlations between molecules, becomes

$$f_2(q) = \frac{1}{\left|\sum_i^m \overline{b}_i\right|^2}\left\langle\sum_{k,l}^m \overline{b}_k\overline{b}_l^*\frac{\sin(qr'_{kylz})}{(qr'_{kylz})}\right\rangle, \tag{2.56}$$

where $r'_{kylz} = |\boldsymbol{r}'_{ky} - \boldsymbol{r}'_{lz}|$ and $\boldsymbol{r}'_{ky} \equiv \boldsymbol{r}_{ky} - \boldsymbol{R}_{cy}$, $\boldsymbol{r}'_{lz} \equiv \boldsymbol{r}_{lz} - \boldsymbol{R}_{cz}$ are the coordinates of atom k in molecule y and of atom l in molecule $z \neq y$ defined relative to their respective molecular centres. In the limit as $q \to 0$, we see that $f_1(q) \to 1$ and $f_2(q) \to 1$ such that

$$S_{\rm mol}(q) = 1 + \frac{1}{N_{\rm mol}}\left\langle\sum_{y,z\neq y}^{N_{\rm mol}} {\rm e}^{-{\rm i}\boldsymbol{q}\cdot(\boldsymbol{R}_{cy}-\boldsymbol{R}_{cz})}\right\rangle. \tag{2.57}$$

Comparison with equations (2.13) and (2.17) shows that the structure factor $S_{\rm mol}(q)$ becomes equivalent to that for a liquid of 'super-atoms', each having a coherent scattering length of $\overline{b}_{\rm mol} \stackrel{\rm def}{=} \sum_i^m \overline{b}_i$. We can thereby regain the thermodynamic limit of equation (2.31) for a molecular liquid:

$$\frac{1}{N_{\rm mol}\overline{b}_{\rm mol}^2}\left[\frac{{\rm d}\sigma}{{\rm d}\Omega}(q \to 0)\right]^{\rm coh} = \rho_{\rm mol}\chi_T k_B T, \tag{2.58}$$

where $\rho_{\rm mol} = \rho_o/m$ is the number density of molecules. In the case of an ideal gas, $\chi_T^{-1} = P = \rho_{\rm mol}k_B T$ such that χ_T is increased by a factor of m for a molecular gas as compared with an atomic gas having the same total atomic density ρ_o and temperature T.

The above formulae are similar to those presented by, e.g. Powles (1973) and can be generalized to mixtures of molecular liquids (e.g. Pfleiderer *et al* (2001), Bowron *et al* (1998a), Soper and Luzar (1992)) as well as adapted to the case of ions in aqueous solution (e.g. Bruni *et al* (2001), Enderby and Gullidge (1987), Enderby and Neilson (1981), Soper *et al* (1977)).

3. Neutron diffraction by liquids and glasses

Some of the earliest neutron diffraction studies of liquids were carried out by Chamberlain (1950) on molten sulfur, lead and bismuth, followed by Henshaw *et al* (1953) on liquid nitrogen, oxygen and argon and by Sharrah and Smith (1953) on molten lead and bismuth at two temperatures. North *et al* (1968) reviewed the method of obtaining structure factors from neutron diffraction and presented experimental results for some liquid metals, while Enderby (1968) discussed other neutron scattering studies on liquids. Page (1973) gives an early pedagogical presentation of the neutron diffraction technique as applied to liquids. As concerns glasses, Breen *et al* (1957) performed variable-wavelength total neutron scattering experiments on vitreous silica and compared their radial distribution functions with those obtained from x-ray diffraction measurements. More accurate results were obtained using conventional neutron diffraction methods by Lorch (1969) on vitreous germania and silica, by Leadbetter and Wright (1972a) on BeF_2 and other binary glasses and by Hansen *et al* (1975) on amorphous selenium. Wright (1974) and Wright and Leadbetter (1976) give early reviews of studies of glass structure using methods that include neutron diffraction.

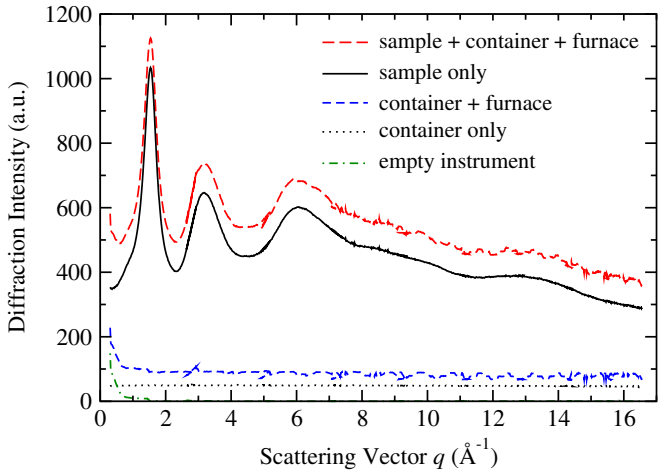

Figure 4. Measured diffraction intensities (diffractograms) for a typical neutron diffraction experiment on a liquid sample at a reactor source (D4c diffractometer at ILL). From top to bottom: sample in its container and sample environment, the final sample diffractogram after proper subtraction of the other intensities, the sample environment and empty sample container, the sample container after proper subtraction of the sample environment, and the background counts of the empty instrument. For clarity, the diffractogram of the empty sample environment (i.e. no sample nor container) is not shown.

3.1. Data treatment for neutron diffraction

To obtain a sample's $d\sigma/d\Omega$ from a real neutron diffraction experiment, it is of course necessary to subtract the diffraction intensities coming from the sample container, the sample environment (e.g. furnace, cryostat) and the background (arising from neutrons and electronic noise). Therefore, separate diffractograms are necessary for the sample in its container in the sample environment, the empty container (i.e. no sample) with sample environment, the empty environment (i.e. no container nor sample) and the background or empty instrument (see figure 4). In subtracting these intensities, account must be made of attenuation (from absorption and scattering) and multiple scattering, which originate not only from the sample environment but also from the sample itself. In other words, we now need to go beyond the 'small sample limit' wherein the mean free path of a neutron is very much larger than the linear dimensions of the sample so that virtually all the incident neutrons pass undisturbed through the sample (e.g. Sears (1978, 1975)). Furthermore, use of the static approximation means that inelasticity corrections to the measured diffraction intensity are generally required and are particularly large when the sample contains light atoms. A practical summary of the data treatment and corrections for neutron scattering by liquids is given by Egelstaff (1987). The basics for the case of a reactor source experiment are discussed by Johnson *et al* (1983), while Salmon *et al* (2004) offer a more recent summary for reactor–source data, including a comparison between different inelasticity corrections as well as a deconvolution procedure to take into account the q-space resolution function.

Our brief review of neutron diffraction data analysis is somewhat general but more pertinent to reactor sources. At pulsed sources, additional complications arise because of the distribution of incident wavelengths and the need to combine data accurately from different detector banks, each requiring different corrections, into a single diffractogram $d\sigma/d\Omega$ as a function of q. For more information on experimental technique and data treatment

for neutron diffraction at pulsed sources, the reader is referred to Postorino *et al* (1994) (molecular liquids), Soper and Luzar (1992) (mixtures of molecular liquids), Grimley *et al* (1990) (glasses), Soper (1990) (maximum entropy method), Hannon *et al* (1990) (general), Howe *et al* (1989) (liquids), Carpenter (1985) (glasses), Windsor (1981) (general), as well as internal reports/publications of the ISIS pulsed neutron facility (UK): Hannon *et al* (2005), Soper *et al* (2000) and Benmore and Soper (1998). Bermejo *et al* (1989) have made a useful and critical comparison of the measured static structure factor, $S(q)$, of a liquid as measured by diffraction at reactor and pulsed sources.

The normalization of a sample's diffraction intensity to an absolute cross-section can be effected via a comparison with the measured intensity of a different sample of known scattering cross-section, whose volume in the beam is known with respect to the sample's. In general vanadium is used as a normalization standard because its accurately known cross-section is almost completely incoherent and therefore isotropic and easily quantified even for pulsed neutron sources (see Mayers (1984) for theoretical calculations). Lack of a vanadium or other standard may necessitate an 'auto-normalization' of $\mathrm{d}\sigma/\mathrm{d}\Omega$ by aligning the self-scattering with the theoretical value for the sample's composition. Additional checks on normalization can be effected by, for example, the use of a sum-rule as in equation (2.44) for $S(q)$ or $S_{\alpha\beta}(q)$ after corrections for attenuation, multiple scattering and inelasticity have been made.

Attenuation corrections (resulting from both absorption and scattering, i.e. the total cross-section) have been treated by Paalman and Pings (1962) for the case of a completely and uniformly illuminated sample of cylindrical geometry in an annular container, being a simple but common sample configuration (the work was extended to incomplete illumination by Kendig and Pings (1965) and by Soper and Egelstaff (1980)). They provide coefficients, dependent on scattering angle, that permit the proper subtraction of the empty-container diffractogram taking into account the attenuation of the sample and its container (e.g. Salmon (1988) for a thorough application). Their method can be simply extended to other sample and container geometries (e.g. Mitchell *et al* (1976)). However, these results presuppose that each neutron contributing to the diffractogram is scattered only once, thereby ignoring the effects of multiple scattering. Numerical solutions for multiple scattering corrections, based on quadrature (e.g. Soper (1983), Soper and Egelstaff (1980), Blech and Averbach (1965)), generally assume that a neutron undergoes one or more scattering events in the sample, where each individual scattering event is both elastic and isotropic. These corrections are complicated and highly dependent on sample and sample environment geometries. Monte Carlo simulations have also been used for complex sample environments (e.g. Bausenwein *et al* (1991), Poncet (1978)), but their precision has in general been limited by simulation counting statistics.

For high-precision or small-sample experiments, the background diffraction intensities (e.g. from sample environment and empty instrument) must be carefully subtracted. By replacing the sample under study by a nearly perfectly absorbing specimen of like dimensions (e.g. cadmium or $^{10}B_4C$), one can separate the sample-attenuated and non-attenuated background intensities, to which different coefficients can be applied during subtraction (e.g. Bertagnolli *et al* (1976)).

The inelasticity correction has been treated by Placzek (1952) and others (see Salmon *et al* (2004) for a comparison of different methods). As mentioned earlier, an inelasticity correction becomes necessary when the energy exchange, $\hbar\omega$, between the neutron and the sample becomes comparable to the incident energy E_o, leading to a breakdown of the static approximation. An additional consequence is that, for a given λ_o, loci of equal 2θ in the detector plane no longer correspond well to loci of equal q, as the scattering angle depends not only on q but also on $\hbar\omega$ (e.g. Yarnell *et al* (1973), appendix A). The integral of equation (2.7) is, therefore, no longer performed at constant q, as required for the static approximation.

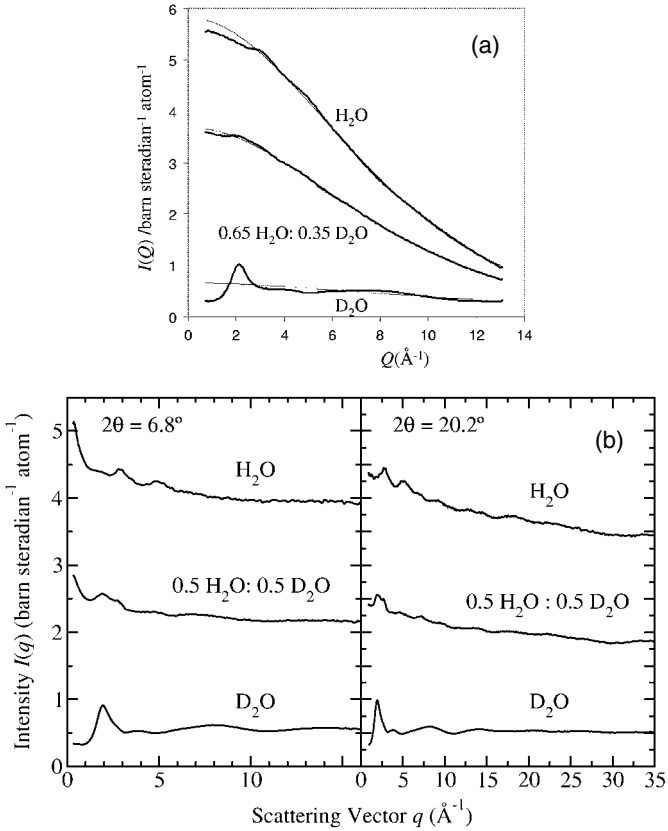

Figure 5. Measured diffraction intensities, $I(q)$, comparing inelasticity effects for liquid samples containing light atoms: (*a*) 2 molal solutions of $NiCl_2$ in light water, 'null' water or heavy water as measured using the D20 diffractometer at the ILL (reactor source) by Powell *et al* (1989)—figure reproduced with permission from IOP Publishing Limited (Bristol); (*b*) light water, heavy water or a 1 : 1 mixture at 25 °C as measured at two different scattering angles, 2θ, using the SANDALS instrument at ISIS (pulsed neutron source) by Soper (2005a). The inelasticity effects are represented by (*a*) smooth fitted lines or (*b*) data sets that have a slope at smaller q-values that becomes more significant with decreasing nuclear mass. In (*b*) the data sets at fixed 2θ-values cover different q-ranges since $q = 4\pi \sin\theta/\lambda_o$ equation (2.10) and the range of incident neutron wavelengths is fixed. Also, at a given 2θ-value, smaller incident neutron energies correspond to smaller q-values and hence larger inelasticity effects. Note that the general slope on the $2\theta = 20.2^\circ$ data at large q-values is a consequence of a detector deadtime artefact which is most prevalent for strongly scattering samples.

In general, only the self part of the differential scattering cross-section is appreciably affected by inelasticity. For neutron diffraction from reactor sources, the self-scattering 'falls off' with increasing q, as shown in figure 5(*a*)—intuitively, one can think of the nuclear scattering length passing from the 'bound' to the 'free' value with increasing scattering angle at a given wavelength, since the atom receives an increasing 'jolt' of momentum transfer from the neutron (Soper *et al* (1977) appendix, Powles (1973)). Except for the lightest atoms, the correction for reactor sources can be expressed in the form

$$\left[\frac{d\sigma}{d\Omega}(q)\right]^{\text{self}}_{\text{measured}} = \left[\frac{d\sigma}{d\Omega}(q)\right]^{\text{self}}_{\text{corrected}} [1 + P(q)], \tag{3.1}$$

where $P(q)$ is a polynomial expansion in powers of q^2 and the ratio m_n/M_α of the neutron's mass to that of atoms in the sample. In practice, it is therefore oftentimes a simple matter of subtracting a polynomial in q^2 from the measured $\mathrm{d}\sigma/\mathrm{d}\Omega$ to obtain directly the distinct part after normalization. It should be noted that the function $P(q)$ needs to be calculated for each instrument used as it depends on the precise details of the detector efficiency. Yarnell *et al* (1973) provide convenient formulae for calculating the coefficients of the polynomial.

A neutron striking an atom of small mass will transfer more energy, making the static approximation less valid. The 'Placzek falloff' with increasing q (for a reactor source) is steeper and of greater magnitude for light atoms. For H and other very light atoms, there is in fact no suitable polynomial in q^2 that can be used to correct the data for inelasticity effects. In this case several heuristic schemes for 'fitting' the Placzek falloff have been used for reactor-source data. For example, a linear combination of a Lorentzian function and a Gaussian function of equal full-width at half-maximum or FWHM (i.e. a pseudo-voigt function) fits well the intensity falloff (as a function of q and not 2θ) for H concentrations greater than about 20 at.% (e.g. Fischer (1997) pp 73–4 and figure 5(*a*) for H_2O).

The inelasticity effects on the distinct part of $\mathrm{d}\sigma/\mathrm{d}\Omega$ are generally much weaker than for the self part (e.g. Soper *et al* (1977) appendix). The physical intuition is that the momentum transfer of the neutron, $\hbar\boldsymbol{q}$, is not localized to a single atom, as in isotropic self-scattering, but to all the atoms in its coherence volume (of size increasing with the tightness of the collimation and the fineness of the wavelength resolution). Therefore, not only is the inelastic 'shock' more distributed but the atoms tend to move together so that their relative distances, seen in the distinct term of $\mathrm{d}\sigma/\mathrm{d}\Omega$, are less distorted. In spite of the effect being weaker, an inelasticty correction to the distinct term, often imprecisely referred to as the coherent scattering term, should in principle still be applied. Again the inelastic effects are expected to be larger for spatial correlations between light atoms and may produce inaccurate distances in the $g(r)$ obtained by Fourier transformation. However, in order to correct the distinct part for inelasticity effects, a complete description of the response, i.e. $S(q,\omega)$, is needed, leading to supplementary inelastic scattering experiments and an iterative solution at best. Certain aspects of inelasticity corrections for neutron scattering by molecular fluids are discussed in a recent review by Guarini (2003)—see also Egelstaff and Soper (1980a, 1980b) and Powles (1973).

Inelasticity effects are generally weaker for diffraction measurements at pulsed neutron sources due to higher incident energies, provided the diffraction patterns are measured at small scattering angles, and occur principally at low q-values in the diffractogram (thus weakening the effect on the Fourier transform), but the effects are more difficult to parametrize than for reactor sources. For information on inelasticity corrections for pulsed-source diffraction data, the reader is referred to, for example, Grimley *et al* (1990), Howe *et al* (1989) or the 'ATLAS manual' (Soper *et al* 2000). The SANDALS instrument (Soper 1989) at the ISIS pulsed neutron source (UK) was designed to minimize inelasticity corrections through small-angle detection of high-energy neutrons, while maintaining a high maximum q-value for good resolution in r-space. Figure 5(*b*) shows an example of the effects of inelasticity on a diffractogram measured by SANDALS.

Finally, although neutron absorption resonances are rare at diffraction wavelengths (Sinclair 1993), the scattering length $b = b' + \mathrm{i}b''$ generally shows strong variation at such resonances, as a function of incident neutron wavelength. Figure 6 shows this variation for the case of ^{113}Cd. For pulsed-source neutron diffractometers a broad range of incident wavelengths is used, so that absorption resonances must either be avoided (by excluding certain isotopes in the sample) or taken into account as accurately as possible.

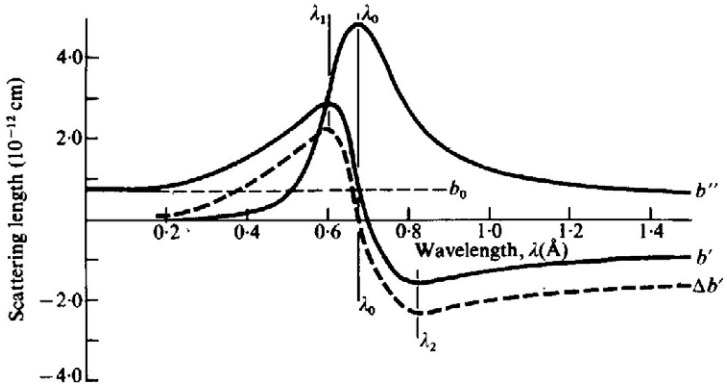

Figure 6. Variation of the real and imaginary parts b', b'' of the neutron scattering length of ^{113}Cd, as a function of incident wavelength, near the absorption resonance occurring at $\lambda_o = 0.68$ Å. Note that b_o is the limiting value of b' for zero wavelength and $\Delta b' = b' - b_o$. Figure from Bacon (1975) and reproduced by permission of Oxford University Press.

3.2. *Neutron diffraction with isotopic substitution (NDIS)*

In order to determine experimentally the partial structure factors $S_{\alpha\beta}(q)$ (and therefore the $g_{\alpha\beta}(r)$ by Fourier transformation) from measurements of the differential scattering cross-section $\mathrm{d}\sigma/\mathrm{d}\Omega$ for a polyatomic system, one can use the technique of neutron diffraction with isotopic substitution (NDIS). The pioneering NDIS experiment was performed by Enderby *et al* (1966) who determined the partial structure factors of liquid Cu_6Sn_5. The method was then applied to molten CuCl in the study by Page and Mika (1971). A later NDIS study by Edwards *et al* (1975) on molten NaCl used a more sophisticated data analysis technique that was discussed in detail. Better values for the Cl scattering lengths were incorporated into later studies by Eisenberg *et al* (1982) on molten CuCl and by Biggin and Enderby (1982) on molten NaCl. Enderby *et al* (1973) discussed the feasibility of doing NDIS on aqueous solutions, where the partial structure factors of water can dominate even when D_2O is used, and then Soper *et al* (1977) applied the technique to ionic solutions in heavy water. McGreevy and Mitchell (1982) have discussed and compared different self-consistent methods for smoothing/fitting the partial structure factors obtained by NDIS.

As described by Chieux (1993, 1978), Page (1973) and others, the NDIS technique consists of measuring $\mathrm{d}\sigma/\mathrm{d}\Omega$ and hence $F(q)$ for several samples of identical structure and chemical composition (i.e. the same c_α) but having different isotopic compositions for one or more of the species α (of atomic number Z_α):

$$F_i(q) = \sum_{\alpha,\beta}^{n} c_\alpha c_\beta \bar{b}_{\alpha i} \bar{b}_{\beta i} [S_{\alpha\beta}(q) - 1], \tag{3.2}$$

where $\bar{b}_{\alpha i}$ is the average scattering length of the α atoms in sample i (in this subsection we will assume for simplicity that all scattering lengths are real-valued—see, e.g. Sears (1992) for a table).

A sample of n chemical species has $m = n(n+1)/2$ independent partial structure factors, requiring m samples of differing isotopic composition for a complete determination of the $S_{\alpha\beta}(q)$ (Price and Pasquarello (1999) give a detailed analysis of this requirement). Therefore, equation (3.2) is generally expressed in matrix form which in the case of a binary system,

having two species x and y, becomes

$$\begin{bmatrix} F_1(q) \\ F_2(q) \\ F_3(q) \end{bmatrix} = \begin{bmatrix} c_x^2\bar{b}_{x1}^2 & c_y^2\bar{b}_{y1}^2 & 2c_xc_y\bar{b}_{x1}\bar{b}_{y1} \\ c_x^2\bar{b}_{x2}^2 & c_y^2\bar{b}_{y2}^2 & 2c_xc_y\bar{b}_{x2}\bar{b}_{y2} \\ c_x^2\bar{b}_{x3}^2 & c_y^2\bar{b}_{y3}^2 & 2c_xc_y\bar{b}_{x3}\bar{b}_{y3} \end{bmatrix} \begin{bmatrix} S_{xx}(q) - 1 \\ S_{yy}(q) - 1 \\ S_{xy}(q) - 1 \end{bmatrix} \equiv \begin{bmatrix} a_{11} & a_{12} & a_{13} \\ a_{21} & a_{22} & a_{23} \\ a_{31} & a_{32} & a_{33} \end{bmatrix} \begin{bmatrix} S_{xx}(q) - 1 \\ S_{yy}(q) - 1 \\ S_{xy}(q) - 1 \end{bmatrix}, \tag{3.3}$$

that is,

$$[F(q)] = [A][S(q) - 1], \tag{3.4}$$

which can be inverted to solve for the partial structure factors $S_{\alpha\beta}(q)$:

$$[S(q) - 1] = [A]^{-1}[F(q)]. \tag{3.5}$$

The determinant $|A|_n$, normalized by dividing each row i of $[A]$ by $(\sum_j a_{ij}^2)^{1/2}$, is a measure of the conditioning of the matrix (Westlake 1968), i.e. of the robustness in the determination of the $S_{\alpha\beta}(q)$, resulting from the scattering length 'contrast' between the $F_i(q)$. Although $|A|_n = 1$ is the ideal case, values less than 0.1 are in general encountered in NDIS experiments. It is observed that $|A|_n$ is oftentimes a rough indication of the maximum fractional statistical uncertainty permissible for each measured diffractogram if statistically significant partial structure factors are to be obtained.

It can also be convenient to display the matrix using another normalization, obtained by dividing each row i of the original matrix by $\sum_j a_{ij}$, which ensures that the sum of the coefficients of the partial structure factors is unity for each $F_i(q)$, that is $\sum_j a_{ij} = 1$. This is equivalent to dividing each $F_i(q)$ by the square of its overall average scattering length $\langle b_i\rangle^2 = \sum_{\alpha,\beta}^n c_\alpha c_\beta \bar{b}_{\alpha i}\bar{b}_{\beta i} = (\sum_\alpha^n c_\alpha \bar{b}_{\alpha i})^2$, e.g. in the case of a binary system $\langle b_i\rangle^2 = (c_x\bar{b}_{xi} + c_y\bar{b}_{yi})^2$.

When a NDIS matrix is very poorly conditioned, i.e. almost singular, it is preferable to make an analysis using the technique of singular value decomposition (SVD) (Press *et al* (1999) pp 59–70). The advantage of this numerical technique is that one obtains the relative error and its sign (+/−) for each of the $n(n + 1)/2$ partial structure factors, $S_{\alpha\beta}(q)$. For example, one might find that a positive error in $S_{\alpha\alpha}(q)$ produces a negative error in $S_{\alpha\beta}(q)$ (for $\alpha \neq \beta$). The absolute errors can then be obtained for each partial structure factor via an analysis of the 'Turing number', a method that is well explained by Ludwig *et al* (1987c).

As NDIS experiments generally last several days, it is important to have very good stability in the detectors and sample environment, and this can be monitored by dividing or subtracting diffractograms from successive time segments of a long acquisition (e.g. Jal *et al* (1990)). The D4c neutron diffractometer (Fischer *et al* 2002, 1998) at the Institut Laue-Langevin (ILL) has been optimized for high-accuracy measurements (minimization of both random and systematic errors) on liquids and glasses and is particularly useful for isotopic substitution experiments (see also Cuello *et al* (2005), Cicognani (2005)). Since the differences between the $F_i(q)$ diffractograms are at times less than 1%, it is necessary to control very precisely the production of the NDIS samples to assure that their structures are identical, and difficulty therein arises because of the high price and small quantities of available isotopes.

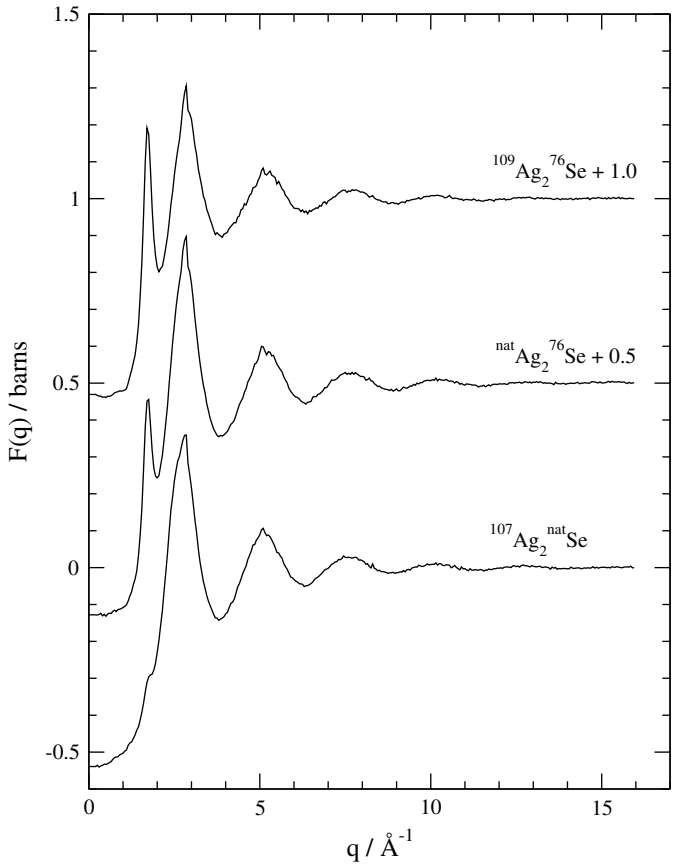

Figure 7. Neutron diffraction data for liquid Ag_2Se samples of three different isotopic compositions ('nat' = natural composition), shown as total interference functions $F(q)$—i.e. as $d\sigma/d\Omega$ per atom after subtraction of the self-scattering. Figure from Barnes *et al* (1997) and reproduced with permission from IOP Publishing Limited (Bristol).

NDIS experiments involving substitution on both chemical species in binary systems have been carried out, among others, by Penfold and Salmon (1991) on liquid $GeSe_2$, by Barnes *et al* (1997) on liquid Ag_2Se and by Salmon and Petri (2003) on glassy $GeSe_2$. Figures 7, 8 and 9 show the results of the Ag_2Se study (D4b instrument at ILL), for which the normalized determinant was $|A|_n = 0.029$, and illustrate the quality of partial structure factors that can be obtained in a careful NDIS experiment. It is important to note that in modern neutron diffraction experiments it is usual to obtain the full set of $S_{\alpha\beta}(q)$ directly from the measured total interference functions by the application of equation (3.5), i.e. additional constraints (see, e.g. Edwards *et al* (1975)) are not applied. The efficacy of the procedure is then rigorously tested—see, e.g. Salmon and Petri (2003) for a recent discussion.

When it is not possible to perform a sufficient number of NDIS experiments to resolve the matrix for all the partial structure factors, some information can still be gained from a limited number of experiments (e.g. Enderby *et al* (1973)). In the case of only two experiments wherein the isotopic composition of only one chemical species x is varied, a simple subtraction of the measured $F_i(q)$ for samples 1 and 2 leads to a *first-difference* function

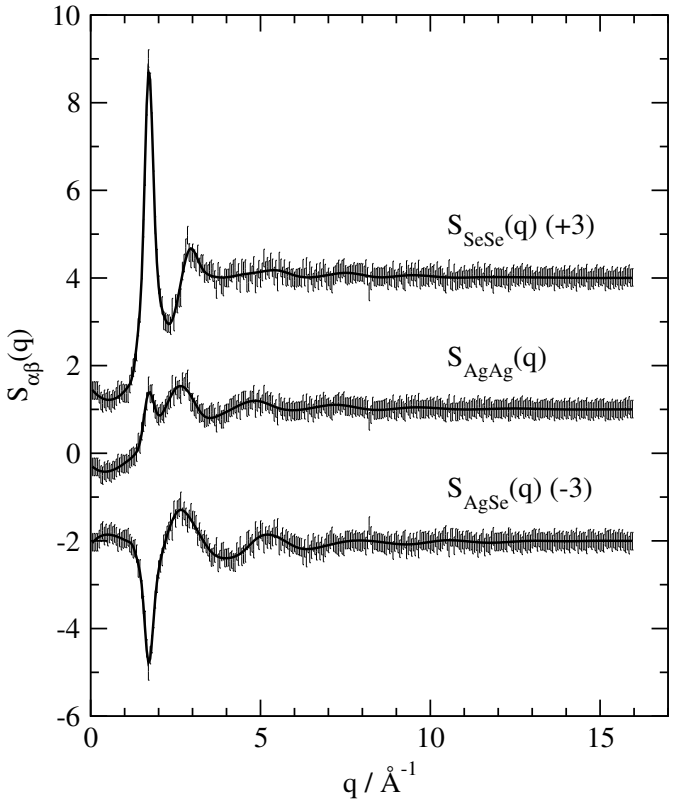

Figure 8. Partial structure factors $S_{\alpha\beta}(q)$ for liquid Ag_2Se obtained via NDIS, from the data of figure 7 (Barnes *et al* 1997). Figure reproduced with permission from IOP Publishing Limited (Bristol).

(e.g. Eckersley *et al* (1988), Soper *et al* (1977)):

$$\Delta_{x\{1-2\}}F(q) \stackrel{\text{def}}{=} F_1(q) - F_2(q)$$

$$= c_x^2(\overline{b}_{x1}^2 - \overline{b}_{x2}^2)[S_{xx}(q) - 1] + \sum_{\alpha\neq x}^{n} 2c_\alpha c_x \overline{b}_\alpha(\overline{b}_{x1} - \overline{b}_{x2})[S_{\alpha x}(q) - 1], \qquad (3.6)$$

which contains only the partial structure factors involving atoms of chemical species x. Alternatively, it is clear from equation (2.34) that a weighted subtraction of the two measured $F_i(q)$ can be used to eliminate any single partial structure factor, such as $S_{xx}(q)$ or $S_{xy}(q)$. In addition, a weighted subtraction of a first-difference function $\Delta_x F(q)$ from one of the measured (total) $F_i(q)$ eliminates all partial structure factors involving x except $S_{xx}(q)$. Such first-difference techniques can be useful for the study of, for example, modified network glasses having three or more chemical species (Penfold and Salmon 1990). The relevant equations, allowing for complex-valued scattering lengths, are given by Wasse *et al* (2000a).

Even complex systems such as clays are amenable to accurate NDIS studies (e.g. Powell *et al* (1998)). Very dilute systems are also accessible if the scattering length contrast is sufficiently high, as is the case for Ar dissolved in water where the substitution ^{36}Ar/^{nat}Ar has been used (Sullivan *et al* 2001). The first-difference study by Wasse *et al* (2000b) on Li

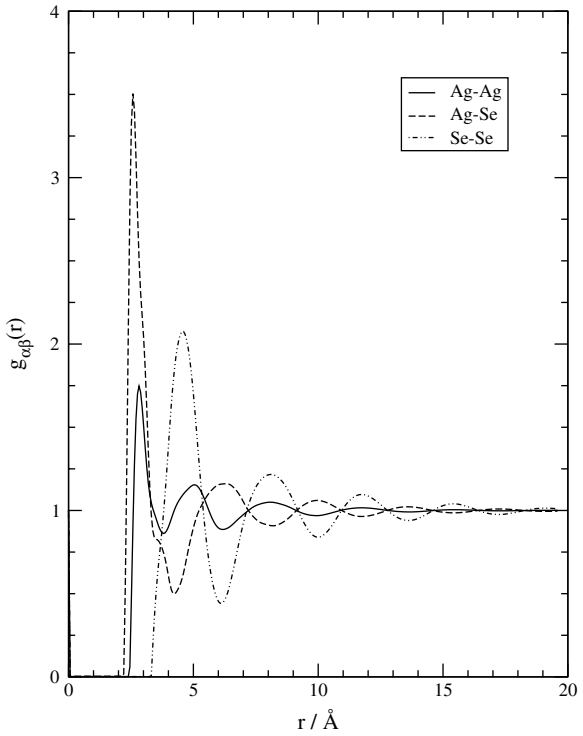

Figure 9. Partial pair-distribution functions $g_{\alpha\beta}(r)$ for liquid Ag_2Se obtained via NDIS, resulting from Fourier transformation of the partial structure factors of figure 8 (Barnes *et al* 1997). Figure reproduced with permission from IOP Publishing Limited (Bristol).

dissolved in ammonia is interesting in that the isotopic substitution was performed on all three chemical species: H, Li and N.

By analogy with equation (2.40), we can Fourier transform $\Delta_x F(q)$ to obtain the first-difference function for samples 1 and 2 of the total pair-correlation function:

$$\Delta_{x\{1-2\}}G(r) \stackrel{\text{def}}{=} \frac{1}{2\pi^2 r\rho_o}\int_0^\infty q\,\Delta_{x\{1-2\}}F(q)\sin(qr)\,\mathrm{d}q$$

$$= c_x^2(\bar{b}_{x1}^2 - \bar{b}_{x2}^2)[g_{xx}(r) - 1] + \sum_{\alpha\neq x}^{n} 2c_\alpha c_x \bar{b}_\alpha(\bar{b}_{x1} - \bar{b}_{x2})[g_{\alpha x}(r) - 1] \qquad (3.7)$$

$$= G_1(r) - G_2(r).$$

For a liquid or glass having $n > 2$ chemical species, it is nevertheless possible to use a series of only 3 NDIS experiments to determine the partial structure factor $S_{xx}(q)$ corresponding to one of the species x, through the technique of *double-difference* also called the *second-difference* (e.g. Salmon *et al* (1998), Gaskell *et al* (1991), Enderby and Neilson (1981)). In this procedure, only $\bar{b}_x$ is varied among the 3 samples via isotopic substitution of x atoms. A weighted subtraction of two first-difference functions leads to

$$\Delta_x^2 F(q) \stackrel{\text{def}}{=} (\bar{b}_{x2} - \bar{b}_{x3})[\Delta_{x\{1-2\}}F(q)] - (\bar{b}_{x1} - \bar{b}_{x2})[\Delta_{x\{2-3\}}F(q)]$$

$$= c_x^2[(\bar{b}_{x2} - \bar{b}_{x3})(\bar{b}_{x1}^2 - \bar{b}_{x2}^2) - (\bar{b}_{x1} - \bar{b}_{x2})(\bar{b}_{x2}^2 - \bar{b}_{x3}^2)][S_{xx}(q) - 1], \qquad (3.8)$$

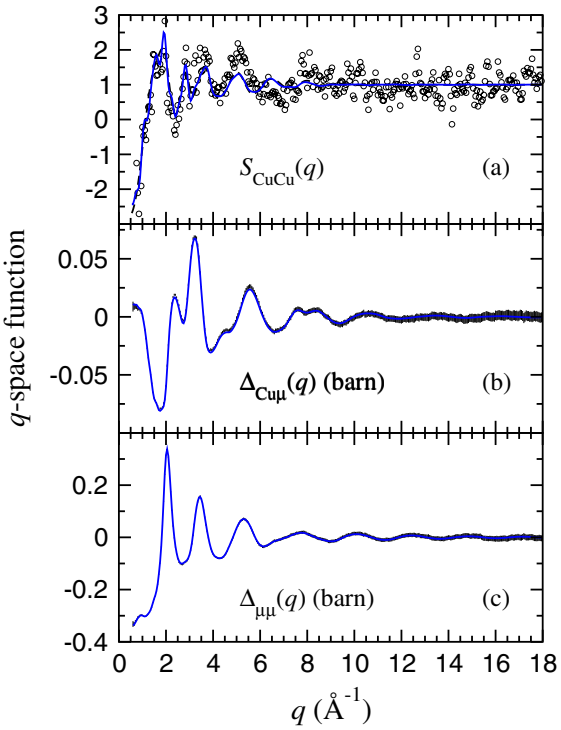

Figure 10. The partial structure factor $S_{\mathrm{CuCu}}(q)$ and the difference functions $\Delta_{\mathrm{Cu}\mu}(q)$ and $\Delta_{\mu\mu}(q)$ for the four component chalcohalide glass $(\mathrm{CuI})_{0.6}(\mathrm{Sb_2Se_3})_{0.4}$, where μ denotes a matrix atom (Sb, Se or I). In (*a*) the measured data points are represented by the circles, a spline fit to the data is given by the dashed curve and a so-called minimum noise (MIN) solution (Soper *et al* 1993) is given by the solid curve. In (*b*) and (*c*) the vertical bars represent the errors on the data points and the solid curves give the MIN solutions. Note that the total interference function measured in a single diffraction experiment has been resolved into its contributions from the Cu–Cu partial structure factor and the two difference functions $\Delta_{\mathrm{Cu}\mu}(q)$ and $\Delta_{\mu\mu}(q)$ that describe either the Cu–μ or μ–μ correlations alone (see Salmon and Xin (2002)).

which can be solved for $S_{xx}(q)$. The latter can then be used, along with the first-difference functions, to produce other difference functions which involve linear combinations of $S_{x\mu}(q)$ and $S_{\mu\mu}(q)$, where μ represents any type of atom other than x. In such a way 3 NDIS experiments, by substituting on a single element x, can produce 3 difference functions ($S_{xx}(q)$ and combinations of the $S_{x\mu}(q)$ or $S_{\mu\mu}(q)$) pertinent to structural studies of polyatomic systems such as glasses (e.g. Salmon and Xin (2002), Benmore and Salmon (1994)). The results that can be obtained are illustrated in figures 10 and 11 for the case of the chalcohalide glass $(\mathrm{CuI})_{0.6}(\mathrm{Sb_2Se_3})_{0.4}$ where only Cu was isotopically substituted.

If 4 NDIS experiments are made when $n > 2$, it is then possible to resolve for any partial structure factor $S_{xy}(q)$ (where $x \neq y$) by taking a (possibly weighted) difference of two first-difference functions, $\Delta_{x\{1-2\}}F(q)$ and $\Delta_{x\{3-4\}}F(q)$, thus producing a *second-difference* function, where samples 1 and 2 have a different isotopic composition for species y than do samples 3 and 4. For example, in the study of Pasquarello *et al* (2001) on the first solvation shell of the Cu(II) aqua ion, a first-difference function involving Cu isotopes was taken for each of the two aqueous solutions having different H/D ratios. These first-difference functions were then combined to obtain $g_{\mathrm{CuH}}(r)$. The results were compared with first-principles molecular dynamics simulations.

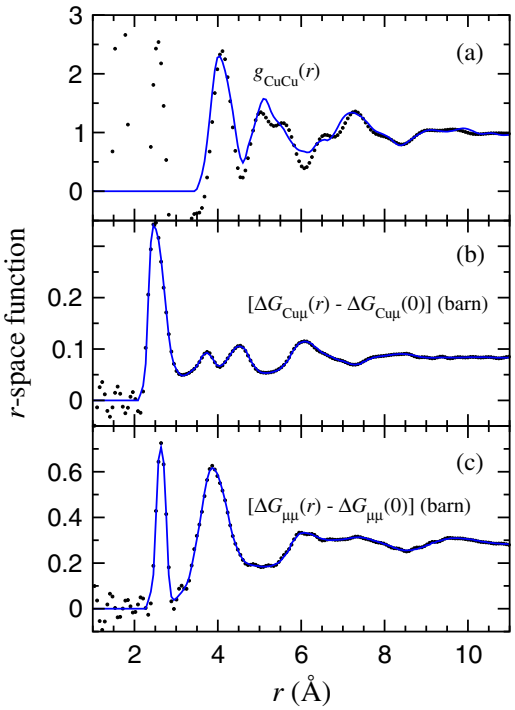

Figure 11. The partial pair-distribution function $g_{CuCu}(r)$ and the difference functions $\Delta G_{Cu\mu}(r)$ and $\Delta G_{\mu\mu}(r)$ for glassy $(CuI)_{0.6}(Sb_2Se_3)_{0.4}$ as obtained from the reciprocal space data sets of figure 10 (Salmon and Xin 2002). The solid curves represent the MIN solutions while the dotted curves represent the Fourier transforms of either (*a*) the spline fitted $S_{CuCu}(q)$ or (*b*) and (*c*) the raw reciprocal space data sets. The difference functions $\Delta G_{Cu\mu}(r)$ and $\Delta G_{\mu\mu}(r)$ describe either the Cu–μ or μ–μ correlations alone where μ denotes a matrix atom (Sb, Se or I). Figure after Salmon and Xin (2002).

All procedures for obtaining partial structure factors, $S_{\alpha\beta}(q)$, from NDIS experiments involve linear algebra. It should be recognized that these mathematical techniques are numerically unstable and that it is very easy, if care is not taken, to obtain misleading results. The SVD method discussed above (Press *et al* (1999) pp 59–70) is numerically stable and is also more general in application. For a system of equations (i.e. diffractograms) that is over-determined, SVD is formally equivalent to least-squares methods and will find the optimum solution with the minimum error. In addition, for an under-determined system (e.g. in the case of a double difference experiment), SVD produces the optimum solution for the sub-set of the $S_{\alpha\beta}(q)$ that can be obtained from the data as well as estimates of their errors, including the sign of the error. It is therefore practical to employ SVD regularly to obtain the partial structure factors from any set of diffractograms, irrespective of whether the system is over-determined (all partial structures factors can be obtained) or under-determined (a sub-set of partial structure factors can be obtained).

As certain elements (e.g. H, Ni, Cr, Dy) have isotopes that have both positive and negative scattering lengths, it is possible to create isotopic mixtures for which $\overline{b}_\alpha = b_{coh,\alpha} = 0$. In this case, for binary systems containing a 'zero' scattering element, the partial structure factor of the other element can be measured directly in a single diffraction experiment. Enderby and Barnes (1990) exploited the negative scattering length of ^{62}Ni to obtain a zero mixture of Ni isotopes in molten $NiSe_2$ and thereby obtained the Se–Se partial structure factor from

a single measurement. The '$b_{\mathrm{coh},\alpha} = 0$' technique has also been used to produce a 'double null' amorphous alloy Dy_7Ni_3 (Hannon *et al* 1991, Wright *et al* 1985) for which $\overline{b}_{\mathrm{Dy}} = 0$ and $\overline{b}_{\mathrm{Ni}} = 0$, i.e. the contribution to the diffractogram from nuclear correlations is removed, in order to observe the scattering from the magnetic correlations alone.

A null average coherent scattering length can also be achieved if two chemical species, one having a negative coherent scattering length and the other positive, are mixed such that $\langle b \rangle = c_1\overline{b}_1 + c_2\overline{b}_2 = 0$. Ideally, the two chemical species would occupy the same sites in the structure without any chemical correlation between those sites (i.e. the case of isomorphic substitution, which is discussed below). In the case of the Ti–Zr 'zero alloy' used as a sample container material in neutron scattering (e.g. for pressure cells), the substitution is not perfect (i.e. the measured $S_{CC}(q)$ has some q-dependence) but the coherent scattering (e.g. Bragg peaks) is greatly reduced.

In neutron diffraction experiments on aqueous solutions, it has been proved useful to use 'null water', consisting of approximately 2 parts H_2O and 1 part D_2O, for which the average coherent scattering length of the $Z = 1$ sites is zero. The neutrons then 'see' only the oxygen atoms of the water molecules—see, e.g. Powell *et al* (1989) for a study of $NiCl_2$ in aqueous solutions of D_2O, H_2O and null water. Note that the assumption is made that the H and D isotopes exchange (i.e. substitute for each other) freely and without correlation. If there was no exchange, the equilibrium concentration of HDO would be zero.

In general, hydrogen/deuterium or H/D substitution in neutron diffraction has become a valuable and widely used technique for probing the $Z = 1$ environments of organic liquids, especially at pulsed neutron sources where the inelasticity corrections can be made smaller (except at small q) using higher incident energies, as compared with reactor sources. Of course, care must be taken in H/D substitution experiments to know clearly the timescales of exchange or non-exchange, between the $Z = 1$ sites on all the molecules in the sample. Apart from questions of exchangeability at different sites, some recent studies have added qualifications (discussed below) to the assumption that the structure of organic liquids is not appreciably affected by deuteration. Since the structure of two classical systems of atoms interacting via the same potentials, and at the same temperature and atomic density, should not depend on the atomic masses (e.g. Egelstaff (1992) sections 5.3 and 8.4, Tomberli *et al* (2002, 2001c)), any additional effects on the structure coming from H/D substitution are referred to as 'quantum effects' or 'quantum isotope effects'.

An analysis of quantum effects in water has been made by comparing high-energy x-ray diffractograms of H_2O and D_2O for samples under ambient pressure and either at the same temperature or at the same atomic density (Hart *et al* 2005, Badyal *et al* 2002, Neuefeind *et al* 2002, Tomberli *et al* 2000). They have also been studied by comparing the x-ray diffractograms of D_2O at the same density but two different temperatures about the density maximum (Bosio *et al* 1983). All these experimental studies, supported by computer simulations (e.g. Kuharski and Rossky (1985)), find evidence for quantum isotope effects in water (e.g. coming from differences in ground-state motions for H and D), leading to differences in the structure factors at the level of about 1%. As these structure factor differences often resemble those produced by temperature differences, it has been suggested that H/D substitution experiments in neutron diffraction may be improved somewhat by using appropriately different temperatures for different isotopic samples (e.g. Tomberli *et al* (2002)).

In general, the large contrast in neutron scattering length between H and D leads to differences in NDIS diffractograms that are comfortably larger than those arising from isotope effects, especially if a temperature shift can be taken into account. Isotope effects in H/D substitution have also been studied for liquid hydrogen (Zoppi 2003), liquid methanol (Tomberli *et al* 2001a, 2001b, 2001c), liquid ethanol (Tomberli *et al* 2002), liquid benzene

(Benmore *et al* 2001) and low-density amorphous ice (LDA) (Urquidi *et al* 2003). A short review of quantum effects in hydrogenous liquids and glasses is given by Egelstaff (2002, 2003).

Apart from isotope effects, the measurement of (partial or total) structure factors for hydrogen-containing systems is nevertheless experimentally difficult due to large inelasticity effects and the large incoherent scattering from H in neutron diffraction and due to the low electron density around hydrogen sites in x-ray diffraction (see section 4). These difficulties are well illustrated in the case of water, where the partial structure factors determined via H/D substitution in neutron diffraction were the subject of much debate (see, e.g. Soper (2000) for a review), after some results showed discrepancies with certain computer simulations (Soper *et al* 1997, Soper 1997, 1996b).

When appropriate isotopes do not exist or are too expensive for an NDIS study, it is often possible to exploit the technique of *isomorphic* substitution, wherein similar chemical species are substituted, rather than the different isotopes of a given species. One chooses two species that are as chemically identical as possible, with nearly equivalent atomic radii, such that if a sample is prepared using a mixture of both species, they substitute freely for each other without chemical correlation. When appropriate samples can be reliably produced, and sufficient care is taken, the results of isomorphic substitution experiments can be comparable to those of NDIS, as illustrated by the study by Martin *et al* (2003a, 2003b). It is sometimes also possible to obtain partial structure factors in neutron diffraction by controlling the relative orientations of the atomic and neutron magnetic moments and thereby the total nuclear+magnetic scattering length, for example, using polarized neutron diffraction (Schweizer (1982), see Blétry and Sadoc (1975) for an application to amorphous $Co_{0.834}P_{0.166}$).

4. X-ray diffraction by liquids and glasses

The theoretical approach to x-ray diffraction by liquids and glasses was introduced and developed by Zernicke and Prins (1929, 1927) and by Debye and Menke (1930). Some of the earliest experiments performed on liquid water are reported by Bernal and Fowler (1933) who employed impressively modern techniques of data modelling and interpretation. An x-ray diffraction experiment on vitreous SiO_2 and GeO_2 was carried out by Warren (1934) using an 'evacuated camera' and monochromatic Cu K_α radiation. Gingrich (1943) gives an early but comprehensive review of x-ray diffraction by liquid elements. An accurate study of liquid structure factors by x-ray diffraction was carried out by Kaplow *et al* (1965) on liquid lead and mercury, and included a thorough discussion of the treatment of measurement errors. The structure of simple liquids by x-ray diffraction was also discussed early on by Pings (1968), while Narten and Levy (1971) made measurements on liquid water and, for example, Pálinkás *et al* (1980) on aqueous solutions. Early x-ray diffraction studies on polyatomic glasses, using Fourier transforms to obtain real-space functions, were performed by Leadbetter and Wright (1972c) on germania and other binary glasses and by Renninger and Averbach (1973) on As–Ge glasses. Both teams used data correction and analysis techniques developed principally by Warren and Mozzi (1970, 1966), Kaplow *et al* (1965) and Norman (1957). All these studies employed conventional 'tube' x-ray sources. Wright (1974) and Wright and Leadbetter (1976) gave early reviews of glass structure studies that include x-ray diffraction.

Since x-ray diffraction measurements on liquids and glasses involve relatively weak 'diffuse' scattering, the continued development of high-flux, high-energy synchrotron x-ray sources (Als-Nielsen and McMorrow 2001, Raoux 1993a) has significantly increased the possibilities for such studies. The BW5 beamline (Bouchard *et al* 1998) at HASYLAB in Hamburg exploits high-energy synchrotron x-rays to reduce absorption by the sample. Neuefeind (2002) has reviewed high-energy x-ray diffraction on liquid samples, while,

for example, Hoppe *et al* (2003) and Petkov *et al* (2000) present applications to glasses. The ID1 beamline (Lequien *et al* 1995) at the European Synchrotron Radiation Facility (ESRF) in Grenoble has been designed for anomalous x-ray diffraction (AXD), a technique discussed in section 4.2. Synchrotron x-ray sources are also extensively used when only small samples are available, e.g. liquid samples in pressure cells (Crichton *et al* 2001) or levitated aerodynamically (Krishnan and Price 2000).

The technique of extended x-ray absorption fine structure (EXAFS) spectroscopy has also benefitted from the high-resolution and variable energy range of synchrotron sources, and although it is not a diffraction technique, it is becoming increasingly useful for structure measurements (Gurman 1995), including liquids (Filipponi 2001). In general, EXAFS can provide satisfactory results for simple (e.g. monatomic) liquids and glasses and is a sensitive probe of small changes in structure (e.g. as a function of temperature). Diffraction techniques are, however, generally more accurate for complex disordered systems and provide a more extended r-range after Fourier transformation than does EXAFS.

4.1. Data treatment for x-ray diffraction

To obtain $\mathrm{d}\sigma/\mathrm{d}\Omega$ for a sample via x-ray diffraction, it is of course necessary to subtract the scattering contributions from the background and sample environment, which are generally larger than in the case of neutron diffraction, while taking into account very large attenuation corrections (due to high x-ray absorption) and also multiple scattering corrections (e.g. Fajardo *et al* (1998), Poulsen and Neuefeind (1995), Serimaa *et al* (1990)) that can be significant for light elements and for high incident x-ray energies. In general, the corrections and data analysis necessary to produce a proper $S(q)$ or $F(q)$ are more complicated and difficult for x-ray diffraction as compared with neutron diffraction. One advantage is, however, that the static approximation holds to a high degree of accuracy for x-ray diffraction, so no corresponding corrections to the data are necessary. For details on the treatment of data from conventional (tube source) x-ray diffraction studies of liquids and glasses, see for example Magini (1988), Hajdu and Pálinkás (1972), Warren and Mozzi (1970), Levy *et al* (1966) and Kaplow *et al* (1965). The experimental technique and data corrections for $S(q)$ measurements made using high-energy synchrotron x-rays ($\gtrsim$50 keV), which have some advantages over lower-energy x-rays, are discussed by Tomberli *et al* (2000), Weitkamp *et al* (2000) and Poulsen *et al* (1995).

As discussed in the introduction, the scattering lengths for atoms in x-ray diffraction are dependent on both the energy E_o of the incident photons (the so-called anomalous dispersion) and the magnitude of the scattering vector q (due to the finite size of the electron clouds). Recall that the effects of anomalous dispersion in neutron diffraction are more rare (Sinclair 1993, Cossy *et al* 1989). We adopt the convention of retaining the symbol b for scattering lengths (units of femtometre) and using f for form factors (units of number of electrons). In the case of x-rays, then, the atomic scattering length can be written as

$$b(q, E_o) = r_e f(q, E_o) = r_e[Z f_{\text{falloff}}(q) + f'(E_o) + \mathrm{i} f''(E_o)], \tag{4.1}$$

where $r_e = 2.818$ fm is the classical radius of the electron also known as the Thomson scattering length, $f(q, E_o)$ the atomic form factor, Z the atomic number, $f_{\text{falloff}}(q)$ the atomic form factor's modulation varying from 1 ($q = 0$) to 0 ($q = \infty$), and finally $f' = \Re(f_a)$ and $f'' = \Im(f_a)$ are the real and imaginary parts of the 'anomalous' term $f_a(E_o) = f'(E_o) + \mathrm{i} f''(E_o)$ of the atomic form factor (electron units). Since the anomalous term involves inner core electron clouds having small radii, its q-dependence is generally weak enough to be ignored. However, the variation of the anomalous term near an absorption edge is considerably dependent on the

chemical environment of the chemical species in question. In practice, f' is often determined by applying a Kramers-Kronig relation (Kubo and Ichimura 1972) to theoretically extrapolated absorption measurements (giving $f''(E_o)$) on the sample under study. Theoretical values of f' and f'' at different energies and for different chemical species are given by Chantler *et al* (2005), Gullikson (2001) and Chantler (2000, 1995). Atomic form factors are discussed by Kissel and Pratt (1990, 1985) and have been tabulated for the elements (both neutral atoms and chemically significant ions) by, for example, Maslen *et al* (1995 pp 476–505) and Hubbell *et al* (1975). Zhou *et al* (1992) treat in particular the detailed structure of f' resulting from near-edge structure in f'', and Kissel *et al* (1995) give a general assessment of certain theoretical approximations to atomic form factors. A basic discussion of atomic scattering factors, including numerical methods of calculation, is given by James (1962 chapter 3). Figure 12 shows how f' and f'' vary near the K-edge of a Se atom (i.e. the absorption edge for electrons in the K shell) and should be compared with figure 6 which shows an example of how the real and imaginary parts of the neutron scattering length vary near a neutron absorption resonance. Note that at x-ray energies far from an absorption edge, f'' is approximately proportional to $1/E_o^2$ or λ_o^2, and at a fixed wavelength it varies approximately as Z^4 across the periodic table (e.g. Als-Nielsen (1993)).

As compared with neutron scattering, x-ray scattering involves additional inelastic scattering and re-emission processes having significant cross-sections in the q-range of interest for diffraction, as illustrated in figure 13 for the case of carbon atoms. These processes include Compton scattering, fluorescence and resonant-Raman scattering, and they must be accurately subtracted from the measured total differential scattering cross-section to obtain the 'elastic' or Rayleigh–Thomson differential scattering cross-section pertinent to diffraction:

$$\left[\frac{\mathrm{d}\sigma}{\mathrm{d}\Omega}(q,E_o)\right]_{\mathrm{X}}^{\mathrm{total}} = \left[\frac{\mathrm{d}\sigma}{\mathrm{d}\Omega}(q,E_o)\right]_{\mathrm{X}}^{\mathrm{Ray-T}} + \left[\frac{\mathrm{d}\sigma}{\mathrm{d}\Omega}(q,E_o)\right]_{\mathrm{X}}^{\mathrm{fluo}} + \left[\frac{\mathrm{d}\sigma}{\mathrm{d}\Omega}(q,E_o)\right]_{\mathrm{X}}^{\mathrm{r-Raman}} + \left[\frac{\mathrm{d}\sigma}{\mathrm{d}\Omega}(q,E_o)\right]_{\mathrm{X}}^{\mathrm{Compton}} + \left[\frac{\mathrm{d}\sigma}{\mathrm{d}\Omega}(q,E_o)\right]_{\mathrm{X}}^{\mathrm{other}}, \tag{4.2}$$

where the 'other' processes are only relevant at very high incident x-ray energy, E_o, as shown in figure 13. Note that we show explicitly the q and E_o dependences of all the x-ray differential scattering cross-sections. The Rayleigh–Thomson or x-ray diffraction differential cross-section can then be written in the same way as in equation (2.32) for neutrons:

$$\frac{1}{N}\left[\frac{\mathrm{d}\sigma}{\mathrm{d}\Omega}(q,E_o)\right]_{\mathrm{X}}^{\mathrm{Ray-T}} = \tilde{F}(q,E_o) + \sum_{\alpha}^{n} c_\alpha \overline{b_\alpha(q,E_o) b_\alpha^*(q,E_o)} = \tilde{F}(q,E_o) + \overline{b(q,E_o)^2}, \tag{4.3}$$

where again the average runs over all atoms in the sample. By convention, a tilde is superposed for functions resulting from the use of x-ray rather than neutron scattering lengths. We remind the reader that for reasons of consistency with neutron diffraction, the terms in the above formulae have units of barn per steradian or femtometre squared per steradian (per atom), even though x-ray diffraction data are often quoted in electron units.

In the q-range appropriate to atomic-scale diffraction, the incident energy E_o of x-rays is very large compared with that of neutrons, so that only a small percentage of the former is exchanged with atomic displacement energies, $\hbar\omega$, in the sample. In addition, even when a crystal analyser is used, the energy resolution of detection is generally much broader than the maximum energy exchange, $\hbar\omega_{\max}$, so that the measured Rayleigh–Thomson

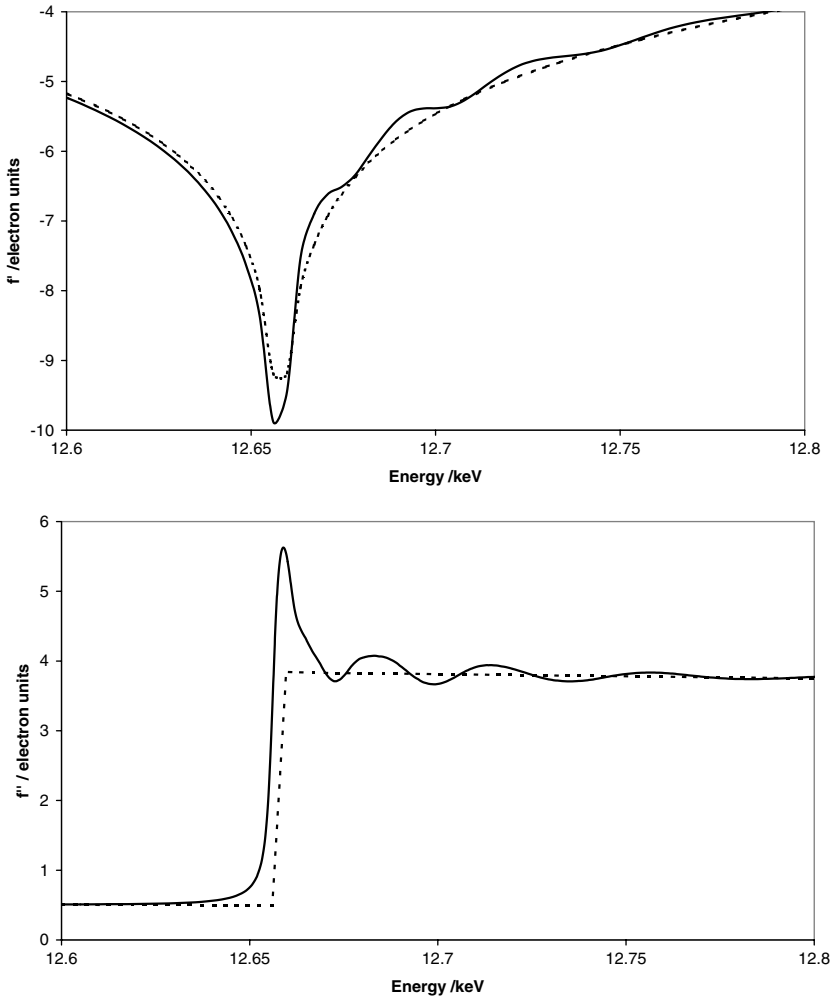

Figure 12. Variation of $f'(E_o)$ (upper curve) and of $f''(E_o)$ (lower curve) near the x-ray absorption K-edge of Se, in electron units. The solid lines represent measurements (Barnes 2005) and the dashed lines are theoretical calculations for an isolated atom that are consistent with the Kramers-Kronig relations (Creagh and McAuley 1995, Cromer and Liberman 1970). Note that the EXAFS oscillations in f'', which depend on the chemical environment of the Se atom, also have a manifestation on the high-energy side of the dip in f'.

differential cross-section effectively integrates $S(q, \omega)$ over all energy exchanges, assuring the validity of the static approximation and making the associated inelasticity corrections unnecessary.

For diffraction experiments at synchrotron sources, the nominal nearly complete horizontal polarization of the incident beam (e.g. Raoux (1993a) pp 58–63) permits polarization effects to be ignored in equation (4.3) for diffraction in a vertical scattering plane, as is commonly practiced. For an un-polarized incident beam, as from an x-ray tube source, the polarization factor (e.g. Cullity (1978))

$$P(\theta) = \frac{1 + \cos^2(2\theta)}{2} \tag{4.4}$$

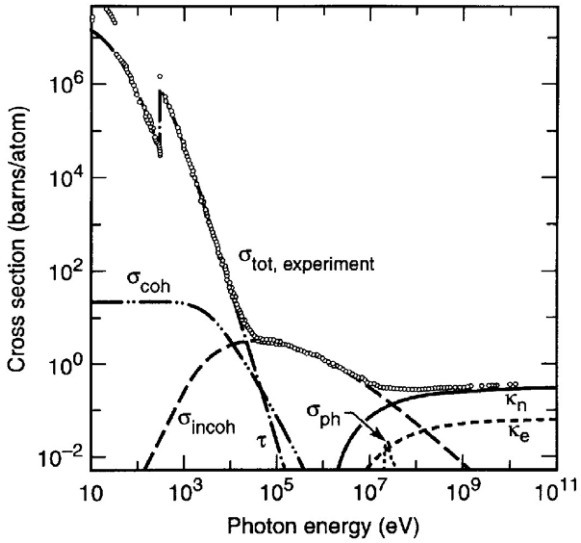

Figure 13. Photon scattering cross-sections for carbon as a function of incident energy, plotted on logarithmic axes. Here 'tot' is the total cross-section, 'coh' represents the Rayleigh–Thomson cross-section and 'incoh' the Compton scattering. The absorption cross-section τ includes fluorescence and resonant-Raman scattering and dominates for energies below 20 keV, above which Compton scattering dominates until 20 MeV. The K-edge absorption is visible at 284 eV. The cross-sections for photonuclear absorption (σ_{ph}) and for pair-production in nuclear (κ_n) and electron fields (κ_e) are significant only at very high energy. Figure from Kirz (2001).

must be taken into account when comparing measured and calculated x-ray diffraction intensities (recall in figure 1 that 2θ is the scattering angle with respect to the incident beam). A polarization correction must also be made for any diffracting element in the detector system (again usually not necessary for synchrotron sources). Dwiggins (1983) has made a general calculation of the polarization factor for any number of pre- and post-sample scatterers of any orientation, while Vincent (1982) considers several special cases, and Lawrence (1982) has analysed the case for a pyrolytic graphite monochromator. The latter functions as a mosaic crystal and can be mounted downstream of the sample as an analyser, effectively translating energy dispersion into angular dispersion, useful, for example, for monitoring fluorescence intensity. De Bergevin (1999) incorporates the polarization factor into the definition of the atomic scattering length for x-ray diffraction.

For incident x-ray energies at or above an absorption-edge energy E_{edge} (corresponding to electrons in K, L or M shells), the photoelectric effect causes the ejection of an electron after which the atom may de-excite radiatively via fluorescence (e.g. Krause (1979)) and emit x-rays isotropically of energy $E_{fluo} < E_{edge}$, or non-radiatively via the Auger process. Note that in the case of K-edge absorption, the hole in the K shell can be filled either by relaxation to the L shell, emitting an x-ray of energy $E_{fluo,\alpha} = W_K - W_L$, or to the M shell whereupon $E_{fluo,\beta} = W_K - W_M$, where W_i is the (positive) binding energy or work function for electrons in the i shell (e.g. Eisenberger *et al* (1976))—see the energy level diagram of figure 14. Energies for x-ray absorption edges and x-ray emission lines have been tabulated by Williams (2001) and by Kortright and Thompson (2001), respectively, for almost all elements of the periodic table.

When the incident energy E_o is below but near E_{edge} (within a few tens of electronvolts for K-edges), the x-ray can interact with a virtual electronic state of the atom and lose energy, in a process known as resonant-Raman scattering, and then be re-emitted at energy

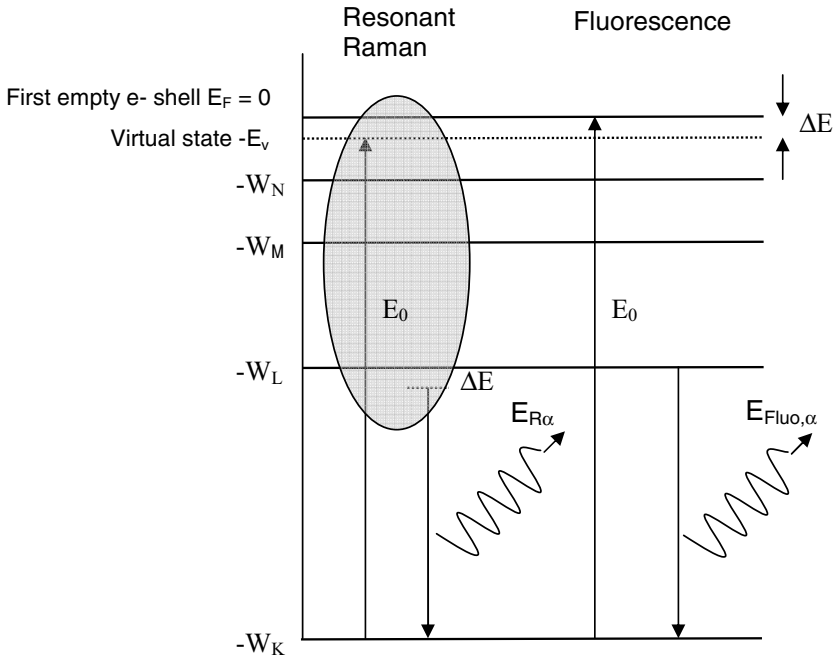

Figure 14. Schematic of the atomic energy levels involved in K-edge absorption and resonant-Raman scattering. In this case, $E_{\text{edge}} = W_K > 0$ where zero energy is defined at the Fermi level, E_F. For $E_o \geqslant E_{\text{edge}}$, an electron in the K shell is ejected and subsequent atomic relaxation from the L or M shells produces fluorescence, in which photons of constant energies $E_{\text{fluo},\alpha} = E_{\text{edge}} - W_L$ (K_α fluorescence) and $E_{\text{fluo},\beta} = E_{\text{edge}} - W_M$ (K_β fluorescence) are emitted. An incident photon of energy $E_o < E_{\text{edge}}$, insufficiently high for absorption, can nevertheless excite the atom to a virtual state from which it relaxes to the L or M states by emitting a resonant-Raman photon of energy $E_{R\alpha}$ or $E_{R\beta}$, respectively. The shaded oval indicates that the resonant-Raman excitation and relaxation processes form a single scattering event. Note that the energy of the emitted resonant-Raman photon is shifted below E_{fluo} by an amount $\Delta E = E_{\text{edge}} - E_o$ and therefore depends on the incident energy E_o. As E_o approaches E_{edge}, the virtual state becomes more active and the resonant-Raman intensity increases greatly. For clarity, the fine structure of the atomic states is not shown. Note that elements of $Z < 36$ have no N shell.

$E_R < E_{\text{fluo}} < E_o$. Furthermore, as both K_α and K_β fluorescence processes take place when E_o is above a K absorption edge, there are both K_α (where $E_o - E_{R\alpha} = W_L$) and K_β (where $E_o - E_{R\beta} = W_M$) resonant-Raman processes when E_o is just below the K absorption edge (see figure 14). Note that in both cases, as E_o varies, it is the energy loss between the incident and emitted photon that remains constant in resonant-Raman scattering, whereas in fluorescence the emission energy is constant. The resonant-Raman energy loss serves to eject an outer-shell electron, for example, an L shell electron in the case of the K_α process. As E_o approaches E_{edge}, the interaction with the virtual state becomes more and more probable, leading to a strong increase in the resonant-Raman intensity near E_{edge} (Bannett and Freund (1975), Alexandropoulos and Cooper (1995) pp 577–8). Once the absorption edge is attained, the energy of the re-emitted x-rays E_R becomes equal to E_{fluo}, for both K_α and K_β processes. Effectively, since resonant-Raman scattering is also isotropic, it can be thought of as 'anticipating' fluorescence.

Although energy discrimination at the x-ray detector is usually sufficient to separate fluorescence from the desired Rayleigh–Thomson intensity at energy E_o, the energy E_R, at

least in the case of K_β resonant-Raman scattering, is generally too close to E_o and requires a combination of a monocrystal analyser and collimation between the sample and detector to be blocked. For example, $E_o - E_{R\beta} = W_M$ is only 53 eV for the K-edge of Fe at 7112 eV, and in general $(E_o - E_{R\beta})/E_o \approx 1\%$ for the K-edges of the transition metals (Williams 2001).

In the method developed by Raoux (1993b) and co-workers (e.g. Armand *et al* (1993)), the ratio of the K_α and K_β fluorescence intensities is measured above the absorption edge, where a solid state detector (or else a linear detector after a pyrolytic graphite analyser) can easily discriminate these intensities from the elastic intensity. If one then assumes that the ratio of the K_β to K_α intensities remains roughly constant as a function of incident energy then a measure of the resonant-Raman K_α intensity below the absorption edge allows an estimation of the resonant-Raman K_β intensity which can then be subtracted.

Compton scattering is essentially inelastic 'billiard ball' scattering of the x-ray photons from quasi-free electrons in the sample. Its intensity depends on the initial momentum state (k) of the electron as well as the incident x-ray energy. For an initially static ($k = 0$) electron of rest mass, m_e, the energy loss (in terms of the wavelength shift of the scattered x-ray) is given by

$$\Delta\lambda = (\lambda_f - \lambda_o) = \frac{h}{m_e c}[1 - \cos(2\theta)], \tag{4.5}$$

where the incident energy $E_o = hc/\lambda_o$, and we ignore here the effects of binding energy. In practice the Compton scattering spectrum shows a wide distribution around this energy loss, due to the momenta of the bound electrons in the scattering atom (see upper plot of figure 15).

It turns out that the differential scattering cross-section for Compton scattering, $[\mathrm{d}\sigma/\mathrm{d}\Omega(q, E_o)]_{\mathrm{X}}^{\mathrm{Compton}}$, in equation (4.2) (as obtained by integrating the Compton scattering spectrum over final photon energies) for a given chemical species is more or less independent of the incident energy, E_o. It is, however, an increasing function of q and at high-q tends towards a value of $b(q = 0, E_o)^2/Z \approx Zr_e^2$, i.e. towards $1/Z$ of the self-scattering, provided that final state effects are unimportant (Alexandropoulos and Cooper (1995) pp 576–7). In experiments, however, the detector is not always 'black', i.e. it does not always have a uniform efficiency for detecting final energy photons, and the Compton spectrum is not uniformly integrated (see figure 16). The contribution of Compton scattering to the measured intensity $[\mathrm{d}\sigma/\mathrm{d}\Omega(q, E_o)]_{\mathrm{X}}^{\mathrm{total}}$ can therefore be strongly dependent on the energy response of the detector—hence the Breit–Dirac correction which is often used for laboratory x-ray sources (e.g. Warren (1990) p 12). In the free atom case, the Compton scattering contribution can be calculated from tabulated cross-sections, binding energies and detector efficiencies. Pálinkás (1973) has provided analytical approximations for calculating Compton intensities for elements of $Z \geqslant 20$.

Oftentimes, Compton scattering can be eliminated from detection at high scattering angles via moderate energy discrimination at the detector (e.g. by use of an analyser crystal placed just upstream of the detector), but at small scattering angles it can be difficult to suppress because its energy spectrum approaches closely the incident energy, E_o (e.g. Tonnerre (1989)). This situation is somewhat alleviated for electrically insulating samples wherein a binding energy must be surpassed before electrons can become 'free' and thereby subject to Compton scattering, causing a small but convenient shift in the beginning of the Compton spectrum away from the incident x-ray energy (particularly evident in the lower plot of figure 15 at about 17.598 keV, as compared with $E_o = 17.61$ keV). The use of a longer incident wavelength (i.e. smaller incident energy) will push the constant-q features in a diffractogram out to larger scattering angles (see equation (2.10)), but this does not help to separate the Compton scattering

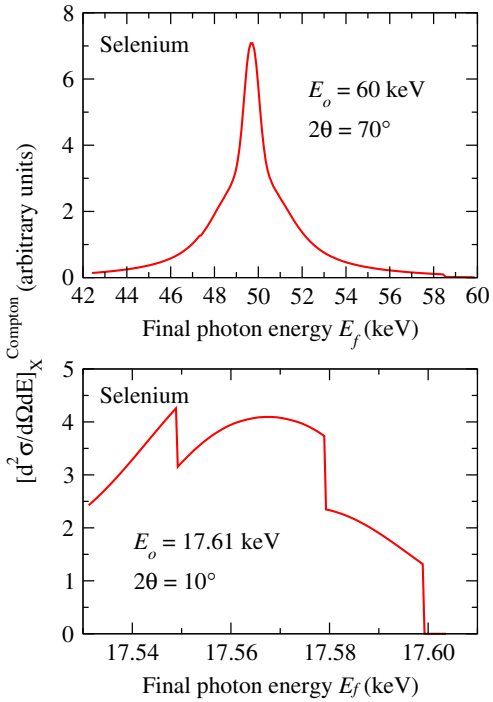

Figure 15. Compton scattering spectra, as a function of the final photon energy, for x-ray scattering from Se atoms. Upper plot: incident energy $E_o = 60$ keV and detector angle $2\theta = 70^\circ$. Lower plot: $E_o = 17.61$ keV and $2\theta = 10^\circ$. The discontinuities occur at electron binding energies. The detector is assumed to have perfect efficiency. Calculations by Barnes (2005) using the theory of Biggs *et al* (1975).

because equation (4.5) implies that a *small* Compton energy loss $\delta E = E_o - E_f \propto q^2$ is independent of E_o for a given q-value in the diffractogram. It can be useful to keep in mind, nevertheless, the rather simple result for Compton scattering that both δE and the differential scattering cross-section (obtained for a 'black' detector) are functions of q and roughly independent of E_o.

The Warren–Mavel fluorescence detection method (Warren and Mavel 1965) for eliminating Compton scattering from diffraction experiments has been adapted to synchrotron sources by Bushnell-Wye *et al* (1992). At high x-ray energy and high q-values, the Breit–Dirac approximation is no longer accurate, and the full relativistic expression of Klein and Nishina (1929) should be used for calculating the Compton scattering cross-section (Poulsen *et al* 1995). A thorough theoretical treatment of the Compton scattering of photons from bound electrons is given by Bergstrom *et al* (1993), and Kane (1992) has given a review of Compton scattering measurements.

As mentioned earlier, the use of high incident x-ray energies (i.e. 50–200 keV), as opposed to lower energies, has some advantages for diffraction measurements on liquids and glasses. At high energies the small wavelength permits diffraction to be performed at small angles, allowing the use of a flat detector and reducing polarization corrections (Poulsen *et al* 1995), while maintaining a high maximum q-value. In addition, the x-ray absorption is greatly decreased at high incident energies, so that scattering becomes the dominant process, permitting sample environments similar to those used for neutron diffraction experiments (see, e.g. Neuefeind (2002), Badyal *et al* (2000)). Although the multiple scattering contribution to the diffractogram

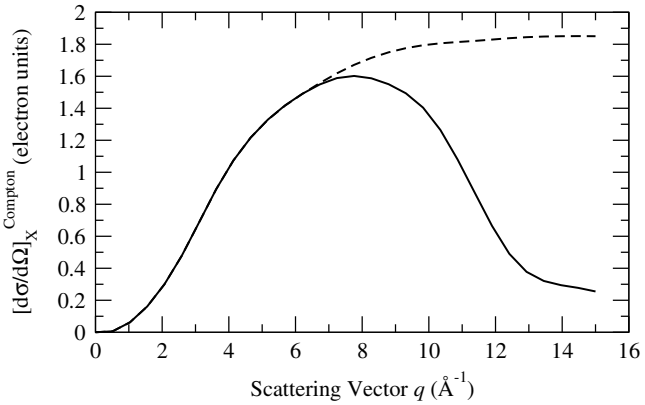

Figure 16. Effect of the detector energy response on the differential scattering cross-section for Compton scattering, $[d\sigma/d\Omega(q, E_o)]_X^{Compton}$, from a Li^+ ion ($Z = 2$) at an incident energy E_o = 17.479 keV (i.e. Mo $K_{\alpha 1}$, $\lambda_o = 0.709\,26$ Å). The dashed curve corresponds to an integration of the Compton scattering spectrum over final photon energies, E_f, by a 'black' detector having a uniform efficiency of detection. The solid curve shows the effect of applying a sharp cut-off to the detector response at an energy $E_f = E_o - 0.5$ keV.

can become more important at high energies as absorption decreases (Fajardo *et al* 1998), most of this contribution is from photons that are Compton-scattered at large angles and therefore have large energy shifts that can be discriminated at the detector (Poulsen and Neuefeind 1995).

In summary, to properly perform x-ray diffraction on liquids and glasses it is necessary either to block or subtract the unwanted contributions to $[d\sigma/d\Omega(q, E_o)]_X^{total}$ so as to isolate the Rayleigh–Thomson term. Note that there is no equivalent to vanadium, as used in neutron diffraction, for normalizing x-ray diffraction intensities. Instead, an auto-normalization technique can be used to fit the self-scattering at higher q-values, taking into account the atomic form factors of the elements in the sample (e.g. Hoppe *et al* (2004)), a variant being the 'Krogh-Moe/Norman' normalization technique (Norman 1957, Krogh-Moe 1956) which employs the sum-rule of equation (2.44). In practice, it is in fact very difficult to calculate accurately all the necessary corrections to x-ray diffraction data for a particular experimental setup, and this inexorably leads to uncertainties in the structure factors $S(q)$ or total interference functions $\tilde{F}(q)$ that are obtained.

4.2. *Anomalous x-ray diffraction (AXD)*

As shown by equation (4.1) and discussed in section 4.1, the x-ray scattering length $b(q, E_o)$ for a particular chemical species exhibits variation close to an absorption-edge energy. The technique of anomalous x-ray diffraction (AXD) (described by, e.g. Bienenstock (1993), Fischer-Colbrie and Fuoss (1990) appendix 2.2, Warburton *et al* (1987), Waseda (1984)) consists of performing diffraction measurements on a single sample at several incident energies E_o both near and far from absorption edges of atoms present in the sample. As a general rule, one always works below the absorption-edge energy so as to reduce absorption and to avoid EXAFS oscillations in f'' and especially in f' (see figure 12). Such experiments are most conveniently performed at a synchrotron light source, offering highly monochromatic beams over a wide range of x-ray energies.

The partial structure factor equations for NDIS can then be reformulated for a series of m AXD experiments, where again $m = n(n + 1)/2$ diffraction experiments are necessary

for a determination of all the partial structure factors of a sample having n chemical species. The diffractogram of each AXD experiment yields a total interference function $\tilde{F}_i(q)$, and equation (3.2) becomes

$$\tilde{F}_i(q) = \sum_{\alpha,\beta}^{n} c_\alpha c_\beta b_{\alpha i}(q) b^*_{\beta i}(q)[S_{\alpha\beta}(q) - 1], \tag{4.6}$$

where $b_{\alpha i}(q) = b_\alpha(q, E_{oi})$ is the scattering length of chemical species α for an incident x-ray energy E_{oi}. Note that here we cannot ignore the imaginary part of the scattering lengths as we did for NDIS. However, an isotropic system is effectively 'centro-symmetric' such that Friedel's law (e.g. Als-Nielsen and McMorrow (2001) pp 246–53, Sands (1993) pp 107–8) is satisfied, i.e. $\tilde{F}_i(\boldsymbol{q}) = \tilde{F}_i(-\boldsymbol{q})$ in spite of the non-real scattering lengths. Provided $S_{\alpha\beta}(q) = S_{\beta\alpha}(q)$, as given in equation (2.36), the weighting factors of the partial structure factors in equation (4.6) are all real-valued.

Each $\tilde{F}_i(q)$ is obtained from the $[\mathrm{d}\sigma/\mathrm{d}\Omega]_{\mathrm{X}}^{\mathrm{Ray-T}}$ term of equation (4.2) using equation (4.3) after normalization and correction of the measured $[\mathrm{d}\sigma/\mathrm{d}\Omega]_{\mathrm{X}}^{\mathrm{total}}$ for background, attenuation, multiple scattering, fluorescence, resonant-Raman and Compton scattering, as discussed earlier. For a binary system the matrix for AXD becomes (cf equation (3.3)):

$$\begin{bmatrix} \tilde{F}_1(q) \\ \tilde{F}_2(q) \\ \tilde{F}_3(q) \end{bmatrix} = \begin{bmatrix} c_x^2\, b_{x1}^2(q) & c_y^2\, b_{y1}^2(q) & c_x c_y[b_{x1}(q)b^*_{y1}(q) + b_{y1}(q)b^*_{x1}(q)] \\ c_x^2\, b_{x2}^2(q) & c_y^2\, b_{y2}^2(q) & c_x c_y[b_{x2}(q)b^*_{y2}(q) + b_{y2}(q)b^*_{x2}(q)] \\ c_x^2\, b_{x3}^2(q) & c_y^2\, b_{y3}^2(q) & c_x c_y[b_{x3}(q)b^*_{y3}(q) + b_{y3}(q)b^*_{x3}(q)] \end{bmatrix} \begin{bmatrix} S_{xx}(q) - 1 \\ S_{yy}(q) - 1 \\ S_{xy}(q) - 1 \end{bmatrix}$$

$$\equiv \begin{bmatrix} a_{11}(q) & a_{12}(q) & a_{13}(q) \\ a_{21}(q) & a_{22}(q) & a_{23}(q) \\ a_{31}(q) & a_{32}(q) & a_{33}(q) \end{bmatrix} \begin{bmatrix} S_{xx}(q) - 1 \\ S_{yy}(q) - 1 \\ S_{xy}(q) - 1 \end{bmatrix} \tag{4.7}$$

that is,

$$[\tilde{F}(q)] = [A(q)][S(q) - 1], \tag{4.8}$$

which can be inverted to solve for the partial structure factors, $S_{\alpha\beta}(q)$:

$$[S(q) - 1] = [A(q)]^{-1}[\tilde{F}(q)], \tag{4.9}$$

where again b^2 denotes $bb^* = |b|^2$. It is clear that each element $a_{ij}(q)$ of the matrix is purely real-valued (here normalized to units of barns). The q-dependent normalized determinant $|A(q)|_n$ is calculated after dividing each row i of $[A(q)]$ by $\left[\sum_j a_{ij}^2(q)\right]^{1/2}$.

The expression for a first-difference function (between x-ray energies E_{o1} and E_{o2}) in AXD for species x becomes

$$\begin{aligned} \Delta_{x\{1-2\}}\tilde{F}(q) &\stackrel{\mathrm{def}}{=} \tilde{F}_1(q) - \tilde{F}_2(q) \\ &= c_x^2[b_{x1}^2(q) - b_{x2}^2(q)][S_{xx}(q) - 1] + \sum_{\alpha\neq x}^{n} c_\alpha c_x[b_\alpha(q)(b^*_{x1}(q) - b^*_{x2}(q)) \\ &\quad + b^*_\alpha(q)(b_{x1}(q) - b_{x2}(q))][S_{\alpha x}(q) - 1]. \end{aligned} \tag{4.10}$$

However, since the imaginary part of x-ray scattering lengths cannot in general be ignored, an exact solution for a double-difference in AXD does not exist for $n > 2$ chemical species when only three $\tilde{F}_i(q)$ are measured, i.e. it is not possible to take a weighted difference of two AXD first-difference functions that cancels all the $S_{\alpha x}(q)$ where $\alpha \neq x$. For a binary system ($n = 2$) of species x and y, the exact expression for a double-difference function in AXD is

given by

$$\begin{aligned}\Delta_x^2\tilde{F}(q) \stackrel{\text{def}}{=} & [b_y(q)(b^*_{x2}(q) - b^*_{x3}(q)) + b^*_y(q)(b_{x2}(q) - b_{x3}(q))][\Delta_{x\{1-2\}}\tilde{F}(q)] \\ & - [b_y(q)(b^*_{x1}(q) - b^*_{x2}(q)) + b^*_y(q)(b_{x1}(q) - b_{x2}(q))][\Delta_{x\{2-3\}}\tilde{F}(q)] \\ = & \, c_x^2[S_{xx}(q) - 1][b_y(q)[(b^*_{x2}(q) - b^*_{x3}(q))(b^2_{x1}(q) - b^2_{x2}(q)) \\ & - (b^*_{x1}(q) - b^*_{x2}(q))(b^2_{x2}(q) - b^2_{x3}(q))] + b^*_y(q)[(b_{x2}(q) - b_{x3}(q)) \\ & \times (b^2_{x1}(q) - b^2_{x2}(q)) - (b_{x1}(q) - b_{x2}(q))(b^2_{x2}(q) - b^2_{x3}(q))]]. \end{aligned} \tag{4.11}$$

Note that this expression, which can be solved for $S_{xx}(q)$, includes the scattering length $b_y(q)$, which is not the case for the NDIS double difference of equation (3.8) wherein the scattering lengths are assumed to be real-valued. Note also that the coefficients of the partial structure factors $S_{\alpha\beta}(q)$ and the measured intensity differences $\Delta_x\tilde{F}(q)$ are real-valued in equations (4.7), (4.10) and (4.11) since they can be re-written as, for example, $f_1 f_2^* + f_1^* f_2 = 2(f_1' f_2' + f_1'' f_2'')$ where $f_1 = f_1' + \mathrm{i}f_1''$ and $f_2 = f_2' + \mathrm{i}f_2''$ are two complex numbers.

A fundamental difference between equations (4.10) and (4.11) for AXD and those for NDIS is that for AXD we must assume that the $b_\alpha(q)$ and $b_y(q)$ of the α and y atoms (where $\alpha, y \neq x$) do not change very much near an absorption edge of species x, whereas in NDIS it is generally true that isotopic substitution of species x does not affect the neutron scattering lengths of other species in the prepared samples. In addition, f' and f'' for a given chemical species in a liquid or glass depend on the immediate chemical environment (e.g. Bienenstock (1993)), producing a correlation between local structure and scattering length for that chemical species. This correlation is implicitly assumed to be non-existent in the definition of the total interference function given by equation (4.6) and is reduced, in experiment, by working with incident x-ray energies below the absorption edge (see figure 12). Chihara (1987) has shown that both the atomic form factors and Compton scattering are different for an atom in metallic versus non-metallic states. Finally, the Fourier transforms of the AXD equations (4.6) and (4.10) do not result in linear combinations of the $g_{\alpha\beta}(r)$, as is the case for the $G(r)$ obtained through neutron diffraction in equations (2.40) and (3.7), because x-ray scattering lengths are q-dependent. It is however useful to define an 'x-ray modified' total pair-correlation function $\tilde{G}(r)$ as the Fourier transform of the corresponding total interference function $\tilde{F}(q)$ and thereby a real-space first-difference function $\Delta_x\tilde{G}(r)$ for anomalous dispersion performed on species x:

$$\Delta_x\tilde{G}(r) \stackrel{\text{def}}{=} \frac{1}{2\pi^2 r\rho_o}\int_0^\infty q\,\Delta_x\tilde{F}(q)\sin(qr)\,\mathrm{d}q, \tag{4.12}$$

which converges to zero at large r. Narten and Levy (1972) have shown that x-ray modified partial pair-correlation functions $\tilde{g}_{\alpha\beta}(r)$, obtained by the Fourier transformation of each term in equation (4.6), are related to the true pair-correlation functions $g_{\alpha\beta}(r)$ via convolution by known functions involving the average breadth of the atomic electron density distribution. Note, however, that in a double difference experiment a full correction is made for the q-dependent scattering lengths (see equation (4.11)) and the true partial structure factor, $S_{xx}(q)$, is obtained directly.

The AXD approach to partial structure factor determination was originally suggested by Krogh-Moe (1966), and the idea was developed and extended to anomalous neutron diffraction by Ramesh and Ramaseshan (1971a, 1971b). Bondot (1974) used x-ray wavelengths from two tube sources (Cu K_α and Ag K_α), combined with a neutron diffractogram, in an effort to derive the partial pair-correlation functions of amorphous GeO_2. Some of the earliest AXD synchrotron experiments were carried out by Fuoss *et al* (1981, 1980) on amorphous $GeSe_2$

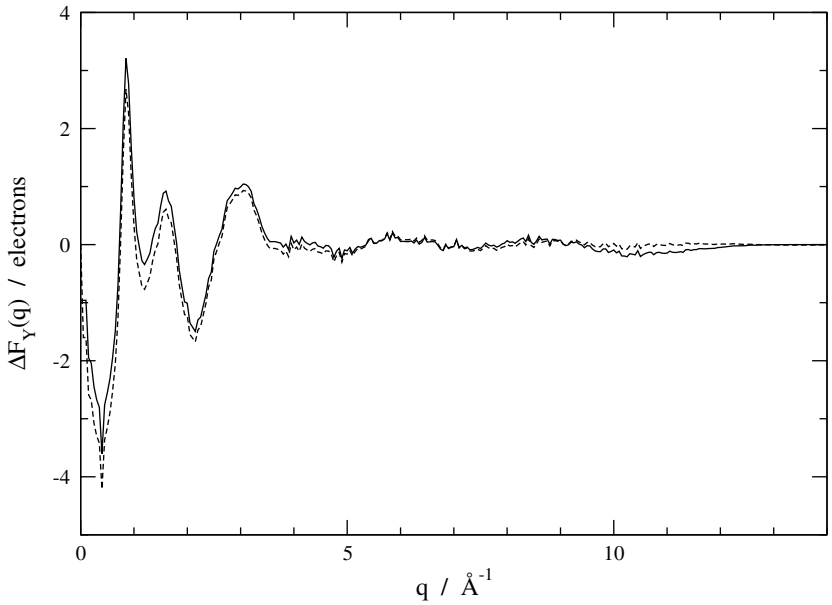

Figure 17. Corrected and normalized difference $\Delta_Y \tilde{F}(q)$ for a 3.5 molal YCl_3 aqueous solution obtained via AXD at the Y (yttrium) K-edge. The dashed line represents the back Fourier transform of the (edited) $\Delta_Y \tilde{G}(r)$ curve shown in figure 18 and thereby gives an estimate of the accuracy of the experimental data. Figure from Ramos *et al* (2001) and reproduced with permission from the American Chemical Society.

and GeSe. The AXD technique is particularly valuable for the study of $GeSe_x$ glasses or liquids since Ge ($Z = 32$) and Se ($Z = 34$) have nearly the same nominal x-ray scattering length. The scattering length contrast is therefore greatly increased by using an incident energy just below the K-edge of Ge or Se. See for example the results of Hosokawa (2001) on $GeSe_x$ glasses, Fischer–Colbrie and Fuoss (1990) on amorphous $GeSe_2$ and Armand *et al* (1993) on $GeSe_3$ and $GeSe_5$ glasses.

Ludwig *et al* (1987a) compared AXD and EXAFS results on concentrated metal bromide aqueous solutions. Their thorough study on liquid $GeBr_4$ (Ludwig *et al* 1987b, 1987c) concluded that high accuracy in AXD depends on a cancellation of systematic errors when subtracting data sets taken at two nearby incident photon energies. The Munro (1982) method uses differences to determine the partial pair-distribution functions (PDFs) from AXD data obtained at a total of 5 incident energies, and hence takes advantage of the cancellation of some systematic errors. Note, again, that in these fully constrained or over-constrained methods, the effect of the q-dependent scattering lengths is removed and the true partial structure factors are obtained.

Some AXD experiments and analyses by Ramos *et al* (2000) have determined the hydration structures of Br^- and Rb^+ ions in concentrated aqueous solution by combining first-difference functions from x-ray energies near and far from both the Br^- K-edge and the Rb^+ K-edge. The same group has obtained good results for YCl_3 aqueous solutions using anomalous dispersion at the Y (yttrium) K-edge (Ramos *et al* 2001), as shown in figures 17 and 18. The Munro (1982) method, as well as the SVD numerical technique discussed earlier, was employed by Burian (1998) to obtain the partial structure factors of amorphous Cd-As films by AXD.

Rather than being limited by the availability of isotopes as in NDIS, the AXD technique is constrained by the existence of absorption-edge energies E_{edge} for the atoms in the sample

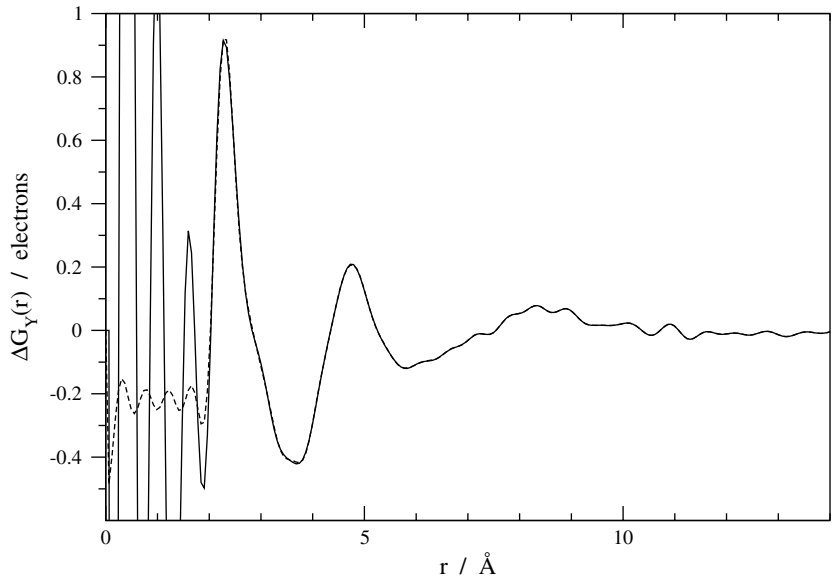

Figure 18. Real-space first-difference function $\Delta_Y\tilde{G}(r)$ obtained by Fourier transformation of the data in figure 17. The dashed line was obtained from a best fit to the q-space experimental data when a cut off is applied to $\Delta_Y\tilde{G}(r)$ in the region between 0 and 1.96 Å. The dashed line in figure 17 represents its back Fourier transform. Figure from Ramos *et al* (2001) and reproduced with permission from the American Chemical Society.

that are at once accessible and high enough to give a good maximum wavevector transfer $q_{max} = 4\pi E_{edge} \sin\theta_{max}/hc$, where $2\theta_{max}$ is the maximum scattering angle. To obtain a $g_{\alpha\beta}(r)$ with sufficient resolution in r-space via the Fourier transformation of a measured $S_{\alpha\beta}(q)$, a range of at least 10 Å^{-1} in q is generally necessary, corresponding to $E_{edge} \geqslant 10$ keV. For structural studies of glasses, especially those having covalent bonds (e.g. oxide glasses) which lead to well-defined interatomic distances, a maximum q of at least 20 Å^{-1} is generally desirable. The elements having absorption energies between 10 and 50 keV (the latter being the highest commonly available at 3rd-generation synchrotrons) vary from Ga ($Z = 31$) to Gd ($Z = 64$) for the K-edge and from Tm ($Z = 69$) to U ($Z = 92$) for the L-edge (which offers a weaker variation in f' than for the K-edge). We see therefore that AXD is a technique best exploited for elements of $Z > 30$ (see figure 19).

When absorption edges are not at appropriate energies, one can also employ isomorphic substitution in x-ray diffraction, as mentioned in section 3.2 for neutron diffraction. The study by Skipper *et al* (1989) concluded that the Mg^{2+} and Ni^{2+} ions are sufficiently isomorphic, in concentrated aqueous chloride solution, to provide useful information on their hydration environment. Powell (1989) has pointed out, however, that care must be taken that the differences in the water–water partial structure factors between the 2 samples are smaller than those coming from the scattering length contrast, which can be more problematic for neutron diffraction with isomorphic substitution where the water–water contributions are generally weighted more strongly than for x-ray diffraction.

For high-Z elements, the scattering length contrast offered by AXD is generally comparable to or higher than that for NDIS. The convenience of using a single sample in AXD is countered by the considerably greater difficulty in data analysis as compared with NDIS. As mentioned earlier, the energy dependence of f' is not easily determined experimentally nor theoretically and depends as well on the chemical environment of the atom. In addition,

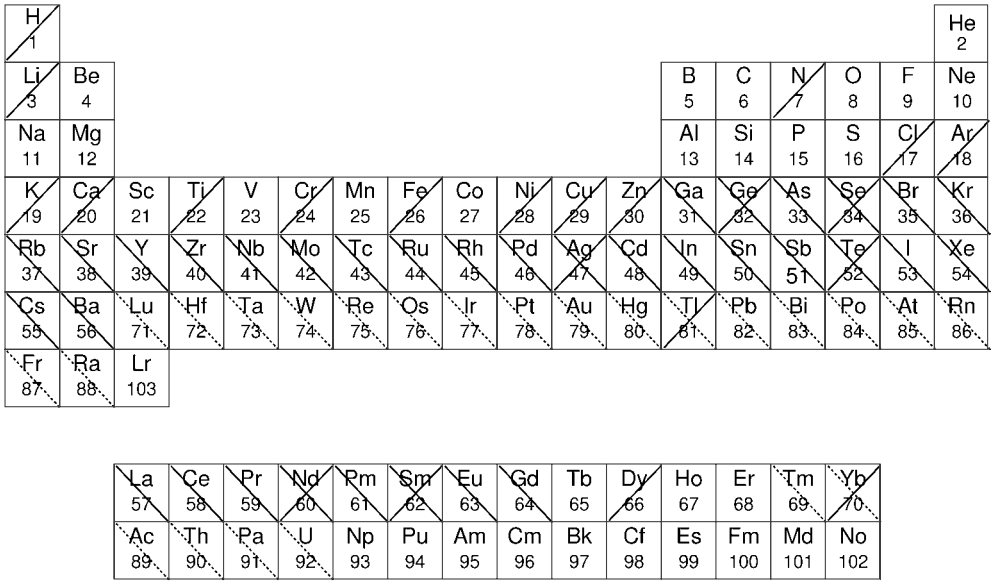

Figure 19. Periodic table showing those elements for which NDIS has already been performed (positive slope solid lines), as well as those having K (negative slope solid lines) and L (negative slope dashed lines) absorption edges between 10 and 50 keV.

for x-ray diffraction it is necessary to subtract or eliminate the fluorescence, Compton and resonant-Raman intensities (none of which are present in neutron scattering) and to correct for attenuation effects (scattering and absorption) that are in general significantly larger than for neutron diffraction measurements. Finally, the q-dependence of the scattering lengths in AXD first-difference functions (see equation (4.10)) leads, after Fourier transformation, to r-space resolution that is generally poorer as compared with neutron first-difference functions (see equation (3.6)). Nevertheless, AXD offers an oftentimes valuable alternative and some useful complementarity to NDIS.

5. Combined neutron and x-ray diffraction

As neutron scattering lengths depend on nuclear mass and the strong interaction (the theory of quantum chromodynamics or QCD), whereas x-ray scattering lengths depend on the number of electrons and the electromagnetic interaction (the theory of quantum electrodynamics or QED), the two are *a priori* uncorrelated across the Periodic Table, as illustrated in figure 20. A combination of the two diffraction techniques therefore offers good possibilities for increasing the contrast between measured $F_i(q)$ in the determination of partial structure factors, $S_{\alpha\beta}(q)$. The matrix expressing the $F_i(q)$ as functions of the $S_{\alpha\beta}(q)$ will then contain q-independent neutron (N) rows coming from equation (3.2) and q-dependent x-ray (X) rows from equation (4.6), the ensemble becoming therefore q-dependent.

5.1. Advantages for partial structure factor determination

The combined use of the two techniques therefore permits one to exploit not only two types of scattering lengths (as illustrated in figure 20) for each element in the sample but also two independent ways of varying the scattering lengths (NDIS and AXD). This versatility is central

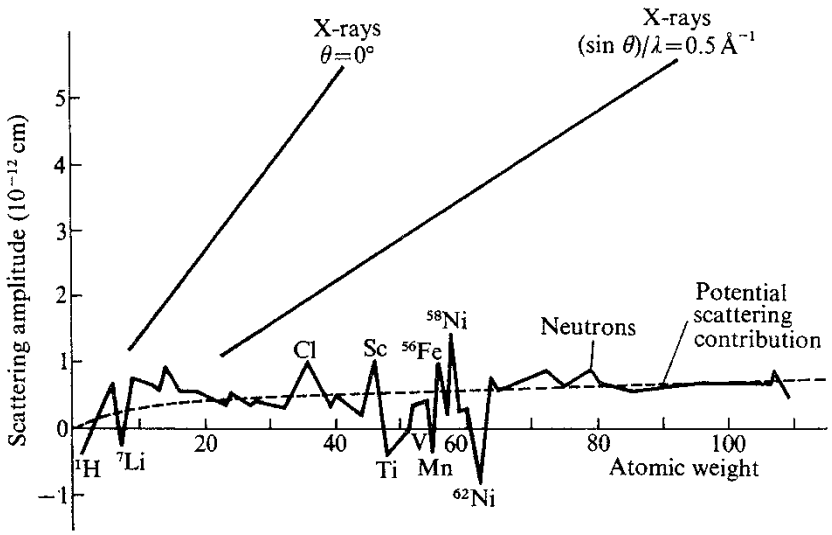

Figure 20. Coherent scattering lengths for x-rays ($r_e f$) and neutrons (b) as a function of atomic number. Note the dependence on $q \propto \sin\theta/\lambda_o$ for x-rays but not for neutrons. Figure after Bacon (1975).

to the effective complementarity of neutron (N) and x-ray (X) diffraction for the determination of the $S_{\alpha\beta}(q)$ and thus the $g_{\alpha\beta}(r)$ for a polyatomic liquid or glass. Although the addition of an x-ray diffractogram can lead to a greatly increased contrast in H/D substitution studies, such as for water (e.g. Fischer *et al* (2003) pp 383–5), we prefer to illustrate the advantage of combining N and X diffractograms for a higher-Z system which allows for 'cleaner' x-ray diffraction measurements.

The study of liquid TlSe by Barnes *et al* (1998) offers an excellent example of the utility of combining an x-ray diffractogram with a NDIS determination of partial structure factors. The electron density distributions of Tl and Se are quite spherical, and the relatively high mass and medium Z of these elements lead to small inelasticity corrections for neutrons and a low Compton intensity for x-rays, respectively. In this case, therefore, 2 neutron and 1 x-ray diffractograms (2N + X) can be combined quite accurately to derive partial structure factors.

Let us first review the results for standard NDIS applied to liquid TlSe, where the 3 samples measured by neutron diffraction have isotopic compositions of $^{\mathrm{nat}}\mathrm{Tl}^{\mathrm{nat}}\mathrm{Se}$, $^{205}\mathrm{Tl}^{\mathrm{nat}}\mathrm{Se}$ and $^{203}\mathrm{Tl}^{76}\mathrm{Se}$ (where 'nat' indicates the natural isotopic composition). After all the corrections are applied, the 3 $F_i(q)$ so obtained have an 'NDIS' matrix of

$$\begin{bmatrix} {}^{\mathrm{nat}}_{\mathrm{nat}}F(q) \\ {}^{205}_{\mathrm{nat}}F(q) \\ {}^{203}_{76}F(q) \end{bmatrix} = \begin{bmatrix} 0.2749 & 0.2263 & 0.4988 \\ 0.2968 & 0.2072 & 0.4960 \\ 0.1327 & 0.4042 & 0.4631 \end{bmatrix} \begin{bmatrix} S_{\mathrm{TlTl}}(q) - 1 \\ S_{\mathrm{SeSe}}(q) - 1 \\ S_{\mathrm{TlSe}}(q) - 1 \end{bmatrix}, \tag{5.1}$$

which gives a very small normalized determinant $|A|_{\mathrm{NDIS}} = 0.005$, in spite of the combination of isotopes being nearly optimal for TlSe. Even though the Barnes *et al* (1998) study used a very precise liquids diffractometer (D4b at ILL), the NDIS-only partial structure factors are barely discernable over the statistical noise, as shown in figure 21. Note that the matrix elements mentioned above are normalized such that $\sum_j a_{ij} = 1$. It is thus clear that there is not much contrast between the $^{\mathrm{nat}}\mathrm{Tl}^{\mathrm{nat}}\mathrm{Se}$ and $^{205}\mathrm{Tl}^{\mathrm{nat}}\mathrm{Se}$ samples since their matrix rows contain very similar values.

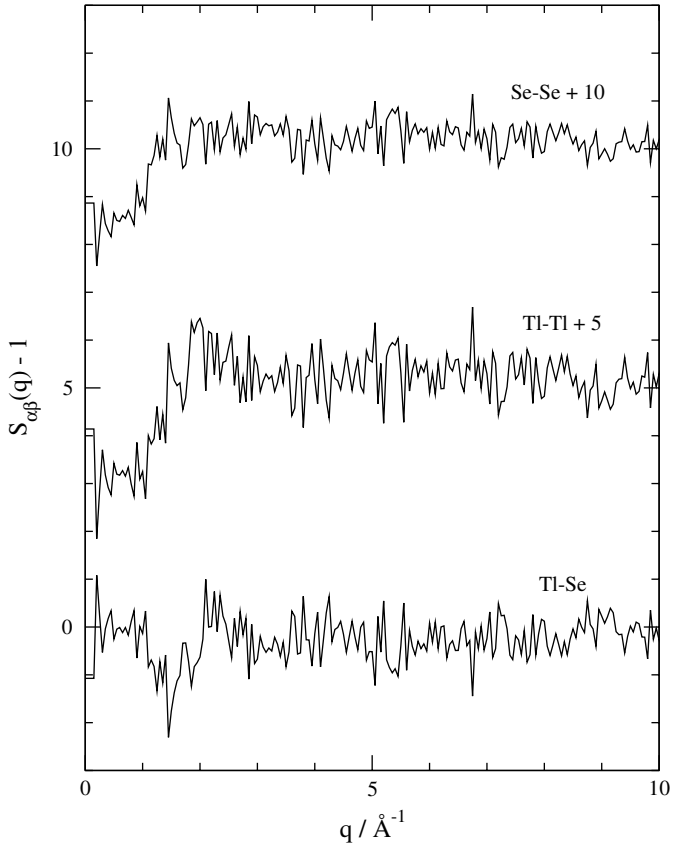

Figure 21. Partial structure factors, $S_{\alpha\beta}(q)$, for liquid TlSe obtained via NDIS only, using 3 samples of different isotopic compositions. The statistical noise indicates the spread in data points. Figure from Barnes *et al* (1998) and reproduced with permission from IOP Publishing Limited (Bristol).

The nat–nat sample's neutron diffractogram was then replaced by an x-ray diffractogram taken at an incident energy of $E_o = 38$ keV. The '2N + X' matrix becomes q-dependent and at $q = 5$ Å^{-1} is given by

$$\begin{bmatrix} {}^{\mathrm{X}}\tilde{F}(q) \\ {}^{205}_{\mathrm{nat}}F(q) \\ {}^{203}_{76}F(q) \end{bmatrix} = \begin{bmatrix} 0.5184 & 0.0784 & 0.4032 \\ 0.2968 & 0.2072 & 0.4960 \\ 0.1327 & 0.4042 & 0.4631 \end{bmatrix} \begin{bmatrix} S_{\mathrm{TlTl}}(q) - 1 \\ S_{\mathrm{SeSe}}(q) - 1 \\ S_{\mathrm{TlSe}}(q) - 1 \end{bmatrix}, \tag{5.2}$$

where the normalized determinant $|A|_{\mathrm{2N+X}} = 0.088$ is a factor of 17 larger than $|A|_{\mathrm{NDIS}}$. This exceptionally good contrast results in an inverse matrix at $q = 5$ Å^{-1} given by

$$\begin{bmatrix} S_{\mathrm{TlTl}}(q) - 1 \\ S_{\mathrm{SeSe}}(q) - 1 \\ S_{\mathrm{TlSe}}(q) - 1 \end{bmatrix} = \begin{bmatrix} -5.625 & 1.983 & 4.643 \\ -8.290 & 6.105 & 3.184 \\ 8.846 & -3.737 & -4.109 \end{bmatrix} \begin{bmatrix} {}^{205}_{\mathrm{nat}}F(q) \\ {}^{203}_{76}F(q) \\ {}^{\mathrm{X}}\tilde{F}(q) \end{bmatrix}, \tag{5.3}$$

which has small-valued elements and therefore gives a precise and robust determination of the $S_{\alpha\beta}(q)$ (figure 22) and finally the $g_{\alpha\beta}(r)$ via Fourier transformation (figure 23).

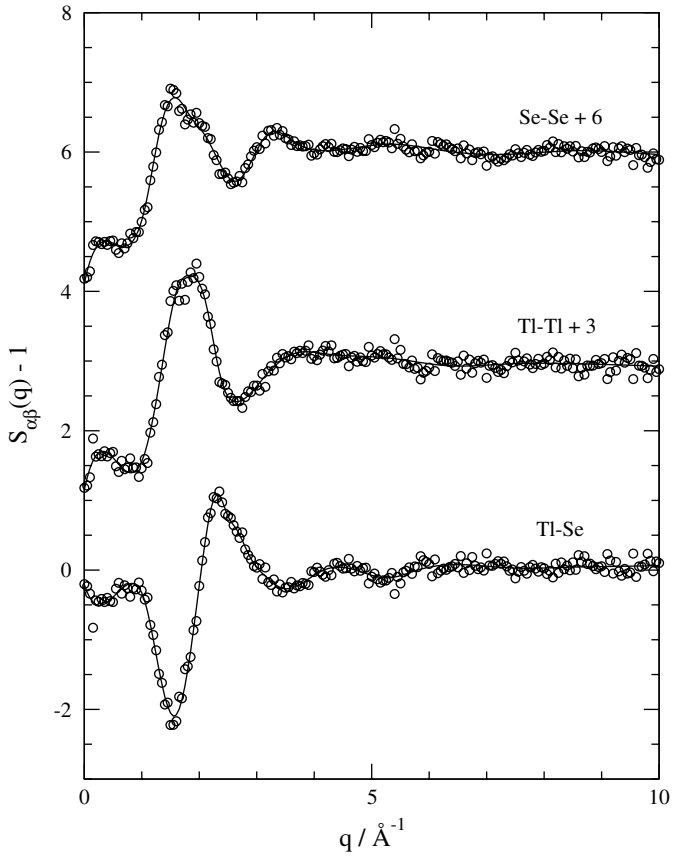

Figure 22. Partial structure factors, $S_{\alpha\beta}(q)$, for liquid TlSe obtained from a 2N + X experiment, i.e. combining 2 neutron diffractograms for samples having different isotopic compositions with 1 x-ray diffractogram. Figure from Barnes *et al* (1998) and reproduced with permission from IOP Publishing Limited (Bristol).

5.2. *Difficulties in combining neutron and x-ray diffractograms*

In general, the combination of neutron and x-ray diffractograms engenders several new difficulties in the data analysis. In particular, certain systematic errors of measurement will no longer 'cancel out' through subtractive linear combinations in the matrix, as can be the case for diffractograms coming from a single technique—for example, the inelasticity effects for neutron diffraction from ionic solutions in heavy water will cancel to a large extent in the first difference obtained via isotopic substitution of a dissolved ion (Soper *et al* 1977). When combining the results from x-ray and neutron diffraction, however, it is necessary to correct, in absolute and not just in relative terms, the measured differential scattering cross-sections $[\mathrm{d}\sigma/\mathrm{d}\Omega]_{\mathrm{N}}$ and $[\mathrm{d}\sigma/\mathrm{d}\Omega]_{\mathrm{X}}$ sufficiently well that residual systematic errors are much smaller than the differences between them—i.e. much smaller than the contrast. For example, the subtraction of the diffraction intensity measured for the container and sample environment, as well as any other background intensity, must be made very accurately when N and X diffractograms are combined.

In addition, an accurate absolute normalization of the measured $\mathrm{d}\sigma/\mathrm{d}\Omega$ (in barn per steradian) is required, a task that is especially difficult in the case of x-rays. It may also

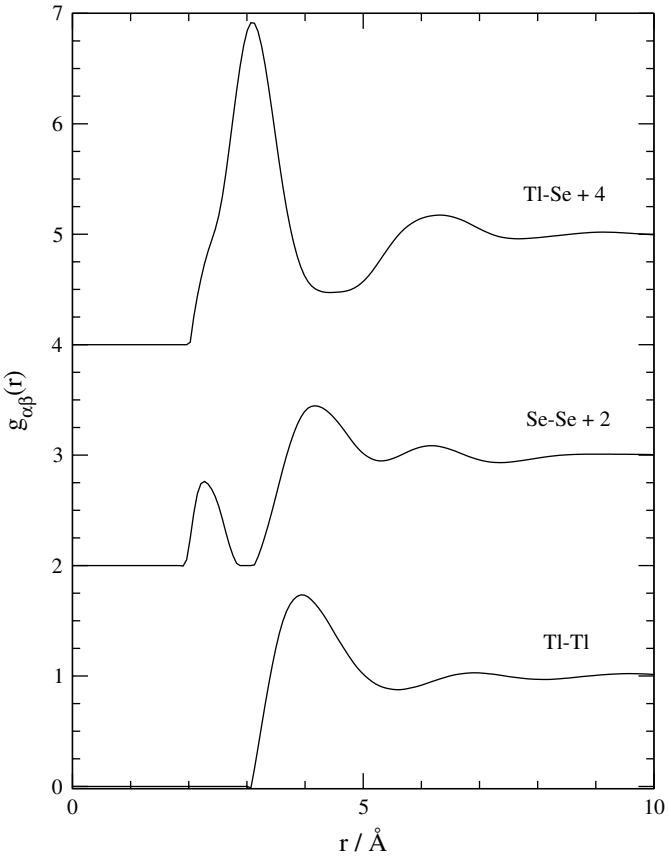

Figure 23. Partial pair-distribution functions, $g_{\alpha\beta}(r)$, for liquid TlSe obtained from a 2N + X experiment, after Fourier transformation of the curves fitted to the partial structure factors of figure 22 (Barnes *et al* 1998). Figure reproduced with permission from IOP Publishing Limited (Bristol).

be necessary to confirm that equivalent parts of the sample are probed by both techniques, x-rays having shorter extinction lengths and therefore being more surface-sensitive. Finally, the difference in the q-space resolution of neutron diffractometers (Finger *et al* 1994, van Laar and Yelon 1984, Caglioti *et al* 1960, 1958) and x-ray diffractometers (almost always more than sufficient for liquid and glass diffraction studies) requires consideration before the measured $F_i(q)$ from the two techniques can be put into the matrix. Oftentimes, the x-ray q-space data can simply be convolved with the poorer neutron-diffraction resolution function, as was the case in the liquid TlSe study of Barnes *et al* (1998). Alternatively, a modulation can be applied to the neutron-diffraction r-space results that takes into account the convolution of the structure factor with the instrument resolution function in q-space.

Aside from the above experimental difficulties in combining N and X diffractograms, one should remember that any significant non-sphericity of the atomic electron densities in the sample will invalidate the assumption of isotropy of the atomic form factor's modulation $f_{\text{falloff}}(q)$ in equation (4.1). For example, molten covalent systems can have strong directional bonds carrying significant electron density between the atomic centres. For a metallic liquid, the x-ray scattering from the conduction electrons may need to be taken into account (e.g. Salmon *et al* (2004)). In some of these cases the electron density will no

longer have spherical symmetry around the nucleus, meaning that x-rays and neutrons will no longer diffract from the same set of scattering centres, and will therefore be measuring slightly different structures.

A good example concerns the partial structure factors of water, where most of the electron density of the $Z = 1$ sites has been 'absorbed' by the oxygen orbitals (e.g. see Badyal *et al* (2000) for a comparison of neutron and x-ray diffractograms for water). In addition, the factor of two difference in mass between H and D leads to subtle structure differences, including quantum effects, which are discussed in section 3.2. The neutron diffractograms for samples containing H will also be subject to large incoherent scattering as well as significant inelasticity corrections. Finally, due to the low atomic number $Z = 1$, the x-ray diffractograms will have a high percentage contamination by Compton scattering whose contribution is difficult to calculate since it is dependent on the complex nature of the O–H covalent bond.

The high contrast inherent in a 2N+X diffractogram combination may be larger than the residual systematic errors in the case of water and other systems where H/D substitution is used, but care must be taken in the data analysis and in the interpretation of the results. As an example of the contrast enhancement (recall that no appropriate oxygen isotopes are available for NDIS), consider the case of 3 NDIS samples for water using H/D substitution (0% H, 20% H and 40% H) for which $|A|_{\mathrm{NDIS}} = 0.0236$ (a typical value), as compared with a 2N + X experiment (0% H and 20% H content for the neutron diffractograms and 100% H content for the x-ray diffractogram) for which $|A|_{\mathrm{2N+X}} = 0.159$ is a factor of 7 larger.

Although not really concerned with diffraction from liquids and glasses, the book edited by Furrer (1998) gives a pedagogical presentation of the complementarity between neutron and synchrotron x-ray scattering. Gurman (1990) has discussed the limitations of combining different data sets (from neutron diffraction, x-ray diffraction and EXAFS) for the accurate determination of partial structure factors.

5.3. Some studies to date

Other than the study on amorphous GeO_2 by Bondot (1974) mentioned in section 4.2, one of the earliest attempts at combining neutron and x-ray diffraction results to obtain a partial structure factor, that of S–S in liquid CS_2, was carried out by Orton (1977), who did not use NDIS or AXD but made a few reasonable assumptions in order to eliminate the C–C partial structure factor. A recent study on liquid Ga_2Te_3 (Buchanan *et al* 2001) combined NDIS and AXD (K-edge of Te), producing 3N+2X or 5 diffractograms which were combined in an over-determined application of singular value decomposition (SVD) (Press *et al* (1999) pp 59–70), to give the full set of 3 partial structure factors. The study by Skipper and Neilson (1989) combined NDIS (using ^{107}Ag and ^{109}Ag) with isomorphic substitution in x-ray diffraction (using Ag^+ and Na^+) for concentrated aqueous solutions of $AgNO_3$ and $NaNO_3$. Results for first-differences and partial structure factors have also been obtained for covalent glasses and amorphous semiconductors by combining N and X diffraction (Sampath *et al* 2003, Barnes *et al* 1999). In the case of a liquid metal, the system may be regarded as a binary mixture of ions and valence electrons (Chihara 1987). Neutron and x-ray diffractograms can then be combined, under favourable conditions, to measure the ion–ion and ion–valence electron partial structure factors together with the valence electron form factor—see Salmon *et al* (2004) for a recent overview.

Even if not used to determine partial structure factors, the comparison of neutron and x-ray diffractograms (with theory and/or with each other) for the same system can aid considerably in the interpretation of the total pair-correlation functions (coordination numbers, etc), as each technique will typically be sensitive to different atoms. Early work in this and related areas includes that of Henninger *et al* (1967a, 1967b) on amorphous selenium and vitreous

silica, respectively, that of Narten (1976, 1972a, 1972b) on liquid CCl_4, water and gallium, respectively, and that of Leadbetter and Wright (1972a) on vitreous BeF_2 and other binary glasses. Such dual-beam (X+N) studies have been particularly useful for polyatomic oxide glasses (e.g. Benmore *et al* (2003), Johnson *et al* (2003), Hoppe *et al* (2004, 2001, 1998), Karabulut *et al* (2000)) and for some aqueous solutions (e.g. Bakó *et al* (1999), Andreani and Petrillo (1987)), molecular liquids (e.g. Bellissent-Funel *et al* (1997), Bertagnolli and Zeidler (1978)) and liquid alloys (e.g. Neumann *et al* (1991)).

In addition to combining or comparing N and X data sets in terms of normalized and corrected data sets, the technique of reverse Monte Carlo (RMC) (discussed in section 6) can be employed to generate the theoretical neutron and x-ray diffractograms from a three-dimensional structural model. The procedure can incorporate, for example, effects from the finite-width of the resolution function and from the finite q-range accessible to a diffractometer, and the simulated data are compared iteratively with the experimental results so as to refine the three-dimensional model of the system under study (McGreevy 2001, 1990).

In conclusion, the combination of neutron and x-ray diffractograms has the advantages of increased contrast as well as accessibility to a larger number of elements in the determination of partial structure factors, as compared with using NDIS or AXD alone. Figure 19 shows those elements for which NDIS has already been performed (i.e. those for which isotopes have scattering lengths with sufficient contrast but which are not too expensive—see also Enderby (1993)), as well as those having K and L absorption edges appropriate for AXD. It is clear that many elements not available to one technique are available to the other, whence the advantage of combining the two. However, more progress can be made in improving the experimental techniques and data analysis methods used to combine neutron and x-ray diffractograms, especially for systems containing low-Z elements.

6. Beyond the determination of partial structure factors and pair distribution functions

Until the mid 1980s the interpretation by experimentalists of structure data for liquids and glasses was largely based on interatomic distances observed as peaks in $g(r)$ and the mean coordination number obtained by integration of $g(r)$ between appropriate limits. Three-dimensional local structures and bonding schemes were then inferred from these data, often by comparison to known crystal structures of the same or similar stoichiometry. Since that time, the availability of high-speed computers has improved the accessibility and has extended the range of methods that are used. These fall into two basic categories: (1) modelling of the system by Monte Carlo, molecular dynamics or integral equation methods followed by a comparison of the calculated structures with the experimental data and (2) 'fitting' three-dimensional models of the system to the data, by means of iterative structure refinement methods. All these methods are now readily available to the experimentalist.

Some of the early work using computer simulation and integral equation methods, on systems which include Lennard-Jones liquids (Yarnell *et al* 1973), liquid metals (Cusack 1987), molten salts (Sangster and Dixon 1976, Parrinello and Tosi 1979, Rovere and Tosi 1986) and aqueous solutions (Impey *et al* 1983), is described elsewhere.

6.1. Monte Carlo and molecular dynamics simulation

The modelling of liquid structure by Monte Carlo, molecular dynamics or integral equation methods (such as the hypernetted chain or Percus Yevick method) is now well established. In each of these methods the interactions between the atoms in the material are described in the form of interatomic (usually pair) potentials. For a full description of the methods and their

advantages and disadvantages the reader is referred to the books by Egelstaff (1992), Hansen and McDonald (1990), Allen and Tildesley (1987) and Cusack (1987).

There are now a large number of computer programs generally available that exploit these methods. Similarly a large number of interatomic potentials are widely available in the literature. Hence it is now within the easy grasp of experimentalists to attempt basic computer simulations of simple systems for comparison with experimental results—indeed the comparison with experiment is an important test of the reliability of the potentials. However, in all but the simplest systems it is apparent that methods based on simple pairwise potentials do not give good agreement with the data—see for example the study on liquid Ag_2Se by Barnes *et al* (1997) or the use of a polarizable-ion model as opposed to a rigid-ion model for molten $DyCl_3$ (Takagi *et al* 1999) and other MCl_3 systems (Hutchinson *et al* 2001, 1999).

Over the last decade (1990s), theoretically more complex methods have been developed including *Ab Initio Molecular Dynamics* (Car and Parrinello 1988, 1985) and *Quantum Monte Carlo* (e.g. Allen and Tildesley (1987) chapter 10) methods that attempt to simulate the structure using first-principles quantum mechanical calculations that avoid the need to calculate pair potentials in advance. However, they are computationally intensive and at the present time the calculations are limited at most to a few hundred atoms, and by consequence their agreement with experiment can be poor in the low-q region of the data. In addition, even *ab initio* techniques still require some choice in terms of, for example, the density-functional, and this can affect the results (Massobrio *et al* 1999). Overall, it still remains a difficult theoretical challenge to simulate the structure of liquids, and it is clear that high-quality experimental data are a stringent test of the reliability of these methods. In the case of the simulation of glasses the situation is even more complicated due to the non-equilibrium nature of the systems and the difficulty of 'quenching' liquids sufficiently slowly in the simulations to form glass structures comparable to those found in nature (e.g. Kob (2003)).

6.2. *Structure refinement*

In the 1980s the idea of carrying out a computer refinement of atomistic three-dimensional structural models of liquids and glasses (and other disordered materials) was established. This idea developed in part from original work using 'inverse' Monte Carlo methods applied to glasses by Kaplow *et al* (1968) and Renninger *et al* (1974) and to disordered substitutional alloys by Schweika and Haubold (1988) and Gerold and Kern (1987). At the current time there are two principle methods that are in common use: the reverse Monte Carlo (RMC) method (McGreevy 2001, 1995, McGreevy and Pusztai 1988) and the empirical potential structure refinement (EPSR) method (Soper 2001, 1998, 1996a).

In both methods an initial atomistic three-dimensional model of the liquid or glass in question is created in the computer. The partial pair-distribution functions and/or partial structure factors are then calculated from the computer model and compared with the data. The computer model is then refined until the model data agree sufficiently well with the experimental data. The intention, at the end of the refinement procedure, is that the computer model is a good representation of the actual atomic structure in the liquid or glass.

6.2.1. Reverse Monte Carlo. The RMC method is based on the Metropolis Monte Carlo method (Metropolis *et al* 1953) and involves the successive movement of individual atoms in the simulated structure while a comparison with the measured structure is made in terms of a χ^2 fit to the data. If, as a result of a given move, an improvement in χ^2 is obtained, the move is accepted. If there results a worsening of the fit, the move is accepted according to a certain probability (analogous to a Boltzmann factor in a conventional Monte Carlo simulation).

Eventually χ^2 will reach a stable value, and the structures obtained after additional successive moves are averaged to produce the final refined structure.

An advantage of the RMC method is that it is comparatively easy to use and the program is readily and freely available. In addition, data sets from different techniques (e.g. diffraction, EXAFS, NMR, etc) can be 'fitted' simultaneously while respecting quantitatively their different experimental errors. Furthermore it is relatively easy to build extra constraints into the refined model by, for example, adding coordination number constraints obtained from, e.g. NMR methods, or requiring the model to have agreement with local atomic arrangements known from, e.g. EXAFS measurements. A disadvantage is that it is difficult to build in molecular structure to the model apart from using rather crude constraints that risk trapping the simulation in local minima (see section 6.2.2).

RMC has been used to analyse NDIS data for a number of systems, including superionic conductors (Keen 2002), molten salts (McGreevy and Pusztai 1990, Pusztai and McGreevy 1998), ionically conducting glasses (Cormier *et al* 1998, Lee *et al* 1993), a titanosilicate glass (Cormier *et al* 1997), mixtures of binary molten salts (Badyal and Howe 1996), metallic glasses (Lamparter 1995, Pusztai and Svab 1993) and ions in aqueous solution (Howe 1990), among other examples. Also RMC can straightforwardly take into account the magnetic form factor of particular atoms when necessary (see e.g. Keen *et al* (1995) for amorphous Dy_7Ni_3).

The fact that partial structure factors obtained via an RMC analysis must be consistent with a 3-dimensional model is an added check on the viability of the results, and in this way, among others, RMC serves to eliminate non-physical solutions, even if they had been viable numerical solutions for partial structure factors (e.g. Pusztai and McGreevy 1998). More generally, for multiple data sets, RMC can be effective in identifying which data set (or sets) has significant systematic errors or whether as a whole the data sets are mutually consistent. It is interesting to note that an integral equation method for combining different types of data sets to derive partial structure factors, without producing a 3-dimensional model, was presented by Babanov *et al* (1986).

As suggested by McGreevy (1990), neutron and x-ray diffractograms can be combined using RMC for the determination of partial structure factors. This has been carried out for molten salts (Pusztai and McGreevy 2001) and vitreous silica (Keen and McGreevy 1990), among other systems. Wicks and McGreevy (1995) and McGreevy (1993) have discussed the combination of neutron, x-ray and EXAFS structure data for modelling liquid and amorphous materials, and the method has been applied to ionically conducting glasses by Swenson *et al* (1998) and Wicks *et al* (1995, 1993).

For information on recent applications of RMC modelling (systems include crystalline powders, magnetic structures and disorder in crystals) see Keen *et al* (2005a) and McGreevy (2001). A related data inversion method, useful as an alternative to Fourier transforming $S(q)$ data which can lead to termination and other errors (e.g. Leadbetter and Wright (1972b), Lorch (1969), Waser and Schomaker (1953)), is that of MCGR or MCGOFR (Pusztai and McGreevy 1999, 1997). This method does not develop a 3-dimensional model of the system but produces a $g(r)$ or $G(r)$ whose Fourier transform is consistent with the diffraction data, and thereby offers some estimate of the way in which experimental errors propagate to the real-space function.

6.2.2. Empirical potential structure refinement. Originally named EPMC (empirical potential Monte-Carlo) (Soper 1996a), the EPSR method, like RMC, is based on a fitting procedure through a Monte Carlo simulation, but includes an extra step in the iteration loop so as to allow a refinement of interatomic potentials. Other iterative methods coupling molecular dynamics simulations with interatomic potential inversion schemes (i.e. where

the interatomic potential $u(r)$ is deduced from measured $g(r)$) have been presented by Levesque *et al* (1985) (the LWR method) and Schommers (1983). Pair potentials and ion-electron pseudo-potentials have also been deduced from experimental structure factors using inversion schemes that involve integral equation methods (see e.g. Dharma-wardana and Aers (1983)).

Generally applied to liquid (or fluid) systems, an EPSR refinement begins by constructing via Monte Carlo techniques an initial three-dimensional structural model that has the correct density and temperature, using assumed reference pair-potentials $U_{\alpha\beta}^{\mathrm{ref}}(r)$ between the different atomic sites α and β in the liquid. Each reference potential should, in general, be chosen to be as realistic as possible and, in practice, is usually taken to be a combination of Lennard–Jones and Coulomb terms. From the initial structural model are then calculated the partial pair-distribution functions $g_{\alpha\beta}(r)$ and the corresponding effective potentials of mean force:

$$\psi_{\alpha\beta}(r) = -k_{\mathrm{B}}T \ln[g_{\alpha\beta}(r)], \tag{6.1}$$

which in fact reduce to the true interatomic pair-potentials $u_{\alpha\beta}(r)$ in the limit of an infinitely dilute gas.

An effective potential of mean force is also calculated from each $g_{\alpha\beta}(r)$ of the experimental data (obtained by Fourier transforming the experimental partial structure factors). Empirical pair-potentials $U_{\alpha\beta}^{\mathrm{emp}}(r)$ are then formed by setting them equal to the difference between the data-derived $\psi_{\alpha\beta}(r)$ and those derived from the structural model. These empirical potentials are added as correction terms to the reference potentials, and the model is then re-equilibrated using the new reference potentials, after which comparison with the data leads to a recalculation of the $U_{\alpha\beta}^{\mathrm{emp}}(r)$, and so forth. This iteration is continued until no significant difference remains between the $g_{\alpha\beta}(r)$ of the model and those of the data. The desired outcome is that the model liquid represents the real liquid in a similar way as for the RMC method, while being self-consistent with realistic interatomic potentials.

The EPSR method is increasingly used to refine complex molecular liquids, since the atoms can be more efficiently constrained, as compared with RMC, to maintain the molecular structure as the simulation proceeds. In addition to the modelling of atomic positions, it is also possible to produce orientational correlation maps (e.g. Bowron *et al* (1998a), Andreani *et al* (1997)) and three-dimensional spatial density maps (e.g. Finney *et al* (2002), Soper (2001)) that help to interpret the molecular interactions in the liquid. However, the presentation of such final numerical results, albeit impressive, should *not* preclude the publication of the experimental data along with the fitted curves.

Recent applications of the EPSR method for structure determination include a solution of tertiary butanol in water (Bowron and Moreno 2003), an ionic liquid comprising a large asymmetric organic cation (Hardacre *et al* 2003), high- and low-density amorphous ice (Finney *et al* 2002), liquid alumina (Landron *et al* 2001), high- and low-density water (Soper and Ricci 2000), subcritical and supercritical methanol (Yamaguchi *et al* 2000), water and ice at different temperature/pressure state points (Soper 2000), a solution of LiCl in high-temperature and supercritical water (Yamaguchi and Soper 1999), liquid hydrogen halides (Andreani 1998) and pure tertiary butanol (Bowron *et al* 1998b).

6.2.3. Critique of structure refinement methods. In some circles the use of these refinement methods (RMC and EPSR) has been criticized on the grounds of the non-uniqueness of the solutions (e.g. McGreevy (1995), Soper (2001))—in other words, is it possible to find other solutions that fit the data equally well? The formal answer to this question is that there is no unique solution for any realistic experiment. However, if a satisfactory goodness of fit has been obtained then the model is at least *consistent* with the data. As such, if it supports evidence

obtained from other experimental techniques or a previous hypothesis then clearly relevant conclusions can be made.

It has also been claimed that RMC/EPSR refinement methods allow one to determine partial structure factors from experimentally under-determined systems—this point must be treated with caution. For example, in an experiment on a binary liquid for which the scattering lengths of the elements are exactly the same, there is no information in the diffraction data concerning the arrangement of atoms of type A around those of type B. This is self-evident as we know that we have only measured $S_{NN}(q)$ and hence the atomic positions irrespective of the type of atom. Indeed, if an unconstrained RMC simulation is run on such data, or even if it uses species-independent constraints such as a single minimum interatomic distance, it produces three identical partial structure factors—exactly as predicted. We may choose to add further constraints, for example, on species-dependent coordination numbers or on different minimum interatomic distances (for AA, BB and AB) coming from different atomic sizes, and these constraints will indeed give rise to different partial structure factors in our RMC fit. It is clear, however, that these differences arise purely from the constraints made, and it may be equally possible to choose a different set of constraints that produce an equally valid fit. This highlights a difficulty of the RMC/EPSR methods, i.e. what is the relative weight of the experimental data, compared with the imposed constraints and (in the case of EPSR) the choice of reference potential, on the results of the refinement? An attempt to address some of these problems is given by Soper (2005b).

7. Conclusions and prospective

The experimental and theoretical tools employed in neutron and x-ray diffraction studies of liquids and glasses differ, in general, from those used for diffraction studies of single or powdered crystals. The lack of a crystalline lattice necessitates a probabilistic description of the atomic structures of liquids or glasses and gives rise to weaker and more diffuse diffracted intensity as compared with Bragg peak intensities. There is therefore a requirement for more elaborate data analysis procedures than for the case of crystalline systems, in order to extract useful quantitative information.

In powder diffraction data analysis, it is usual to consider only the elastic scattering that contributes to Bragg peak intensities (e.g. Rietveld refinement) and to disregard the diffuse scattering. Hence the information provided, on only the *time-averaged* atomic positions, is insensitive to any time-dependent (i.e. dynamic) spatial correlations between atoms. By comparison, in the case of diffraction from liquids or glasses an analysis is made of the so-called total scattering (i.e. $S(q)$ or $F(q)$) which provides information on the average of *instantaneous* atomic positions and can therefore be more sensitive to these correlations. Thus, total scattering experiments can be of interest for resolving crystalline structures (e.g. Keen *et al* (2005b), Hui *et al* (2005), Neder and Korsunskiy (2005), Keen (2002)), and an increasing number of powder diffraction groups are adopting techniques such as so-called PDF analysis (Egami and Billinge 2003). The value of the tools developed for diffraction studies of liquids and glasses is therefore being recognized by other diffraction communities, especially as more complex structures are studied.

The inherent complexity of liquids and glasses makes their structure an extremely difficult task to determine. The problem is, therefore, best tackled by obtaining a consistent set of results from a plurality of techniques that include diffraction (both x-ray and neutron) and spectroscopy (e.g. nuclear magnetic resonance, Raman, EXAFS and infra-red)—see e.g. Fischer and Schober (2003). Future advances in x-ray and neutron sources suggest that diffraction data will become increasingly more accurate and lead to much more stringent constraints on structural

models of the materials under study, whether these models are obtained by simulation or structure refinement methods. In the case of neutron diffraction, measurement of the structure of disordered materials has gained enormously from the construction of well-designed and purpose-built instruments. By comparison, the exploitation of x-ray diffraction for accurate structural measurements of liquids and glasses is less well advanced but the advent of third generation x-ray sources means that there is a huge potential for the further development of x-ray methods, especially with regards to anomalous x-ray diffraction (AXD). Recent proposals for dedicated diffractometers at the advanced photon source (e.g. beamline 11-ID as described at http://www.aps.anl.gov/Future/Reports/index.html) and at other sources suggest that huge gains may be made by exploiting x-ray methods alone and by combining the x-ray and neutron diffraction techniques. Finally, the ability to scatter intense x-ray beams from small sample volumes has seen a rapid increase in the use of x-ray diffraction for studying materials under extreme conditions, such as high pressures and temperatures.

In this review we have tried to respect the historical context of the development of neutron and x-ray diffraction studies of liquids and glasses, while explaining pedagogically the experimental techniques and data analysis methods involved, as well as citing recent trends and advances in the field, including those concerned with numerical simulations. We hope that this perspective has produced a coherent and practical review of an area of pure and applied research involving physics, chemistry and biology.

Acknowledgments

We appreciate stimulating conversations with C Alba-Simionesco, R Bellissent, M C Bellissent-Funel, C J Benmore, F J Bermejo, J Blétry, D T Bowron, E Bychkov, D C Champeney, P Chieux, P Convert, G J Cuello, N E Cusack, P Damay, J C Dore, P A Egelstaff, E Elkaim, J E Enderby, R Evans, M Gailhanou, P H Gaskell, J P Gaspard, M A González, A C Hannon, L Hennet, F Hippert, K Hoshino, W S Howells, J F Jal, Y Katayama, J P Lauriat, A J Leadbetter, S Lequien, P A Madden, C Massobrio, R L McGreevy, G W Neilson, J Neuefeind, P Palleau, A Pasquarello, R T Phillips, D H Powell, D L Price, M Silbert, R N Sinclair, N T Skipper, A K Soper, M Sutton, S Takeda, S Tamaki, D Thiaudière, T Usuki, P Verkerk, M Wilson, R M Wood, A C Wright and W H Young.

References

Alexandropoulos N G and Cooper M J 1995 *International Tables for Crystallography* vol C, ed A J C Wilson (Dordrecht: Kluwer) section 7.4.3, pp 574–8

Allen M P and Tildesley D J 1987 *Computer Simulation of Liquids* (Oxford: Clarendon)

Als-Nielsen J 1993 *Neutron and Synchrotron Radiation for Condensed Matter Studies, vol 1: Theory, Instruments and Methods* ed J Baruchel *et al* (Berlin: Springer-Verlag, Les Ulis: Les Editions de Physique) chapter 1, pp 3–33

Als-Nielsen J and McMorrow D 2001 *Elements of Modern X-Ray Physics* (New York: Wiley, Weinheim: Wiley-VCH)

Ambroise J P, Bellissent-Funel M C and Bellissent R 1984 *Rev. Phys. Appl.* **19** 731–4 and http://www-llb.cea.fr/spectros/pdf/7c2-llb.pdf

Andreani C 1998 *J. Mol. Liq.* **78** 217–23

Andreani C, Ricci M A, Nardone M, Ricci F P and Soper A K 1997 *J. Chem. Phys.* **107** 214–21

Andreani C and Petrillo C 1987 *Mol. Phys.* **62** 765

Armand P, Ibanez A, Ma Q, Raoux D and Philippot E 1993 *J. Non-Cryst. Solids* **167** 37–49

Ashcroft N W and Langreth D C 1967 *Phys. Rev.* **156** 685–92

Ashcroft N W and Langreth D C 1968 *Phys. Rev.* **166** 934 (erratum)

Babanov Yu A, Ershov N V, Shvetsov V R, Serikov A V, Ageev A L and Vasin V V 1986 *J. Non-Cryst. Solids* **79** 1–17

Bacon G E 1975 *Neutron Diffraction* 3rd edn (Oxford: Clarendon)

Badyal Y S, Price D L, Saboungi M-L, Haeffner D R and Shastri S D 2002 *J. Chem. Phys.* **116** 10833
Badyal Y S, Saboungi M-L, Price D L, Shastri S D, Haeffner D R and Soper A K 2000 *J. Chem. Phys.* **112** 9206
Badyal Y S and Howe R A 1996 *J. Phys.: Condens. Matter* **8** 3733–54
Bakó I, Pálinkás G, Dore J and Fischer H E 1999 *Mol. Phys.* **96** 743
Bannett Y B and Freund I 1975 *Phys. Rev. Lett.* **34** 372
Barnes A C 2005 private communication
Barnes A C, Fischer H E and Salmon P S 2003 *Neutrons et Systèmes Désordonnés* ed H E Fischer and H Schober (Les Ulis: EDP Sciences) *J. Phys. IV France* **111** 59–96
Barnes A C, Hamilton M A, Buchanan P and Saboungi M-L 1999 *J. Non-Cryst. Solids* **250–252** 393
Barnes A C, Lague S B, Hamilton M A, Fischer H E, Fitch A N and Dooryhee E 1998 *J. Phys.: Condens. Matter* **10** L645
Barnes A C, Lague S B, Salmon P S and Fischer H E 1997 *J. Phys.: Condens. Matter* **9** 6159
Baruchel J, Hodeau J L, Lehmann M S, Regnard J R and Schlenker C (ed) 1993, 1994 *Neutron and Synchrotron Radiation for Condensed Matter Studies* vol 1–3 (Berlin: Springer, Les Ulis: Les Editions de Physique)
Bausenwein T, Bertagnolli H, Tödheide K and Chieux P 1991 *Nucl. Instrum. Methods* B **61** 527
Beé M 1988 *Quasielastic Neutron Scattering: Principles and Applications in Solid State Chemistry, Biology and Materials Science* (Bristol: Hilger, IOP Publishing)
Bellissent-Funel M-C, Nasr S and Bosio L 1997 *J. Chem. Phys.* **106** 7913
Benmore C J, Weber J K R, Sampath S, Siewenie J, Urquidi J and Tangeman J A 2003 *J. Phys.: Condens. Matter* **15** S2413–23
Benmore C J, Tomberli B, Egelstaff P A and Neuefeind J 2001 *Mol. Phys.* **99** 787
Benmore C J and Soper A K 1998 *The SANDALS Manual* Rutherford Appleton Laboratory technical report
Benmore C J and Salmon P S 1994 *Phys. Rev. Lett.* **73** 264
Bergstrom P M Jr, Surić T, Pisk K and Pratt R H 1993 *Phys. Rev.* A **48** 1134–62
Bermejo F J, Dore J C, Howells W S, Chieux P and Enciso E 1989 *Physica* B **156–157** 154–7
Bernal J D and Fowler R H 1933 *J. Chem. Phys.* **1** 515–48
Bertagnolli H and Zeidler M D 1978 *Mol. Phys.* **35** 177
Bertagnolli H, Chieux P and Zeidler M D 1976 *Mol. Phys.* **32** 759
Bhatia A B and Thornton D E 1970 *Phys. Rev.* B **2** 3004
Bienenstock A 1993 *Proc. ILL/ESRF Workshop on Methods in the Determination of Partial Structure Factors (Grenoble)* ed J B Suck *et al* (Singapore: World Scientific) pp 123–9
Biggin S and Enderby J E 1982 *J. Phys. C: Solid State Phys.* **15** L305–9
Biggs F, Mendelsohn L B and Mann J B 1975 *At. Data Nucl. Data Tables* **16** 201–309
Blech I A and Averbach B L 1965 *Phys. Rev.* **137** 1113
Blétry J and Sadoc J F 1975 *J. Phys. F: Met. Phys.* **5** L110–17
Bondot P 1974 *Acta Crystallogr.* A **30** 470–1
Boolchand P (ed) 2000 *Insulating and Semiconducting Glasses* (Singapore: World Scientific)
Bosio L, Chen S-H and Teixeira J 1983 *Phys. Rev.* A **27** 1468
Bouchard R *et al* 1998 *J. Synchrotron Radiat.* **5** 90–101 and http://www-hasylab.desy.de/facility/experimental_stations/BW5/BW5.htm
Bowron D T and Moreno S D 2003 *J. Phys.: Condens. Matter* **15** S121–7
Bowron D T, Finney J L and Soper A K 1998a *J. Phys. Chem.* B **102** 3551
Bowron D T, Finney J L and Soper A K 1998b *Mol. Phys.* **93** 531–43
Brauer S, Stephenson G B, Sutton M, Brüning R, Dufresne E, Mochrie S G J, Grübel G, Als-Nielsen J and Abernathy D L 1995 *Phys. Rev. Lett.* **74** 2010–13
Breen R J, Delaney R M, Persiani P J and Weber A H 1957 *Phys. Rev.* **105** 517–21
Bruni F, Ricci M A and Soper A K 2001 *J. Chem. Phys.* **114** 8056
Buchanan P, Barnes A C, Whittle K R, Hamilton M A, Fitch A N and Fischer H E 2001 *Mol. Phys.* **99** 767
Burian A 1998 *J. Non-Cryst. Solids* **223** 91–104
Burkel E 1991 *Inelastic Scattering of X-rays with Very High Energy Resolution* (*Tracts in Modern Physics* vol 125) (Berlin: Springer) p 71
Bushnell-Wye G, Finney J L, Turner J, Huxley D W and Dore J C 1992 *Rev. Sci. Instrum.* **63** 1153–5
Caglioti G, Paoletti A and Ricci F P 1960 *Nucl. Instrum. Methods* **9** 195–98
Caglioti G, Paoletti A and Ricci F P 1958 *Nucl. Instrum.* **3** 223–28
Car R and Parrinello M 1988 *Phys. Rev. Lett.* **60** 204
Car R and Parrinello M 1985 *Phys. Rev. Lett.* **55** 2471
Carpenter J M and Yelon W B 1986 *Methods of Experimental Physics, vol 23: Neutron Scattering* ed D L Price and K Sköld (London and New York: Academic) part A, chapter 2, pp 99–196

Carpenter J M 1985 *J. Non-Cryst. Solids* **76** 1
Chamberlain O 1950 *Phys. Rev.* **77** 305–13
Champeney D C 1973 *Fourier Transforms and their Physical Applications* (London: Academic)
Chantler C T 2000 *J. Phys. Chem. Ref. Data* **29** 597–1048
Chantler C T 1995 *J. Phys. Chem. Ref. Data* **24** 71–643
Chantler C T, Olsen K, Dragoset R A, Kishore A R, Kotochigova S A and Zucker D S 2005 *X-Ray Form Factor, Attenuation and Scattering Tables (version 2.1)* http://physics.nist.gov/ffast
Chen S-H and Kotlarchyk M 1997 *Interaction of Photons and Neutrons with Matter* (Singapore: World Scientific)
Chieux P 1993 *J. Mol. Struct.* **296** 177
Chieux P 1978 *Neutron Diffraction* (*Topics in Current Physics* vol 6) ed H Dachs (Berlin: Springer) pp 271–302
Chihara J 1987 *J. Phys. F: Met. Phys.* **17** 295–304
Cicognani G (ed) 2005 *The Yellow Book* (Grenoble: Institut Laue-Langevin) http://www.ill.fr/YellowBook
Cormier L, Gaskell P H, Calas G, Zhao J and Soper A K 1998 *Phys. Rev.* B **57** R8067–70
Cormier L, Calas G and Gaskell P H 1997 *J. Phys.: Condens. Matter* **9** 10129–36
Cossy C, Barnes A C, Enderby J E and Merbach A E 1989 *J. Chem. Phys.* **90** 3254–60
Creagh D C and McAuley W J 1995 *International Tables for Crystallography* vol C, ed A J C Wilson (Dordrecht: Kluwer) section 4.2.6, pp 206–22
Crichton W A, Mezouar M, Grande T, Stølen S and Grzechnik A 2001 *Nature* **414** 622
Cromer D T and Liberman D 1970 *J. Chem. Phys.* **53** 1891
Cuello G J, Fischer H E and Palleau P 2005 http://www.ill.fr/YellowBook/D4
Cullity B D 1978 *Elements of X-ray Diffraction* 2nd edn (Reading, MA: Addison-Wesley)
Cusack N E 1987 *The Physics of Structurally Disordered Matter* (Bristol: Hilger)
de Bergevin F 1999 *X-ray and Neutron Reflectivity: Principles and Applications* ed J Daillant and A Gibaud (Berlin: Springer) pp 3–59
Debye P 1915 *Ann. Phys.* **46** 809
Debye P and Menke H 1930 *Phys. Z.* **31** 797
Dharma-wardana M W C and Aers G C 1983 *Phys. Rev.* B **28** 1701–10
Dianoux A J and Lander G (ed) 2002 *Neutron Data Booklet* (Grenoble: Institut Laue-Langevin)
Dwiggins C W Jr 1983 *Acta Crystallogr.* A **39** 773–7
Eckersley M C, Gaskell P H, Barnes A C and Chieux P 1988 *Nature* **335** 525–7
Edwards F G, Enderby J E, Howe R A and Page D I 1975 *J. Phys. C: Solid State Phys.* **8** 3483–3490
Egami T and Billinge S J L 2003 *Underneath the Bragg Peaks: Structural Analysis of Complex Materials* (Oxford: Pergamon)
Egelstaff P A 2003 *Phys. Chem. Liq.* **41** 109
Egelstaff P A 2002 *Phys. Chem. Liq.* **40** 203
Egelstaff P A 1992 *An Introduction to the Liquid State* 2nd edn (Oxford: Oxford University Press)
Egelstaff P A 1987 *Methods of Experimental Physics, vol 23: Neutron scattering* ed D L Price and K Sköld (London and New York: Academic) part B, chapter 14, pp 405–70
Egelstaff P A and Soper A K 1980a *Mol. Phys.* **40** 569
Egelstaff P A and Soper A K 1980b *Mol. Phys.* **40** 553
Egelstaff P A, Page D I and Powles J G 1971 *Mol. Phys.* **20** 881–94
Egry I, Lohöfer G, Gorges E and Jacobs G 1996 *J. Phys.: Condens. Matter* **8** 9363–8
Eisenberg S, Jal J F, Dupuy J, Chieux P and Knoll W 1982 *Phil. Mag.* A **46** 195–209
Eisenberger P, Platzman P M and Winick H 1976 *Phys. Rev.* B **13** 2377
Elliott S R 1990 *Physics of Amorphous Materials* 2nd edn (New York: Wiley)
Ellison A J G, Crawford R K, Montague D G, Volin K J and Price D L 1993 *J. Neutron Res.* **1** 61–70 and http://www.pns.anl.gov/instruments/glad
Enderby J E 1993 *Proc. ILL/ESRF Workshop on Methods in the Determination of Partial Structure Factors (Grenoble)* ed J B Suck *et al* (Singapore: World Scientific) pp 16–29
Enderby J E 1968 *Physics of Simple Liquids* ed H N V Temperley *et al* (Amsterdam: North Holland) chapter 14
Enderby J E and Barnes A C 1990 *Rep. Prog. Phys.* **53** 85
Enderby J E and Gullidge P M N 1987 *Methods of Experimental Physics, vol 23: Neutron Scattering* ed D L Price and K Sköld (London and New York: Academic) part B, chapter 15, pp 471–88
Enderby J E and Neilson G W 1981 *Rep. Prog. Phys.* **44** 593–653
Enderby J E, Howells W S and Howe R A 1973 *Chem. Phys. Lett.* **21** 109–12
Enderby J E, North D M and Egelstaff P A 1966 *Phil. Mag.* **14** 961–70
Evans R 1990 *Mol. Simul.* **4** 409
Faber T E and Ziman J M 1965 *Phil. Mag.* **11** 153

Fajardo P, Honkimäki V, Buslaps T and Suortti P 1998 *Nucl. Instrum. Methods* B **134** 337–45
Falconi S, Lundegaard L F, Hejny C and McMahon M I 2005 *Phys. Rev. Lett.* **94** 125507
Feltz A 1993 *Amorphous Inorganic Materials and Glasses* (New York: Wiley-VCH)
Filipponi A 2001 *J. Phys.: Condens. Matter* **13** R23–60
Finger L W, Cox D E and Jephcoat A P 1994 *J. Appl. Crystallogr.* **27** 892
Finney J L, Hallbrucker A, Kohl I, Soper A K and Bowron D T 2002 *Phys. Rev. Lett.* **88** 225503
Fischer H E and Schober H (ed) 2003 *Neutrons et Systèmes Désordonnés* (Les Ulis: EDP Sciences) *J. Phys. IV France* **111** 1–404
Fischer H E, Salmon P S and Barnes A C 2003 *Neutrons et Matériaux* ed W Paulus and J Meinnel (Les Ulis: EDP Sciences) *J. Phys. IV France* **103** 359–90
Fischer H E, Cuello G J, Palleau P, Feltin D, Barnes A C, Badyal Y S and Simonson J M 2002 *Appl. Phys.* A **74** S160–2
Fischer H E, Palleau P and Feltin D 1998 Results of the D4c prototype tests and review of the project *Institut Laue-Langevin Report* No ILL98FI15T
Fischer H E 1997 *Mémoire présenté pour l'obtention d'une habilitation à diriger les recherches (DHDR)* (Grenoble, France: Université Joseph Fourier)
Fischer-Colbrie A and Fuoss P H 1990 *J. Non-Cryst. Solids* **126** 1–34
Fournet G 1957 *Handbuch der Physik* vol 32 (Berlin: Springer) pp 238–320
Fukunaga T, Misawa M, Fujikawa T and Satoh S 1993 *KENS Report*-IX p 16 and http://neutron-www.kek.jp/kens_e/spectrometer/hit.html
Fuoss P H, Eisenberger P, Warburton W K and Bienenstock A 1981 *Phys. Rev. Lett.* **46** 1537–1540
Fuoss P H, Warburton W K and Bienenstock A 1980 *J. Non-Cryst. Solids* **35–36** 1233–8
Furrer A (ed) 1998 *Complementarity between Neutron and Synchrotron X-Ray Scattering* (Singapore: World Scientific)
Furukawa K 1962 *Rep. Prog. Phys.* **25** 395–440
Gaskell P H, Eckersley M C, Barnes A C and Chieux P 1991 *Nature* **350** 675–7
Gerold V and Kern J 1987 *Acta Metall.* **35** 393–9
Gibson J M and Treacy M M J 1997 *Phys. Rev. Lett.* **78** 1074–7
Gingrich N S 1943 *Rev. Mod. Phys.* **15** 90–110
Gray C G and Gubbins K E 1984 *Theory of Molecular Fluids: vol 1—Fundamentals* (*International Series of Monographs on Chemistry* vol 9) (Oxford: Clarendon)
Gregoryanz E, Degtyareva O, Somayazulu M, Hemley R J and Mao H-k 2005 *Phys. Rev. Lett.* **94** 185502
Grimley D I, Wright A C and Sinclair R N 1990 *J. Non-Cryst. Solids* **119** 49
Guarini E 2003 *J. Phys.: Condens. Matter* **15** R775–812
Guinier A 1994 *X-Ray Diffraction in Crystals, Imperfect Crystals and Amorphous Bodies* (New York: Dover)
Gullikson E M 2001 *X-ray Data Booklet* ed A C Thompson and D Vaughan (Lawrence Berkeley National Laboratory) chapters 1.6 and 1.7, pp 1-38–1-52, and http://www-cxro.lbl.gov/optical_constants/ asf.html
Gurman S J 1995 *J. Synchrotron Radiat.* **2** 56–63
Gurman S J 1990 *Neutron and X-Ray Scattering: Complementary Techniques* (*IOP Conference Series* vol 101) ed M C Fairbanks *et al* (Bristol: IOP Publishing) pp 25–40
Hajdu F and Pálinkás G 1972 *J. Appl. Crystallogr.* **5** 395
Hannon A C 2005 *Nucl. Instrum. Methods* A **551** 88–107
Hannon A C *et al* 2005 http://www.isis.rl.ac.uk/disordered
Hannon A C, Wright A C and Sinclair R N 1991 *Mater. Sci. Eng.* A **134** 883–7
Hannon A C, Howells W S and Soper A K 1990 *Neutron Scattering Data Analysis* (*IOP Conference Series* vol 107) ed M W Johnson (Bristol: IOP Publishing) p 193
Hansen J-P and McDonald I R 1990 *Theory of Simple Liquids* 2nd edn (London: Elsevier Academic)
Hansen F Y, Knudsen T S and Carneiro K 1975 *J. Chem. Phys.* **62** 1556–65
Hardacre C, McMath S E J, Nieuwenhuyzen M, Bowron D T and Soper A K 2003 *J. Phys.: Condens. Matter* **15** S159–66
Hart R T, Benmore C J, Neuefeind J, Kohara S, Tomberli B and Egelstaff P A 2005 *Phys. Rev. Lett.* **94** 47801
Hempelmann R 2000 *Quasielastic Neutron Scattering and Solid State Diffusion* (Oxford: Clarendon)
Hennet L, Thiaudière D, Gailhanou M, Landron C, Coutures J-P and Price D L 2002 *Rev. Sci. Instrum.* **73** 124–9
Henninger E H, Buschert R C and Heaton L 1967a *J. Chem. Phys.* **46** 586–91
Henninger E H, Buschert R C and Heaton L 1967b *J. Phys. Chem. Solids* **28** 423
Henshaw D G, Hurst D G and Pope N K 1953 *Phys. Rev.* **92** 1229–34
Heusel G, Bertagnolli H, Kreitmeir M, Neuefeind J and Lemke A 2002 *Phys. Chem. Chem. Phys.* **4** 4155–60
Hoppe U, Yousef E, Rüssel C, Neuefeind J and Hannon A C 2004 *J. Phys.: Condens. Matter* **16** 1645–63
Hoppe U, Karabulut M, Metwalli E, Brow R K and Jóvári P 2003 *J. Phys.: Condens. Matter* **15** 6143–53

Hoppe U, Ebendorff-Heidepriem H, Neuefeind J and Bowron D T 2001 *Z. Naturf.* A **56** 237–43
Hoppe U, Kranold R, Stachel D, Barz A and Hannon A C 1998 *J. Non-Cryst. Solids* **232–234** 44–50
Hosokawa S 2001 *J. Optoelectron. Adv. Mater.* **3** 199–214
Hosokawa S and Tamura K 2004 *J. Phys.: Condens. Matter* **16** R1465–90
Howe M A 1990 *J. Phys.: Condens. Matter* **2** 741–8
Howe M A, McGreevy R L and Howells W S 1989 *J. Phys.: Condens. Matter* **1** 3433–51
Howells W S and Hannon A C 1999 *J. Phys.: Condens. Matter* **11** 9127–38
Hubbell J H, Veigele W J, Briggs E A, Brown R T, Cromer D T and Howerton R J 1975 *J. Phys. Chem. Ref. Data* **4** 471–538
Hui Q, Tucker M G, Dove M T, Wells S A and Keen D A 2005 *J. Phys.: Condens. Matter* **17** S111–24
Hutchinson F, Wilson M and Madden P A 2001 *Mol. Phys.* **99** 811–24
Hutchinson F, Rowley A J, Walters M K, Wilson M, Madden P A, Wasse J C and Salmon P S 1999 *J. Chem. Phys.* **111** 2028
Impey R W, Madden P A and McDonald I R 1983 *J. Phys. Chem.* **87** 5071
Jal J F, Mathieu C, Chieux P and Dupuy J 1990 *Phil. Mag.* B **62** 351
James R W 1962 *The Optical Principles of the Diffraction of X-Rays* (Woodbridge, CT: Oxbow)
Johnson J A, Holland D, Urquidi J, Gee I A, Benmore C J and Johnson C E 2003 *J. Phys.: Condens. Matter* **15** 4679–93
Johnson P A V, Wright A C and Sinclair R N 1983 *J. Non-Cryst. Solids* **58** 109
Kane P P 1992 *Phys. Rep.* **218** 67
Kaplow R, Rowe T A and Averbach B L 1968 *Phys. Rev.* **168** 1068–79
Kaplow R, Strong S L and Averbach B L 1965 *Phys. Rev.* **138** A1336–45
Karabulut M, Marasinghe G K, Ray C S, Waddill G D, Day D E, Badyal Y S, Saboungi M-L, Shastri S and Haeffner D 2000 *J. Appl. Phys.* **87** 2185
Katayama Y and Tsuji K 2003 *J. Phys.: Condens. Matter* **15** 6085–103
Katayama Y, Mizutani T, Utsumi W, Shimomura O, Yamakata M and Funakoshi K 2000 *Nature* **403** 170–3
Keen D A 2002 *J. Phys.: Condens. Matter* **14** R819–57
Keen D A 2001 *J. Appl. Crystallogr.* **34** 172–7
Keen D A, Pusztai L and Dove M T (ed) 2005a *The First Fifteen Years of Reverse Monte Carlo Modelling* (Bristol: IOP Publishing) *J. Phys.: Condens. Matter* **17** S1–174
Keen D A, Tucker M G and Dove M T 2005b *J. Phys.: Condens. Matter* **17** S15–22
Keen D A, McGreevy R L, Bewley R I and Cywinski R 1995 *Nucl. Instrum. Methods* A **354** 48–52
Keen D A and McGreevy R L 1990 *Nature* **344** 423–5
Kendig A P and Pings C J 1965 *J. Appl. Phys.* **36** 1692
Kimura H *et al* 2001 *Appl. Phys. Lett.* **78** 604–6
Kirz J 2001 *X-Ray Data Booklet* ed A C Thompson and D Vaughan (Berkeley, CA: Lawrence Berkeley National Laboratory) chapter 3.1, pp 3-1–3-4
Kissel L, Zhou B, Roy S C, Sen Gupta S K and Pratt R H 1995 *Acta Crystallogr.* A **51** 271–88
Kissel L and Pratt R H 1990 *Acta Crystallogr.* A **46** 170–5
Kissel L and Pratt R H 1985 *Atomic Inner Shell Physics* ed B Crasemann (New York: Plenum) chapter 11
Klein O and Nishina Y 1929 *Z. Phys.* **57** 853–68
Klotz S, Strässle Th, Nelmes R J, Loveday J S, Hamel G, Rousse G, Canny B, Chervin J C and Saitta A M 2005 *Phys. Rev. Lett.* **94** 25506
Klotz S, Hamel G, Loveday J S, Nelmes R J, Guthrie M and Soper A K 2002 *Phys. Rev. Lett.* **89** 285502
Kob W 2003 *Proc. Les Houches School LXXVII: Slow Relaxations and Nonequilibrium Dynamics in Condensed Matter (Les Houches, 1–25 July 2002)* ed J L Barrat *et al* (Berlin: Springer) 199–270
Kohara S, Suzuya K, Kashihara Y, Matsumoto N, Umesaki N and Sakai I 2001 *Nucl. Instrum. Methods* A **467–468** 1030–3 and http://www.spring8.or.jp/e/bl/BL04B2/BL04B2_exp1.html
Kortright J B and Thompson A C 2001 *X-Ray Data Booklet* ed A C Thompson and D Vaughan (Berkeley, CA: Lawrence Berkeley National Laboratory) chapter 1.2, pp 1-8–1-27
Krause M O 1979 *J. Phys. Chem. Ref. Data* **8** 307–23
Krishnan S and Price D L 2000 *J. Phys.: Condens. Matter* **12** R145–76
Krishnan S, Felten J J, Rix J E, Weber J K R, Nordine P C, Beno M A, Ansell S and Price D L 1997 *Rev. Sci. Instrum.* **68** 3512
Krogh-Moe J 1966 *Acta Chem. Scand.* **20** 2890
Krogh-Moe J 1956 *Acta Crystallogr.* **9** 951
Kruh R F 1962 *Chem. Rev.* **62** 319

Kubo R and Ichimura M 1972 *J. Math. Phys.* **13** 1454–61
Kuharski R A and Rossky P J 1985 *J. Chem. Phys.* **82** 5164
Lamparter P 1995 *Phys. Scr.* T **57** 72–8
Landron C, Hennet L, Thiaudière D, Price D L and Greaves G N 2003 *Nucl. Instrum. Methods* B **199** 481–8
Landron C, Hennet L, Jenkins T E, Greaves G N, Coutures J-P and Soper A K 2001 *Phys. Rev. Lett.* **86** 4839
Landron C, Hennet L, Coutures J-P, Jenkins T, Alétru C, Greaves N, Soper A and Derbyshire G 2000 *Rev. Sci. Instrum.* **71** 1745–51
Landron C *et al* 1997 *Nucl. Instrum. Methods* B **124** 627
Lawrence J L 1982 *Acta Crystallogr.* A **38** 859–63
Leadbetter A J and Wright A C 1972a *J. Non-Cryst. Solids* **7** 156
Leadbetter A J and Wright A C 1972b *J. Non-Cryst. Solids* **7** 141
Leadbetter A J and Wright A C 1972c *J. Non-Cryst. Solids* **7** 37
Leadbetter A J and Wright A C 1972d *J. Non-Cryst. Solids* **7** 23
Lee J H, Owens A P and Elliott S R 1993 *J. Non-Cryst. Solids* **164–166** 139–142
Lequien S, Goirand L and Lesimple F 1995 *Rev. Sci. Instrum.* **66** 1725–7 and http://www.esrf.fr/exp_facilities/ID1/user_guide
Levesque D, Weis J J and Reatto L 1985 *Phys. Rev. Lett.* **54** 451
Levy H A, Danford M D and Narten A H 1966 Data collection and evaluation with an X-ray diffractometer designed for the study of liquid structure *Oak Ridge National Laboratory Report* ORNL-3960
Lomer W M and Low G G 1965 *Thermal Neutron Scattering* ed P A Egelstaff (London and New York: Academic) chapter 1
Lorch E 1969 *J. Phys. C: Solid State Phys.* **2** 229
Lovesey S W 1984 *Theory of Neutron Scattering from Condensed Matter* (*International Series of Monographs on Physics* vol 72) vol 1 and 2 (Oxford: Clarendon)
Ludwig K F Jr, Warburton W K and Fontaine A 1987a *J. Chem. Phys.* **87** 620–9
Ludwig K F Jr, Wilson L, Warburton W K and Bienenstock A I 1987b *J. Chem. Phys.* **87** 613–9
Ludwig K F Jr, Warburton W K, Wilson L and Bienenstock A I 1987c *J. Chem. Phys.* **87** 604–12
Magini M (ed) 1988 *X-Ray Diffraction of Ions in Aqueous Solutions: Hydration and Complex Formation* (Boca Raton: CRC Press)
Mandl F 1988 *Statistical Physics* 2nd edn (Chichester: Wiley)
Martin R A, Salmon P S, Fischer H E and Cuello G J 2003a *Phys. Rev. Lett* **90** 185501
Martin R A, Salmon P S, Fischer H E and Cuello G J 2003b *J. Phys.: Condens. Matter* **15** 8235–52
Maslen E N, Fox A G and O'Keefe M A 1995 *International Tables for Crystallography* vol C, ed A J C Wilson (Dordrecht: Kluwer) section 6.1.1, pp 476–511
Massobrio C, Pasquarello A and Car R 1999 *J. Am. Chem. Soc.* **121** 2943–4
Mayers J 1984 *Nucl. Instrum. Methods* **221** 609
McGreevy R L 2001 *J. Phys.: Condens. Matter* **13** R877–913
McGreevy R L 1995 *Nucl. Instrum. Methods* A **354** 1–16
McGreevy R L 1993 *Proc. ILL/ESRF Workshop on Methods in the Determination of Partial Structure Factors (Grenoble)* ed J B Suck *et al* (Singapore: World Scientific) pp 208–17
McGreevy R L 1990 *Neutron and X-Ray Scattering: Complementary Techniques* (*IOP Conference Series* vol 101) ed M C Fairbanks *et al* (Bristol: IOP Publishing) pp 41–9
McGreevy R L and Pusztai L 1990 *Proc. R. Soc. Lond.* A **430** 241
McGreevy R L and Pusztai L 1988 *Mol. Simul.* **1** 359
McGreevy R L and Mitchell E W J 1982 *J. Phys. C: Solid State Phys.* **15** 5537–50
Metropolis N, Rosenbluth A W, Rosenbluth M N, Teller A H and Teller E 1953 *J. Chem. Phys.* **21** 1087
Mezouar M, Le Bihan T, Libotte H, Le Godec Y and Häusermann D 1999 *J. Synchrotron Radiat.* **6** 1115–9
Mitchell E W J, Poncet P F J and Stewart R J 1976 *Phil. Mag.* **34** 721–32
Mott N F 1962 *Elements of Wave Mechanics* (Cambridge: Cambridge University Press)
Mughabghab S F, Divadeenam M and Holden N E 1981 *Neutron Cross-Sections* (New York: Academic) chapter 1
Munro R G 1982 *Phys. Rev.* B **25** 5037–45
Narten A H 1976 *J. Chem. Phys.* **65** 573
Narten A H 1972a *J. Chem. Phys.* **56** 5681
Narten A H 1972b *J. Chem. Phys.* **56** 1185
Narten A H and Levy H A 1972 *Water: A Comprehensive Treatise* vol 1, ed F Franks (New York: Plenum) chapter 8
Narten A H and Levy H A 1971 *J. Chem. Phys* **55** 2263–9
Neder R B and Korsunskiy V I 2005 *J. Phys.: Condens. Matter* **17** S125–34
Neilson G W and Adya A K 1996 *Annual Reports Section C* (*Royal Society of Chemistry* vol 93) pp 101–45

Neuefeind J 2002 *J. Mol. Liq.* **98–99** 87–95
Neuefeind J, Benmore C J, Tomberli B and Egelstaff P A 2002 *J. Phys.: Condens. Matter* **14** L429–33
Neumann H, Hoyer W and Wobst M 1991 *Z. Naturf.* A **46** 739
Norman N 1957 *Acta Crystallogr.* **10** 370
North D M, Enderby J E and Egelstaff P A 1968 *J. Phys. C: Solid State Phys.* **1** 784
Orton B R 1977 *Z. Naturf.* A **32** 863
Paalman H H and Pings C J 1962 *J. Appl. Phys.* **33** 2635
Page D I 1973 *Chemical Applications of Thermal Neutron Scattering* ed B T M Willis (Oxford: Oxford University Press) chapter 8, pp 173–200
Page D I 1972 *Water: A Comprehensive Treatise* vol 1, ed F Franks (New York: Plenum) chapter 9
Page D I and Mika K 1971 *J. Phys. C: Solid State Phys.* **4** 3034–44
Pálinkás G 1973 *Acta Crystallogr.* A **29** 10–12
Pálinkás G, Radnai T and Hajdu F 1980 *Z. Naturf.* A **35** 107
Parrinello M and Tosi M P 1979 *Riv. Nuovo Cimento* **2** 1
Pasquarello A, Petri I, Salmon P S, Parisel O, Car R, Tóth E, Powell D H, Fischer H E, Helm L and Merbach A E 2001 *Science* **291** 856
Penfold I T and Salmon P S 1991 *Phys. Rev. Lett.* **67** 97
Penfold I T and Salmon P S 1990 *Phys. Rev. Lett.* **64** 2164
Petkov V, Billinge S J L, Shastri S D and Himmel B 2000 *Phys. Rev. Lett.* **85** 3436
Petri I, Salmon P S and Fischer H E 2000 *Phys. Rev. Lett.* **84** 2413
Pings C J 1968 *Physics of Simple Liquids* ed H N V Temperley *et al* (Amsterdam: North Holland) chapter 10
Placzek G 1952 *Phys. Rev.* **86** 377
Poncet P F J 1978 Experimental reports and theory college activities *Institut Laue-Langevin Report* 78PO87S, Grenoble
Postorino P, Ricci M A and Soper A K 1994 *J. Chem. Phys.* **101** 4123–32
Poulsen H F, Neuefeind J, Neumann H-B, Schneider J R and Zeidler M D 1995 *J. Non-Cryst. Solids* **188** 63
Poulsen H F and Neuefeind J 1995 *Nucl. Instrum. Methods* B **95** 509–14
Powell D H, Fischer H E and Skipper N T 1998 *J. Phys. Chem.* B **102** 10899
Powell D H, Neilson G W and Enderby J E 1989 *J. Phys.: Condens. Matter* **1** 8721
Powell D H 1989 *PhD Thesis* University of Bristol, UK
Powles J G 1973 *Adv. Phys.* **22** 1–56
Pfleiderer T, Bertagnolli H, Tödheide K and Fischer H E 2001 *J. Chem. Phys.* **115** 5561
Pfleiderer T, Waldner I, Bertagnolli H, Tödheide K and Fischer H E 2000 *J. Chem. Phys.* **113** 3690
Press W H, Teukolsky S A, Vetterling W T and Flannery B P 1999 *Numerical Recipes in C* 2nd edn (Cambridge: Cambridge University Press)
Price D L, Saboungi M-L and Bermejo F J 2003 *Rep. Prog. Phys.* **66** 407–80
Price D L and Pasquarello A 1999 *Phys. Rev.* B **59** 5–7
Prince E (ed) 2004 *International Tables for Crystallography* vol C, 3rd edn (Berlin: Springer)
Pusztai L and McGreevy R L 2001 *J. Phys.: Condens. Matter* **13** 7213
Pusztai L and McGreevy R L 1999 *J. Neutron Res.* **8** 17
Pusztai L and McGreevy R L 1998 *J. Phys.: Condens. Matter* **10** 525
Pusztai L and McGreevy R L 1997 *Physica* B **234–236** 357
Pusztai L and Svab E 1993 *J. Phys.: Condens. Matter* **5** 8815–28
Ramesh T G and Ramaseshan S 1971a *J. Phys. C: Solid State Phys.* **4** 3029–33
Ramesh T G and Ramaseshan S 1971b *Acta Crystallogr.* A **27** 569–72
Ramos S, Neilson G W, Barnes A C and Mazuelas A 2001 *J. Phys. Chem.* B **105** 2694–8
Ramos S, Barnes A C, Neilson G W and Capitan M J 2000 *Chem. Phys.* **258** 171–80
Raoux D 1993a *Neutron and Synchrotron Radiation for Condensed Matter Studies, vol 1: Theory, Instruments and Methods* ed J Baruchel *et al* (Berlin: Springer, Les Ulis: Les Editions de Physique) chapter 2, pp 37–78
Raoux D 1993b *Proc. ILL/ESRF Workshop on Methods in the Determination of Partial Structure Factors (Grenoble)* ed J B Suck *et al* (Singapore: World Scientific) pp 130–41
Rauch W and Werner S A 2000 *Neutron Interferometry: Lessons in Experimental Quantum Mechanics* (Oxford: Clarendon)
Renninger A L, Rechtin M D and Averbach B L 1974 *J. Non-Cryst. Solids* **16** 1–14
Renninger A L and Averbach B L 1973 *Phys. Rev.* B **8** 1507–14
Richter D, Dianoux A J, Petry W and Teixeira J 1989 *Dynamics of Disordered Materials* (Berlin: Springer)
Roe R J 2000 *Methods of X-Ray and Neutron Scattering in Polymer Science* (Oxford: Oxford University Press)
Rovere M and Tosi M P 1986 *Rep. Prog. Phys.* **49** 1001

Rütt U, Beno M A, Strempfer J, Jennings G, Kurtz C and Montano P A 2001 *Nucl. Instrum. Methods* A **467–468** 1026–9 and https://beam.aps.anl.gov/pls/apsweb/beamline_display_pkg.display_beamline?i_beamline_id=11-ID-C
Salmon P S 2005 *J. Phys.: Condens. Matter* **17** S3537–42
Salmon P S 1994 *Proc. R. Soc. Lond.* A **445** 351–65
Salmon P S 1992 *Proc. R. Soc. Lond.* A **437** 591–606
Salmon P S 1988 *J. Phys. F: Met. Phys.* **18** 2345–52
Salmon P S, Martin R A, Mason P E and Cuello G J 2005 *Nature* **435** 75
Salmon P S, Petri I, de Jong P H K, Verkerk P, Fischer H E and Howells W S 2004 *J. Phys.: Condens. Matter* **16** 195–222
Salmon P S and Petri I 2003 *J. Phys.: Condens. Matter* **15** S1509–28
Salmon P S and Xin S 2002 *Phys. Rev.* B **65** 064202
Salmon P S, Xin S and Fischer H E 1998 *Phys. Rev.* B **58** 6115
Sampath S, Benmore C J, Lantzky K M, Neuefeind J, Leinenweber K, Price D L and Yarger J L 2003 *Phys. Rev. Lett.* **90** 115502
Sands D E 1993 *Introduction to Crystallography* (New York: Dover)
Sangster M J L and Dixon M 1976 *Adv. Phys.* **25** 247
Schweizer J 1982 *Nucl. Instrum. Methods* **199** 115–23
Schenk T, Holland-Moritz D, Simonet V, Bellissent R and Herlach D M 2002 *Phys. Rev. Lett.* **89** 75507
Schiff L I 1968 *Quantum Mechanics* (New York: McGraw-Hill)
Schofield P 1968 *Physics of Simple Liquids* ed H N V Temperley *et al* (Amsterdam: North Holland) chapter 13
Schommers W 1983 *Phys. Rev.* A **28** 3599
Schulke W 1991 *Handbook on Synchrotron Radiation* vol 3, ed G S Brown and D E Moncton (Amsterdam: North Holland) p 565
Schweika W and Haubold H-G 1988 *Phys. Rev.* B **37** 9240–8
Sears V F 1992 *Neutron News* **3** 26 and http://www.ncnr.nist.gov/resources/n-lengths
Sears V F 1978 *Can. J. Phys.* **56** 1261–88
Sears V F 1975 *Adv. Phys.* **24** 1–45
Serimaa R, Pitkänen T, Vahvaselkä S and Paakkari T 1990 *J. Appl. Crystallogr.* **23** 11–17
Sharrah P C and Smith G P 1953 *J. Chem. Phys.* **21** 228–32
Simonet V, Hippert F, Klein H, Audier M, Bellissent R, Fischer H E, Murani A P and Boursier D 1998 *Phys. Rev.* B **58** 6273
Sinclair R N 1993 *Proc. ILL/ESRF Workshop on Methods in the Determination of Partial Structure Factors (Grenoble)* ed J B Suck *et al* (Singapore: World Scientific) pp 107–18
Sinclair R N and Wright A C 1983 *J. Non-Cryst. Solids* **57** 447–64
Sinha S K, Tolan M and Gibaud A 1998 *Phys. Rev.* B **57** 2740–58
Sjölander A 1965 *Thermal Neutron Scattering* ed P A Egelstaff (London and New York: Academic) chapter 7, pp 291–345
Skipper N T and Neilson G W 1989 *J. Phys.: Condens. Matter* **1** 4141
Skipper N T, Neilson G W and Cummings S C 1989 *J. Phys.: Condens. Matter* **1** 3489
Soper A K 2005a private communication
Soper A K 2005b *Phys. Rev.* B **72** 104204
Soper A K 2001 *Mol. Phys.* **99** 1503–16
Soper A K 2000 *Chem. Phys.* **258** 121–37
Soper A K 1998 *J. Mol. Liq.* **78** 179
Soper A K 1997 *J. Phys.: Condens. Matter* **9** 2717
Soper A K 1996a *Chem. Phys.* **202** 295–306
Soper A K 1996b *J. Phys.: Condens. Matter* **8** 9263
Soper A K 1990 *Neutron Scattering Data Analysis* (*IOP Conference Series* vol 107) ed M W Johnson (Bristol: IOP Publishing) pp 57–67
Soper A K 1989 *Advanced Neutron Sources 1988* (*IOP Conference Series* vol 97) ed D K Hyer (Bristol: IOP Publishing)
Soper A K 1983 *Nucl. Instrum. Methods* **212** 337
Soper A K and Ricci M A 2000 *Phys. Rev. Lett.* **84** 2881
Soper A K, Howells W S, Hannon A C, Turner J Z and Bowron D T 2000 ATLAS manual: analysis of time-of-flight diffractometer data from liquid and amorphous samples *Rutherford Appleton Laboratory report for ISIS*
Soper A K, Bruni F and Ricci M A 1997 *J. Chem. Phys.* **106** 247
Soper A K, Andreani C and Nardone M 1993 *Phys. Rev.* E **47** 2598
Soper A K and Luzar A 1992 *J. Chem. Phys.* **97** 1320
Soper A K and Egelstaff P A 1980 *Nucl. Instrum. Methods* **178** 415

Soper A K, Neilson G W, Enderby J E and Howe R A 1977 *J. Phys. C: Solid State Phys.* **10** 1793–801
Squires G L 1978 *Introduction to the Theory of Thermal Neutron Scattering* (Cambridge: Cambridge University Press)
Suck J B, Raoux D, Chieux P and Riekel C (ed) 1993 *Proc. ILL/ESRF Workshop on Methods in the Determination of Partial Structure Factors (Grenoble)* (Singapore: World Scientific)
Sullivan D M, Neilson G W and Fischer H E 2001 *J. Chem. Phys.* **115** 339
Sutton M, Mochrie S G J, Greytak T, Nagler S E, Berman L E, Held G A and Stephenson G B 1991 *Nature* **352** 608–10
Swenson J, McGreevy R L, Börjesson L and Wicks J D 1998 *Solid State Ionics: Diffus. React.* **105** 55–65
Takagi R, Hutchinson F, Madden P A, Adya A K and Gaune-Escard M 1999 *J. Phys.: Condens. Matter* **11** 645–58
Tamura K, Inui M, Nakaso I, Oh'ishi Y, Funakoshi F and Utsumi W 1998 *J. Phys.: Condens. Matter* **10** 11405–17
Temperley H N V, Rowlinson J S and Rushbrooke G S (ed) 1968 *Physics of Simple Liquids* (Amsterdam: North Holland)
Thompson A C and Vaughan D (ed) 2001 *X-Ray Data Booklet* (Lawrence Berkeley National Laboratory) and http://xdb.lbl.gov
Tomberli B, Benmore C J, Neuefeind J and Egelstaff P A 2002 *Can. J. Phys.* **80** 1059
Tomberli B, Egelstaff P A, Benmore C J and Neuefeind J 2001a *J. Phys.: Condens. Matter* **13** 11421–34
Tomberli B, Egelstaff P A, Benmore C J and Neuefeind J 2001b *J. Phys.: Condens. Matter* **13** 11405–20
Tomberli B, Benmore C J, Egelstaff P A, Neuefeind J and Honkimäki V 2001c *Europhys. Lett.* **55** 341–7
Tomberli B, Benmore C J, Egelstaff P A, Neuefeind J and Honkimäki V 2000 *J. Phys.: Condens. Matter* **12** 2597–612
Tonnerre J M 1989 *Thèse Doctorale* Université de Paris-Sud, France
Treacy M M J, Gibson J M, Fan L, Paterson D J and McNulty I 2005 *Rep. Prog. Phys.* **68** 2899–944
Treacy M M J and Gibson J M 1996 *Acta Crystallogr.* A **52** 212–20
Turchin V F 1965 *Slow Neutrons* (Jerusalem: Israel Program for Scientific Translations Ltd)
Turchin V F 1963 *Medlennye Neitrony* (Moscow: Gosatomizdat) (Russian Transl.)
Urquidi J, Benmore C J, Neuefeind J, Tomberli B, Tulk C A, Guthrie M, Egelstaff P A and Klug D D 2003 *J. Phys.: Condens. Matter* **15** 3657–64
van Hove L 1954 *Phys. Rev.* **95** 249–62
van Laar B and Yelon W B 1984 *J. Appl. Crystallogr.* **17** 47
Vincent M G 1982 *Acta Crystallogr.* A **38** 510–12
Wannberg A, Delaplane R G and McGreevy R L 1997 *Physica* B **234–236** 1155–6
Warburton W K, Ludwig K F Jr, Wilson L and Bienenstock A 1987 *Phase transitions in condensed systems—experiments and theory* (*Mater. Res. Soc. Symp. Proc.* vol 57) ed G S Cargill *et al* (Pittsburgh: Materials Research Society) pp 211–25
Warren B E 1990 *X-Ray Diffraction* (New York: Dover)
Warren B E 1934 Phys. Rev. **45** 657–61
Warren B E and Mozzi R L 1970 *J. Appl. Crystallogr.* **3** 59–65
Warren B E and Mozzi R L 1966 *Acta Crystallogr.* **21** 459–61
Warren B E and Mavel G 1965 *Rev. Sci. Instrum.* **36** 196
Waseda Y 1984 *Novel Application of Anomalous (resonance) X-Ray Scattering for Structural Characterization of Disordered Materials* (*Lecture Notes in Physics* vol 204) (Berlin: Springer)
Waser J and Schomaker V 1953 *Rev. Mod. Phys.* **25** 671–90
Wasse J C, Salmon P S and Delaplane R G 2000a *J. Phys.: Condens. Matter* **12** 9539
Wasse J C, Hayama S, Skipper N T and Fischer H E 2000b *Phys. Rev.* B **61** 11993
Wasse J C and Salmon P S 1999 *J. Phys.: Condens. Matter* **11** 1381–96
Weitkamp T, Neuefeind J, Fischer H E and Zeidler M D 2000 *Mol. Phys.* **98** 125
Westlake J R 1968 *A Handbook of Numerical Matrix Inversion and Solution of Linear Equations* (New York: Wiley)
Wicks J D and McGreevy R L 1995 *J. Non-Cryst. Solids* **192–193** 23
Wicks J D, Börjesson L, Bushnell-Wye G, Howells W S and McGreevy R L 1995 *Phys. Rev. Lett.* **74** 726–9
Wicks J D, McGreevy R L and Börjesson L 1993 *Proc. ILL/ESRF Workshop on Methods in the Determination of Partial Structure Factors (Grenoble)* ed J B Suck *et al* (Singapore: World Scientific) pp 238–42
Williams G P 2001 *X-Ray Data Booklet* ed A C Thompson and D Vaughan (Lawrence Berkeley National Laboratory) chapter 1.1, pp 1-1–1-7
Wilson A J C and Prince E (ed) 1999 *International Tables for Crystallography* vol C, 2nd edn (Dordrecht: Kluwer)
Windsor C G 1986 *Methods of Experimental Physics, vol 23: Neutron Scattering* ed D L Price and K Sköld (London and New York: Academic) part A, chapter 3, pp 197–257
Windsor C G 1981 *Pulsed Neutron Scattering* (London: Taylor and Francis)
Wright A C 1996 *X-Ray and Neutron Diffraction: Experimental Technique and Data Analysis* (*NATO ASI Series* 3) pp 83–132

Wright A C 1994 *Neutron and Synchrotron Radiation for Condensed Matter Studies, vol 2: Applications to Solid State Physics and Chemistry* ed J Baruchel *et al* (Berlin: Springer, Les Ulis: Les Editions de Physique) chapter 8, pp 167–196
Wright A C 1993 *Experimental Techniques of Glass Science* ed C J Simmons and O H El-Bayoumi (Westerville, OH: American Ceramic Society) chapter 8, pp 205–314
Wright A C 1980 *Nucl. Instrum. Methods* **176** 623–5
Wright A C 1974 *Advances in Structure Research by Diffraction Methods* vol 5, ed W Hoppe and R Mason (Oxford: Pergamon) pp 1–84
Wright A C, Hannon A C, Clare A G, Sinclair R N, Johnson W L, Atzmon M and Mangin P 1985 *Proc. 3rd Int. Conf. on the Structure of Non-Crystalline Materials (NCM3, Grenoble) J. Phys. Coll.* **46** C8-299–303
Wright A C and Sinclair R N 1985 *J. Non-Cryst. Solids* **76** 351–68
Wright A C and Leadbetter A J 1976 *Phys. Chem. Glasses* **17** 122–45
Yamaguchi T, Benmore C J and Soper A K 2000 *J. Chem. Phys.* **112** 8976–87
Yamaguchi T and Soper A K 1999 *J. Chem. Phys.* **110** 3529–35
Yarnell J L, Katz M J, Wenzel R G and Koenig S H 1973 *Phys. Rev.* A **7** 2130
Zabel H 1993 *Neutron and Synchrotron Radiation for Condensed Matter Studies, vol 1: Theory, Instruments and Methods* ed J Baruchel *et al* (Berlin: Springer, Les Ulis: Les Editions de Physique) chapter 14, pp 285–320
Zachariasen W H 1935 *Phys. Rev.* **47** 277
Zachariasen W H 1932 *J. Am. Chem. Soc.* **54** 3841
Zallen R 1983 *The Physics of Amorphous Solids* (New York: Wiley)
Zernicke F and Prins J A 1929 *Z. Phys.* **56** 617
Zernicke F and Prins J A 1927 *Z. Phys.* **41** 184
Zhou B, Kissel L and Pratt R H 1992 *Phys. Rev.* A **45** 2983
Ziman J M 1979 *Models of Disorder* (Cambridge: Cambridge University Press)
Zoppi M 2003 *J. Phys.: Condens. Matter* **15** R1047–62